Fabrication of tailor-made 2D crystalline and free-standing supramolecular- and metal-organic networks: Use of interfacial assembly of amphiphilic calix[4]arenes

Inauguraldissertation

Zur

Erlangung der Würde eines Doktors der Philosophie

vorgelegt der

Philosophisch-Naturwissenschaftlichen Fakultät

der Universität Basel

von

Mina Moradi

aus dem Iran (Shazand)

Basel, 2019

Genehmigt von der Philosophisch-Naturwissenschaftlichen

Fakultät auf Antrag von:

Prof. Dr. Thomas Jung

Prof. Dr. Patrick Shahgaldian

Prof. Dr. Bruno Therrien

Basel, 11.12.2018

Prof. Dr. Martin Spiess
Dekan

To my parents,
who live their dreams through me.

ACKNOWLEDGMENT

I would like to express my sincere gratefulness to all people who supported me during these four memorable years.

I want to thank my supervisors Prof. Dr. Patrick Shahgaldian and Prof. Dr. Thomas Jung for the great chance of working in their research groups and their valuable patience, guidance, motivation and encouragement. I deeply acknowledge them for everything that I have learned on their sides.

I would like to thank the members of my doctoral committee, Prof. Dr. Catherine E. Housecroft and Prof. Dr. Bruno Therrien for their dedicated time to my PhD defense process.

I would like to acknowledge Mr. Rolf Schelldorfer for his great support and Mr. Marcus Waser who always was available to help.

I acknowledge Nadia Opara very much who performed transmission electron microscopy analysis and deposition experiments of biomolecules on the calixarene-based membranes.

I would like to thank the financial support of the Swiss Nanoscience Institute for my PhD project.

Since I was a lucky PhD student to have a chance of working in two different research groups, I made many collaborations and friendship. I am deeply grateful to my colleagues and "true" friends that became as my family, here in Switzerland: Negar, Carolina, Federica and Alessandro. They have been always present for me in all happy and sad moments. I would like to specially thank my friend and colleague "Mohamed" who supported me all the time as my brother does. I am thankful to my colleagues Rita, Manon, Jenny, Emilie, Yasmin and Lars because of all their helps and friendship. I significantly thank my other friends and colleagues in PSI and university of Basel: Fatemeh, Mehdi, Thomas, Aisha, Deepika, Janek, Milos and Christian.

I should express my deepest and warmest thank to my family in Iran. I would not be able to be here and to do this job without their love, endless support, sacrifices and kindness (I have no more words to express my gratefulness, as it deserves!). My parents always have been like mountains, on the earth, in my life. They neutralize all the pressure and stress simply with their presence and smiles. I deeply thanks my lovely brother, Mahdi, who always has reminded me that "I can do everything if I really want to do it" and my gorgeous sister in law with her faithful support, Parisa, and my sweet nephew, Kourosh.

I want to dedicate my last words of acknowledgement to "Luc" my lovely boyfriend, who appeared in my life in the right time. I thank him for being all the time present to hear and balance my extreme joys and frustrations. I am thankful for his "true" love, priceless support, encouragement and for his presence in my life.

ABSTRACT

This thesis reports new strategies for the fabrication of two-dimensional (2D) free-standing and crystalline tailor-made organic networks via bottom-up assembly of calix[4]arene organic building blocks. Three major areas of work were conducted in this project:

1- Formation of novel 2D metal-organic coordination networks (MOCNs) of calix[4]arene amphiphiles, *i.e.* a 2D MOCN of C_3-*p*-carboxy-calixarene.

2- Fabrication of the first reported free-standing and crystalline linker-free 2D supramolecular-organic network (SON) through dipole-dipole interactions between C_3-*p*-me-cyano-calixarene building units.

3- In-situ synthesis of a bilayered MOCN of C_3-*p*-me-carboxy-calixarene synthons with control over the degree of bilayer formation.

The physical and chemical properties of 2D atomically ordered organic and inorganic architectures, including strong in-plane and weak out-of-plane bonding, are unique and distinct to those of the corresponding 3D structures. Thus, 2D materials have both fundamental and applied importance to various applications ranging from superconductors to catalysis.[1] Rational design and synthesis of 2D hybrid frameworks that enables control over the resulting structures and functionalities can be achieved by applying the concepts of supramolecular and reticular chemistry.[2] Numerous 2D supramolecular organic networks have been produced by taking advantage of non-covalent interactions between organic building units. In addition to supramolecular interactions, coordination bonds have also been employed to link organic building blocks and single metal/metal complex nodes to synthesize 2D architectures, namely 2D MOCNs.[3] A wide range of possible organic and inorganic building blocks that possess coordination centers and electron donator/acceptor properties and containing various selective functional groups and catalytic centers have been used to fabricate 2D architectures with desirable structures, properties and functions.[3]

Several bottom-up techniques for the fabrication of 2D materials have been reported, including wet chemistry synthesis such as direct crystal growth from solvothermal solution, chemical vapor deposition, surfactant-directed synthesis and interfacial self-assembly reactions.[2] In bottom-up fabrication methods, the interfaces - where the reaction happens - plays a pivotal role in the nucleation and growth of 2D materials. Interfacial self-assembly is d

riven by reduction of the interfacial energy between the media.[4] Assembly of nanomaterials at interfaces with various geometries (*e.g.* nanosheets) has led the development of advanced applications in many sectors such as polymer-based photovoltaic devices, magnetic data storage media, polymer composites, oil and mineral refining, coatings, detergents and pharmaceuticals.[5]

In spite of the great progress in the field of 2D organic networks, there is a lack of practical and versatile strategies to design, fabricate and characterize free-standing and crystalline 2D nano-architectures. The research work described in this thesis led to development of a new approach to produce free-standing and crystalline 2D organic networks of calix[4]arene amphiphilic macrocycles. This work demonstrates 2D organic networks with specific desirable properties and functions can be fabricated by tailoring the structure of the amphiphilic calix[4]arene backbone. Indeed, this technique provides precise control over the organization of the molecular building blocks down to the atomic level, *i.e.* enables molecular design.

The first chapter of this thesis reports the first example of a 2D MOCN of calix[4]arene organic building blocks with tunable crystallinity. We show that carefully functionalized calix[4]arene macrocycles containing carboxy functional groups at the upper rim and propyl chains at the lower rim form a free-standing and crystalline MOCN upon coordination with Cu^{2+} ions at the air-liquid interface.

The second chapter provides the first report of linker-free 2D SON that is stabilized via synergistic interactions of the dipole-dipole forces between calix[4]arene derivative building blocks. A functionalized calix[4]arene synthon bearing methyl cyano functional groups at the upper rim and propyl chains at the lower rim was designed. This amphiphilic calix[4]arene self-assembles and forms a crystalline 2D SON at the air-water interface. The crystalline layer can be transferred from the interface onto a solid substrate, while maintaining the homogeneity and crystallinity of the layer. Furthermore, free-standing layers of the 2D SON exhibit high stability and can span perforated substrates with pores as large as 3 × 3 μm. Electron diffraction analysis confirmed the crystallinity of the free-standing 2D SON.

The in-situ formation of a bilayered MOCN, at the air-liquid interface, from a functionalized calix[4]arene carrying methyl carboxy groups at the upper rim and propyl chains at the lower rim is reported in the third chapter. Calix[4]arene derivatives are shown to form monolayers or bilayers upon changing the transition metal ion in the subphase. In the presence of Cu^{2+} ions, a free-standing and crystalline MOCN bilayer forms, in which the degree of bilayer

formation can be kinetically controlled. Substituting the Cu^{2+} ions with Ni^{2+} ions results in formation of a crystalline and free-standing monolayer of MOCN. These observations confirmed that the conformational freedom and flexibility of the modified calix[4]arene building components enable adoption of different coordination geometries in the MOCN, depending on the transition metal ion employed.

These highly stable 2D calix[4]arene-based organic networks can potentially be applied as a new generation of sample supports for transmission electron microscopy imaging and *X*-ray analysis of single biomolecules/assemblies and single-magnetic nanoparticles. Indeed, some examples of biomolecule, assembly and nanoparticle deposition experiments on free-standing coordination networks of calix[4]arene amphiphiles are presented in this thesis. Further work is currently underway to extend this research and define advanced methods to enhance the structural analysis of single biomolecules and the magnetic properties of nanoparticles deposited on free-standing monolayers of calixarenes and related compounds.

Keywords: supramolecular chemistry, reticular chemistry, 2D metal-organic coordination network, 2D supramolecular-organic network, self-assembly, Langmuir-Blodgett technique, calix[4]arene amphiphile, amphiphilic bilayers.

PUBLICATION LIST

During my PhD studies, I contributed to the following publications, in chronological order:

[1] **Mina Moradi**, Ludovico G. Tulli, Jan Nowakowski, Milos Baljozovic, Thomas A. Jung, and Patrick Shahgaldian, "Two-dimensional calix[4]arene-based metal-organic coordination networks of tunable crystallinity", ***Angew. Chem., Int. Ed.,*** **2017**, 56, 14395 –14399. (http://onlinelibrary.wiley.com/doi/10.1002/anie.201703825/abstract)

[2] Vivian Müller, Feng Shao, Milos Baljozovic, **Mina Moradi**, Yao Zhang, Thomas Jung, William B. Thompson, Benjamin T. King, Renato Zenobi, A. Dieter Schlüter, "Structural characterization of a covalent monolayer sheet obtained by two-dimensional polymerization at an air/water interface", ***Angew. Chem., Int. Ed.,*** **2017**, 56, 15262-15266. (http://onlinelibrary.wiley.com/doi/10.1002/anie.201707140/full).

[3] Vivian Müller, Antoine Hinaut, **Mina Moradi**, Milos Baljozovic, Thomas A. Jung, Patrick Shahgaldian, Helmuth Möhwald, Daniel Murray, William B. Thompson, Benjamin T. King, Gregor Hofer, Martin Kröger, Thilo Glatzel, A. Dieter Schlüter, "A two-dimensional polymer synthesized at the air/water interface", ***Angew. Chem., Int. Ed.,*** **2018**, 57, 10584-10588. (https://doi.org/10.1002/anie.201804937)

[4] **Mina Moradi**, Nadia Opara, Ludovico G. Tulli, Christian Wäckerlin, Scott J. Dalgarno, Simon J. Teat, Milos Baljozovic, Olha Popova, Eric v. Genderen, Armin Kleibert, Henning Stahlberg, Jan Pieter Abrahams, Celestino Padeste, Philippe. F.-X. Corvini, Thomas A. Jung, Patrick Shahgaldian, "Supramolecular architectures of molecularly thin yet robust free-standing layers", ***Sci. Adv.*****, 2019,** 5. (https://advances.sciencemag.org/content/5/2/eaav4489)

[5] **Mina Moradi**, Nadia Opara, Catherine E. Housecroft, Ludovico G. Tulli, Henning Stahlberg, Thomas A. Jung, Patrick Shahgaldian, "Controlling in-situ formation of bilayer *vs* monolayer of metal organic coordination networks", to be submitted.

[6] Nadia Opara, **Mina Moradi**, Eric van Genderen, Max Clabbers, Radosav Pantelic, Mohamed Chami, Jan Pieter Abrahams, Thomas A. Jung, Patrick Shahgaldian, Henning Stahlberg, "Calixarene-based free-standing nanomembranes as a protein specimen support for electron microscopy", under preparation.

TABLE OF CONTENTS

LIST OF ABBREVIATIONS AND MOLECULES

1D	one-dimensional
2D	two-dimensional
3D	three-dimensional
MOCN	metal-organic coordination network
SON	supramolecular-organic network
C_3-p-carboxy-calix	*5,11,17,23*-tetra-carboxy-*25,26,27,28*-tetrapropoxycalix[4]arene
C_3-p-me-cyano-calix	*5,11,17,23*-tetra-methylcyano-*25,26,27,28*-tetrapropoxycalix[4]arene
C_3-p-me-carboxy-calix	*5,11,17,23*-tetra-methylcarboxy-*25,26,27,28*-tetrapropoxycalix[4]arene
AFM	atomic force microscopy
XPS	*X*-ray photoelectron spectroscopy
STM	scanning tunneling microscopy
TEM	transmission electron microscopy
^{1}H NMR	proton nuclear magnetic resonance
^{13}C NMR	carbon nuclear magnetic resonance
NEXAFS	near edge *X*-ray absorption fine structure
XRD	*X*-ray diffraction
BAM	Brewster angle microscopy
LB	Langmuir-Blodgett
LS	Langmuir-Schaefer
HOPG	highly-oriented pyrolytic graphite
SBU	secondary building unit
TERS	tip-enhanced Raman spectroscopy
XAS	*X*-ray absorption spectroscopy
PCP	porous coordination polymer
SPM	scanning probe microscopy
SAM	self-assembled monolayer
CB[8]	cucurbit[8]uril
TMV	tobacco mosaic virus
LbL	layer-by-layer deposition
THT	triphenylenehexathiol
GBP	gabapentin
PSI	Paul Scherrer institute

C$_3$-*p*-carboxy-calix 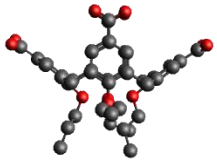

C$_3$-*p*-me-cyano-calix 

C$_3$-*p*-me-carboxy-calix 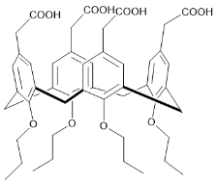

INTRODUCTION

Supramolecular chemistry, Crystal engineering and Reticular chemistry

On the understanding of non-covalent binding – Johannes Diderik van der Waals first introduced the concept of "intermolecular interactions" as the attraction forces between molecules in 1873.[6] Van der Waals forces, named after Diderik van der Waals, are the weakest interactions between atoms or molecules, and arise from polarization of electron clouds by the proximity of an adjacent nucleus. These interactions quickly vanish as the distances between interacting molecules increases.

Two decades later, in 1894, Hermann Emil Fischer introduced the "lock and key" mechanism to describe selective enzyme-substrate/host-guest interactions. In this mechanism, the high selectivity of recognition is attributed to the complementarity between the shape and size of the host/enzyme active site and guest/substrates. Indeed, the binding sites of the receptor/host are perfectly suited to recognize specific guests. This work is considered the fundamental basis of molecular recognition and host-guest chemistry.[7] In 1906, Paul Ehrlich recognized molecules do not act if they do not bind, which led to the emergence of the concept of biological receptors. Some decades after, Daniel Koshland developed the concept of lock-and-key theory and introduced the induced-fit mechanism. The induced-fit mechanism describes how a conformational change occurs in the structure of the binding site of an enzyme upon its interaction with its substrate.[8] The understanding of non-covalent binding was further developed by Latimer and Rodebush in 1920, who described relatively strong and highly directional hydrogen bonding as another type of intermolecular interaction.[9] In 1954, Linus Pauling received the Nobel Prize in Chemistry for his outstanding research into the nature of chemical bonds and their importance in the elucidation of complex structures.[10]

Further knowledge of the nature of non-covalent binding, along with the theory of coordination chemistry, was introduced by Alfred Werner in 1893,[11] which provided the foundation of supramolecular chemistry.

From understanding non-covalent interactions to supramolecular chemistry – The synthesis of crown ethers and cryptands, along with their complexes with metal salts, by Charles J. Pedersen in 1967 was a major breakthrough in the field of supramolecular chemistry.[12] Others, such as Donald J. Cram and Jean-Marie Lehn, focused on the synthesis of shape- and ion-selective receptors. In 1978 Jean-Marie Lehn defined supramolecular chemistry as the: "… chemistry of molecular assemblies and of intermolecular bonds".[13] Lehn, Pedersen and Cram shared the Noble Prize in Chemistry in 1987 for their outstanding

contributions to supramolecular chemistry by synthesizing molecules capable of structure-specific interactions. The initial reports in the realm of supramolecular chemistry described the formation of binary complexes between two components, *i.e.* a host and guest that interact via non-covalent binding. The host is typically a large molecule that possesses a cavity of tunable size, *e.g.* synthetic macrocycles. The guest could be an ion or a more complex molecule that fits perfectly into the cavity of the host.

Organic cyclic oligomers of calix[n]arenes (n = 4, 6, 8) were first named by C. David Gutsche in 1978,[14] and are one of the most well-studied molecules in terms of binary host-guest complexes[15,16] and supramolecular architectures.[17]

Since then, supramolecular chemistry has become a recognized and active domain of chemistry that has gained considerable attention from scientists in a broad range of fields.

From binary complexes to extended 3D structures of organic molecules – Since its emergence in the late 19th century, supramolecular chemistry has evolved towards the production of more complex molecular architectures. However, despite significant progress, the fabrication of predesigned solid-state frameworks with the desired physical and chemical properties remained challenging. In this regard, Feynman stated in 1960 that "what would the properties of materials be if we could really arrange the atoms the way we want them?".[18] Gerhard Schmidt introduced the term "crystal engineering" to describe photodimerization reactions in crystalline cinnamic acids in 1971.[19] Pioneering work by Schmidt revealed the geometry criteria required for a [2+2] photodimerization to occur in the solid-state.[20] Schmidt explained how functional groups or substituents influence the organization of molecules in the solid-state. Since then, several advances have been achieved to facilitate the solid-state reactions. For example, it has been confirmed that intermolecular forces can be effectively exploited as templates to steer the packing of molecules into the desired geometries for reactions in the solid-state (Figure 1).[21,22]

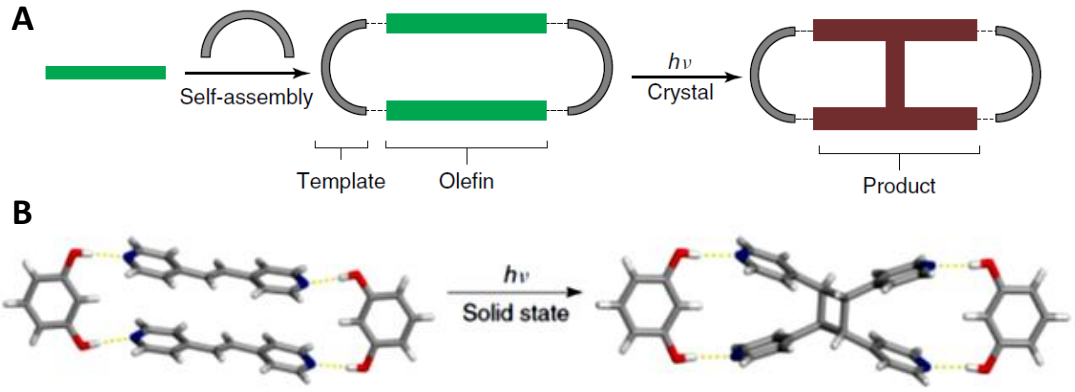

Figure 1: (A) schematic of the template strategy to control the chemical reactivity in the solid-state. (B) An example of a photochemical reaction based on the template approach. The ditopic hydrogen-bond donors were used as template to control the molecular arrangement in the [2+2] photodimerization reaction in order to produce pyridyl-ethylene derivative structure. (Taken with permission from the Ref. 21 and 22. Copyright © 2012. John Wiley and Sons. Copyright © 2008. The American chemical society.)

Continuing Schmidt's work, in 1983 Desiraju published the first report of crystal engineering to provide topochemical control over an organic solid-state reaction by exploiting intermolecular interactions.[23,24,25] Since then, crystal engineering - a sub-discipline within supramolecular chemistry - has been successfully applied to rationally design and synthesize novel extended materials with desirable properties. [25,26-28]

However, an important scientific and technological question remained: would it be possible to predict the crystal structure of a material just by knowing the molecular structure of its components?.[29] In this context, John Maddox - a British scientist who acted as the editor-in-chief of the journal Nature, highlighted this challenge in 1988: "One of the continuing scandals in the physical sciences is that it remains in general impossible to predict the structure of even the simplest crystalline solids from a knowledge of their chemical composition."[30]

The challenge of predicting the crystal structure of a material has aroused a considerable attention amongst scientists interested in the fabrication of "designed" materials.[31] Following seminal work on the synthesis of porous structures in 1994 by Robson,[32] O. Yaghi introduced the term of "reticular chemistry" as a general conceptual approach for the fabrication of robust 3D metal-organic frameworks (MOFs) in 2003. This approach is based on the use of presynthesized polynuclear hybrid clusters, *i.e.* secondary building units (SBUs)[33], to direct the assembly of ordered frameworks.[26] Therefore, rationally designed porous materials including so-called MOFs, porous-coordination polymers (PCPs) and covalent-organic frameworks (COFs), have been fabricated by attaching judiciously rigid SBUs to organic linkers.[31,34-37] The diversity of SBUs and organic/inorganic linkers has enabled the fabrication of thousands of extended crystalline structures. The robust crystalline reticular frameworks exhibit a wide range of functionalities and properties, including conductivity, magnetism, light harvesting, charge transfer and catalytic reactivity.[38-41]

From 3D organic frameworks to 2D organic networks – The discovery of graphene in 2004, and its extraordinary physical and chemical properties opened a new avenue towards the fabrication of novel category of materials, *i.e.* 2D architectures. The subsequent rapid increase in research on 2D materials, both in terms of basic scientific interest and potential technological impact, has led to the introduction of various 2D inorganic materials (*e.g.* boron nitride, layered perovskites and transition metal dichalcogenides).[3,42,43]

Highly organized 2D materials can also be fabricated using organic building units. In recent decades, the principles of supramolecular and reticular chemistry have been adapted to produce a vast array of newly-engineered 2D organic molecular nano-architectures including 2D polymers, 2D MOFs, 2D COFs and 2D supramolecular organic frameworks.[43] Similarly to 2D inorganic materials, these 2D organic layers have attracted ever-increasing scientific attention.[44] The potential of the unique physical and chemical properties of 2D organic layers for various applications in nanotechnology and advanced materials have been clearly recognized.[2,44-46]

Objectives of this thesis

In the absence of carrier materials, *i.e.* free-standing layers, 2D architectures have potential to be used as sensors, catalysts, ionic conductors and sample supports for imaging and structural analysis of molecules.[1,3,47] In such applications, the free-standing monolayers must possess sufficient stability to endure multiple operational cycles, which presents a significant challenge to current fabrication techniques.

In this context, there is a lack of versatile procedures to produce stable and functional 2D free-standing and crystalline organic networks while achieving a high control over the growth process at the nanoscale. This PhD research aimed to identify a reliable protocol to design and synthesize robust crystalline 2D metal-organic coordination networks (MOCNs) and supramolecular-organic networks (SONs). The objective of this work was to use non-planar multivalent macrocycles as organic building blocks to fabricate well-ordered organic networks. It is expected that these 2D organic networks could be employed in further applications, for example, in molecular recognition and host-guest chemistry. In this study, we selected the Langmuir-Bodgett (LB) technique as a tool to manipulate and control interfacial self-assembly of calix[4]arene macrocycles, as the multivalent building components.

Why the LB technique – A mechanism of orientation and alignment mechanism is required to fabricate ordered 2D networks, either in the form of a hosting matrix or directional bonding scheme between the building blocks. The presence of a suitable platform that promotes fine-tuning of the orientation of the molecules, and the interactions between them, plays a key role in the synthesis of 2D materials. The reaction platform defines the homogeneity (versus heterogeneity) of the resulting architecture and its domain size.[41] In this project, the versatile LB technique was chosen to fabricate molecularly precise layers through a self-assembly process and a 2D interfacial assembly between the calix[4]arene building blocks. The air-water interface in LB assembly provides a flat surface with a root-mean-square roughness of approximately 3 Å. This 2D platform confines the molecules to the water surface and enables tuning of the packing density of the amphiphiles by adjusting the surface pressure of the interface.[52] The liquid interface facilitates increased lateral mobility of the molecules in comparison to bulk solution or a solid substrate with fixed terraces and grain boundaries.[2] Thereby the LB technique makes it feasible to fabricate ordered 2D structures from amphiphilic building blocks over an extended area, with control over the morphology of the 2D network.[53]

Calix[4]arenes – chemically configurable synthons as building units for 2D organic networks – Calixarenes are cyclic oligomers produced by the condensation of *p*-tert-butylphenol with formaldehyde and possess guest recognition properties.[48,49] The well-developed synthetic methods and versatility of functionalization of calixarenes are important characteristics that make these units the ideal backbone for the fabrication of ordered 2D structures.[38,50] However, their conformational flexibility makes it challenging to incorporate calixarenes into 2D architectures. In order to overcome this challenge calixarenes are normally functionalized at the lower rim, to reduce their conformational freedom and lock their structure. Additionally, a diverse range of chemical functional groups can be attached to the rim of calixarenes. Therefore, a large variety of organic calixarene synthons can be produced for host-guest assembly, supramolecular and coordination assembly, and covalent linking.
Amphiphilic calixarene macrocycles bearing hydrophilic functional groups at the upper rim and long aliphatic chains at the lower rim have been widely shown to self-assemble into stable insoluble monomolecular films at the air-liquid interface, *i.e.* Langmuir monolayers.[51] In such Langmuir monolayers, the amphiphiles are oriented perpendicular to the interface as the polar functions are attracted into the aqueous phase and the hydrophobic groups orientate into the air (Figure 2). The amphiphilic calixarene synthons within Langmuir monolayers are stabilized by van der Waals interactions between the aliphatic chains, by H-bonding amongst the head groups of calixarene and water molecules and by π-stacking interactions between the arene rings of neighboring calixarene molecules.

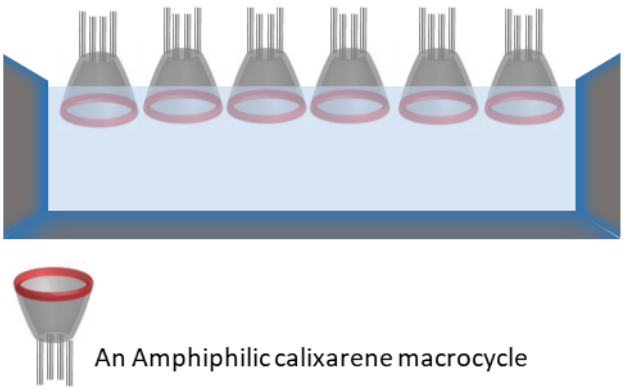

Figure 2: A schematic illustration of a Langmuir monolayer of amphiphilic calixarene molecules floating at the air-water interface.

In this design strategy, we employed a rigid 4-membered macrocycle displaying C_4 symmetry in the cone conformation, *i.e.* calix[4]arene. The symmetrical cone conformation of this 4-membered synthon enables in-plane assembly processes. Calixarene amphiphiles with long alkyl chains exhibit fairly limited 2D crystallization behavior, possibly due to the disorder introduced by thermal motion of the chains.[51] We overcame this issue by functionalizing the calixarene synthons with shorter aliphatic chains, *i.e.* propyl chains. The presence of short

aliphatic chains at the lower rim of the calixarene amphiphiles minimizes the non-directional van der Waals interactions between the propyl chains during the self-assembly process. Therefore, self-assembly is expected to be mainly driven by the strong bonds between the metallic nodes and hydrophilic functional groups of the calixarene molecules and also by the directional π-π interactions between the arene rings of neighboring calix[4]arene amphiphiles.

STATE OF THE ART

2D organic networks have attracted substantial interest from researchers because of their unique physical and chemical properties originating from their low thickness and versatile structures. These 2D materials afford potentials in diverse applications such as gas storage,[54] gas separation[55] and purification.[56] Over the past decades, fabrication techniques of 2D organic networks, classified into two categories of the top-down and the bottom-up routes, have been drastically advanced.

The top-down strategies include the physical and mechanical exfoliation from their corresponding bulk layered materials.[57,58] The chemical exfoliation of 3D structures in solution can also be applied, assisted by ion-intercalation,[59] shear force[60] and ion exchange[61] as well as electrochemical methods.[62] The top-down routes suffer the lack of control over: the layer thickness and lateral size, the arrangement and functionality of molecules in a large area, the synthesis yield and the structural integrity.

The bottom-up methods refer to the direct synthesis of structures from their building components and oppositely, they are highly efficient and provide a precise control on the fabrication process down to the atomic level. The bottom-up synthetic routes involve wet chemistry synthesis such as direct crystal growth from solvothermal solution,[63-65] step-by-step liquid epitaxial growth,[66,67] chemical vapor deposition (CVD),[68] surfactant-directed synthesis[69] and interfacial self-assembly reactions.[2]

It is noteworthy that the interface - where the reaction happens - is an important key point in the most bottom-up synthetic methods. Interface is a 2D confined platform that directs the assembly/reactions of precursors by controlling the morphology and structure of organic/inorganic building blocks. It has been successfully proved that the interfacial self-assembly reactions at gas-liquid, liquid-liquid, liquid-solid and gas/vacuum-solid interfaces produce organic networks upon formation of coordination/covalent bonds and/or non-covalent interactions between the organic linkers and nodes (Figure 1).[2]

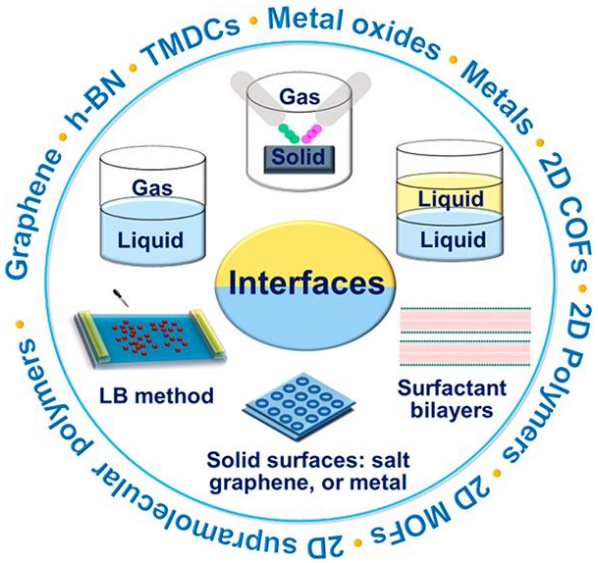

Figure 1: Graphical representation of various interfaces such as gas-liquid, liquid-liquid, gas-solid (or vacuum-solid) and liquid-solid that can be used for chemical synthesis of 2D materials via interfacial self-assembly reactions. (Reprinted with permission from Ref. 2. Copyright © 2018. The American chemical society.)

In this context, considerable efforts have been devoted to fabrication of single or few-layers of 2D metal-organic frameworks (MOFs), supramolecular-organic frameworks (SOFs) and covalent-organic frameworks (COFs) via interfacial self-assembly at liquid-liquid and air-liquid interfaces.[2]

2D metal-organic frameworks – Two-dimensional MOFs are crystalline and porous coordination structures made upon jointing inorganic metal ions or clusters and ditopic or polytopic organic ligands. It has been widely shown that 2D MOFs hold potential for many applications due to their tunable and stable structures, cooperative functions, large surface area and high porosity.[3]

In 2002, Michl *et al.* fabricated the first extended coordination organic network of a carborane cage derivative on the surface of mercury via an electrochemical Langmuir trough. The strategy was based on binding the trigonal carborane cage synthons to each other via a coupling between their thioether containing arms by ligation to mercury cations (Figure 2).[70]

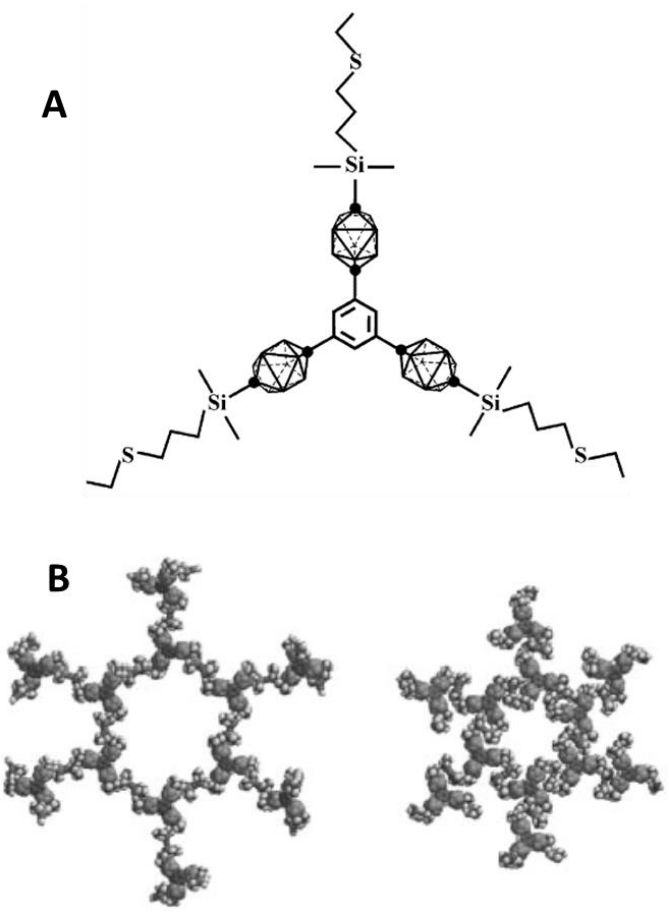

Figure 2: (A) The molecular structure of trigonal carborane cage derivative. (B) Two tentative molecular models of the proposed hexagonal organic networks that are bound through mercury cations. (Reprinted with permission from Ref. 70. Copyright © 2002. The proceeding of the national academy of sciences.)

Talham *et al.* synthesized an array of amphiphilic pentacyanoferrate(III) molecules that coordinate Ni^{2+} ions at the air-water interface and form a 2D network via iron-nickel cyanide-bridges (Figure 3). In this fabrication approach, the amphiphilic dialkylaminopyridine ligands confined the iron complexes at the interface and directed the condensation reaction within the plane of the water surface. Subsequently, any possible 3D growth of the coordination network was suppressed and only a 2D organic network was obtained. Using the Langmuir-Blodgett (LB) deposition technique the monolayers and multilayers of the coordination network were transferred onto solid substrates. It was shown that the 2D coordination network was not formed by homogeneous solution synthesis and the product had only amorphous structure. This result is a proof emphasizing the crucial importance of interfaces, as structure directors, in the assembly of 2D crystalline networks.[71]

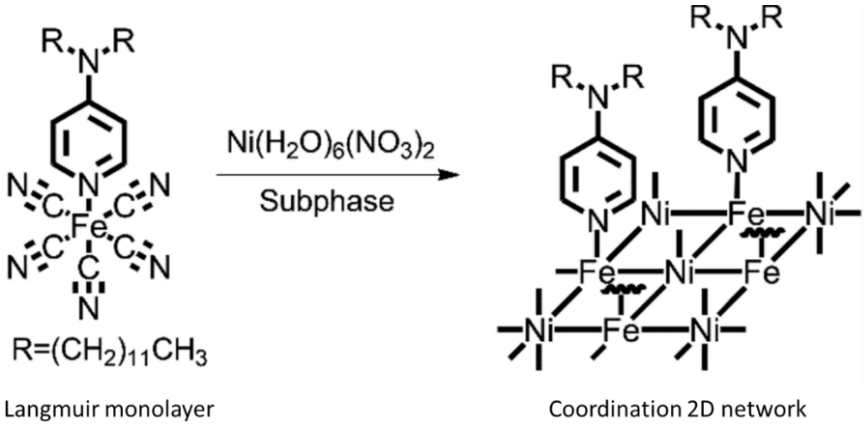

Figure 3: A representative scheme of a 2D square grid coordination network of amphiphilic pentacyanoferrate(III) through coordination with Ni^{2+} ions at the air–water Interface. The formation of iron-nickel cyanide-bridges extends the 2D crystalline network at the interface. (Taken with permission from Ref. 71. Copyright © 2002. The American chemical society.)

Schlüter *et al.* reported the synthesis of a 2D free-standing polymer sheet consisting hexafunctional terpyridine-based monomers held together by Fe^{2+} complexes in an octahedral geometry (Figure 4). The confined, flat and smooth air-water interface in the LB technique was chosen as a platform for performing the polymerization reaction between the terpyridine monomers and the iron ions. The restricted 2D air-water interface prohibits any possible 3D growth of the coordination network during the reaction. It was shown that this type of polymerization provides high control over uniformity of the polymer thickness and lateral size via reversible and dynamic bonds formation. The reversible polymerization leads to fabrication of well-ordered structures with self-correction feature. Synthesizing defect-free coordination monolayers is feasible due to the dynamic nature of this type of interfacial reactions. These are the main advantages of the interfacial-based synthesis compared to other fabrication techniques such as exfoliation of laminar 3D crystals or isolation of sheets from solid substrates.[72]

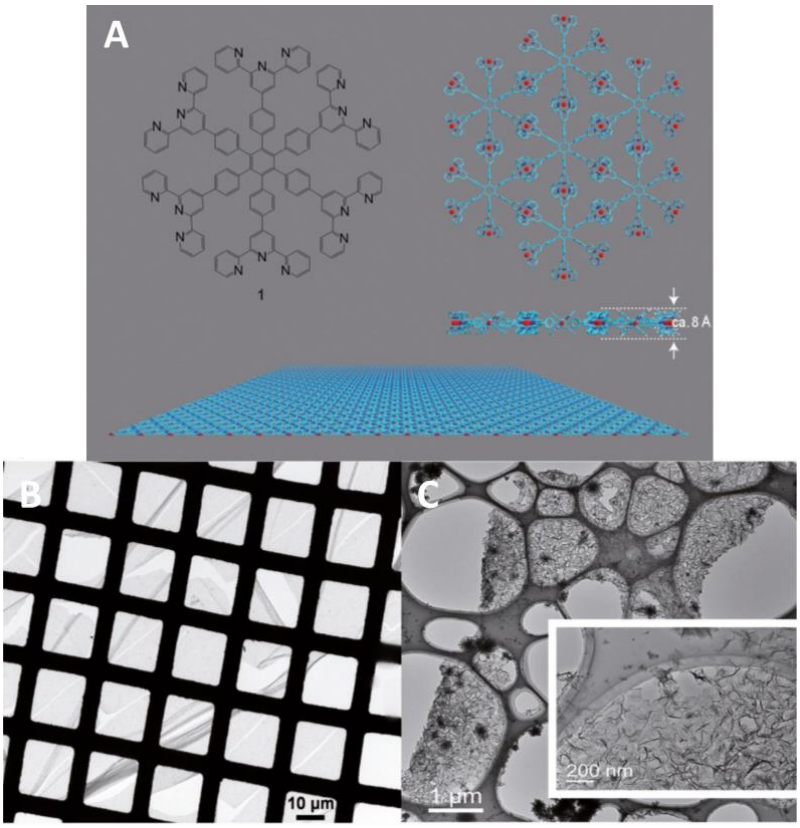

Figure 4: (A) Chemical structure of the terpyridine monomer and a schematic representation showing the resulted 2D coordination network of the monomers and metal ions (metal ion is represented in red, C in turquoise and N in blue). The inset image shows a cross-sectional view of the coordination network to estimate the layer thickness *i.e.* ~8 Å, without counterions. (B & C) TEM images of free-standing layer of the 2D MOF that was transferred from the interface onto a copper and lacey carbon grids. (Taken with permission from Ref. 72. Copyright © 2011. John Wiley and Sons.)

Makiura and co-workers demonstrated an interfacial methodology to synthesize large area crystalline MOF nanofilm on a solid surface, namely NAFS-1. The growth directions and film thickness of the NAFS-1 were controlled via the bottom-up layer-by-layer (LbL) technique combined with the LB method at the air-water interface. Coordination bonds between the functionalized porphyrin carboxylate organic building units and the Cu^{2+} ions formed the extended 2D NAFS-1 nanosheets (Figure 5). In this coordination geometry, every copper ion coordinates four carboxylate linkers, in-plane, and two pillaring molecules (pyridines) complete the coordination sphere, out-of-plane. Both in-plane and out-of-plane crystallinity of NAFS-1 nanosheets were studied by synchrotron *X*-ray surface crystallography. It was confirmed that the organic networks of NAFS-1 can be transferred from the interface onto solid substrates with the LbL deposition technique. The transferred layers of NAFS-1 on a solid substrate exhibited motifs of porphyrine molecules and copper ions. In this motif each pyridine building unit is linked to binuclear $Cu_2(COO)_4$ paddle-wheel complexes. Therefore,

they form a network with large-sized crystalline domains (~140 nm) and a sheet thickness of ~3 Å.[73]

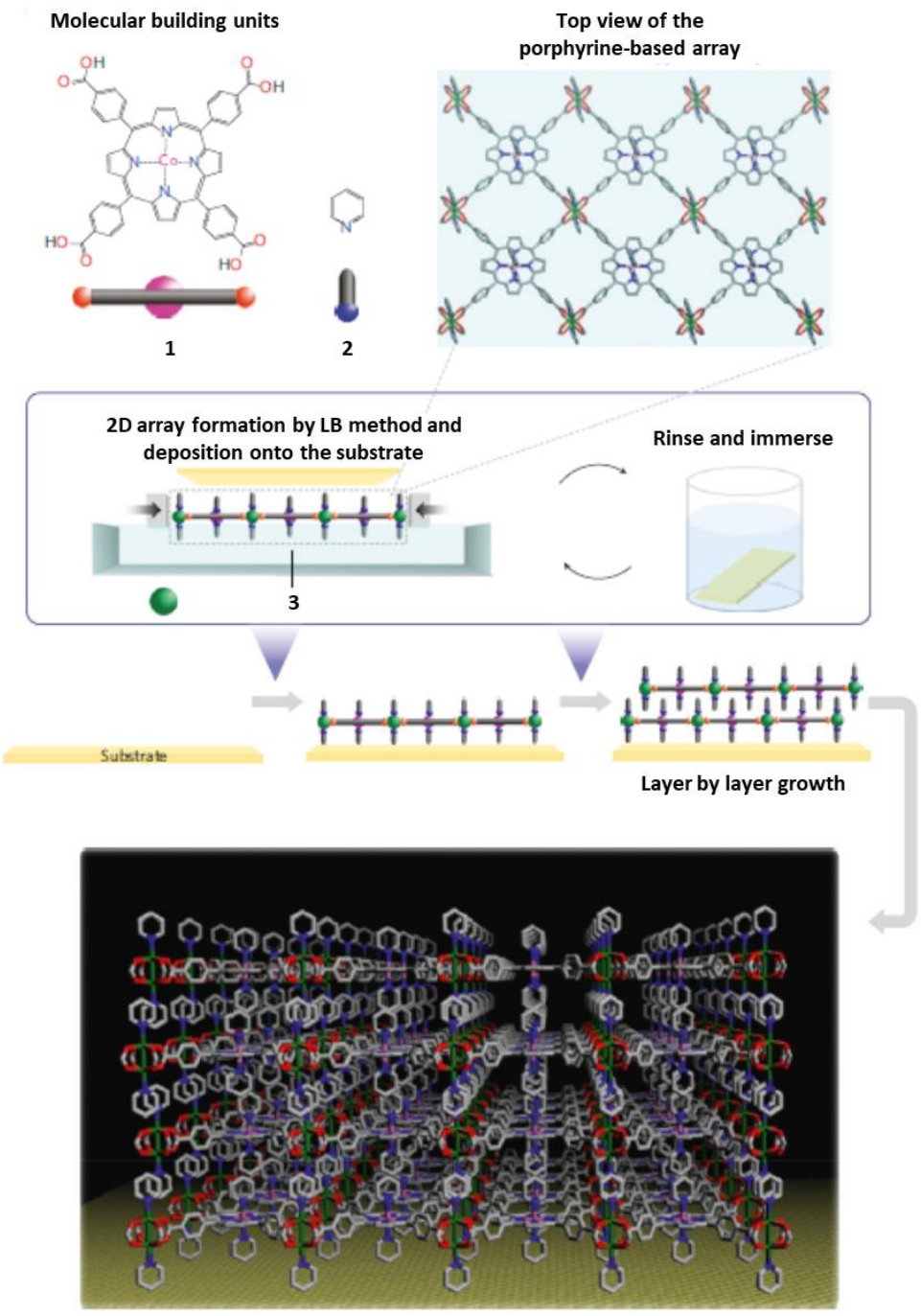

Figure 5: The chemical structures and representative schematics of the porphyrin derivative (**1**) and the pyridine (**2**) building units. The aqueous solution of $CuCl_2.2H_2O$ (**3**) in a LB trough was used as a platform of the interfacial synthesis reaction. Upon compressing the molecules at the interface, a copper-mediated 2D array was formed. The 2D layers of coordination network were deposited onto solid substrates by the LB method. The repetitive process of sheet deposition and rinsing or solvent immersion caused to the sequential LbL growth of the organic network with any desired thickness. C atoms are shown in grey, N in blue, O in red, Co^{2+} ions in pink and Cu^{2+} ions in green. (Reprinted with permission from Ref. 73. Copyright © 2010. Springer nature.)

The same group synthesized a 2D MOF of carboxyphenyl porphyrin derivatives coordinated with copper ions via the LbL technique at the air-water interface, *i.e.* NAFS-2. The only difference between the molecular architectures of NAFS-2 and NAFS-1 is the absence of pillaring components, *i.e.* pyridine molecules, in the structure of NAFS-2 (Figure 6). Upon removing the pyridine building units the interlayer spacing of NAFS-1 nano-architecture was changed. This modification improved the thermal stability of NAFS-2 such that annealing at 200°C does not cause any loss of its structural crystallinity. Multilayers of NAFS-2 were transferred from the interface onto solid surfaces by using the repetitive LbL deposition method. The multilayers of NAFS-2 on gold or silicon solid surfaces have the potential to be integrated as electrodes in devices.[66,73]

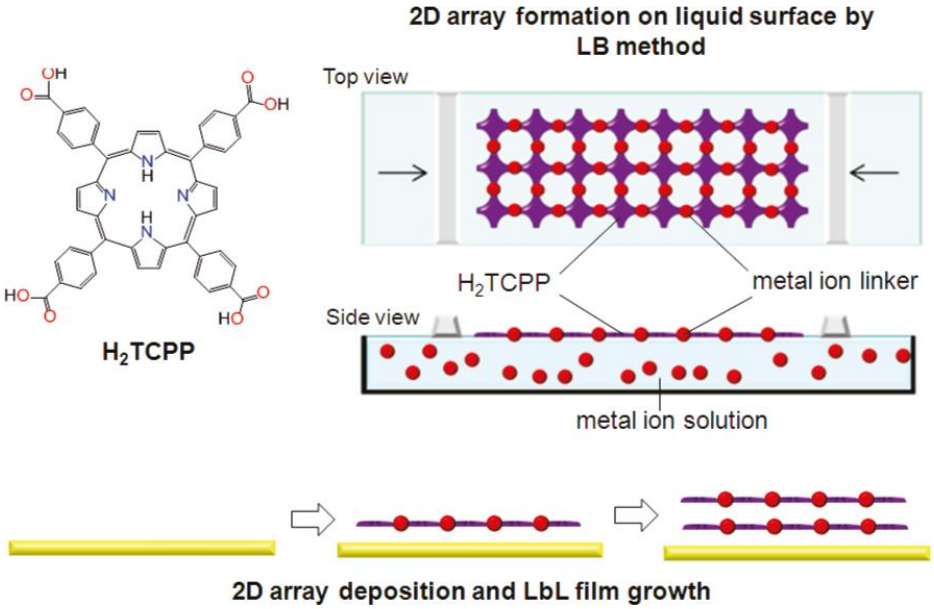

Figure 6: A representative scheme of the combined LbL and LB techniques to synthesize coordination network of NAFS-2, at the air-water interface. The MOF nanosheets of NAFS-2 include carboxyphenyl porphyrine molecules and copper ions. (Reprinted with permission from Ref. 66. Copyright © 2011. The American chemical society.)

Yaghi *et al.* fabricated a new class of 2D extended frameworks with octahedral coordination geometry, *i.e.* metal-catecholates, by coordinating highly conjugated tricatecholate building components with Co(II) ions (Figure 7). It was shown that the porous metal-catecholates have high chemical and thermal stability, porosity, high electrical conductivity and charge storage capacity. Performing *X*-ray analysis revealed the metal atoms are coordinated to two adjacent deprotonated catecholate organic derivatives and two water molecules complete the octahedral coordination sphere. [74]

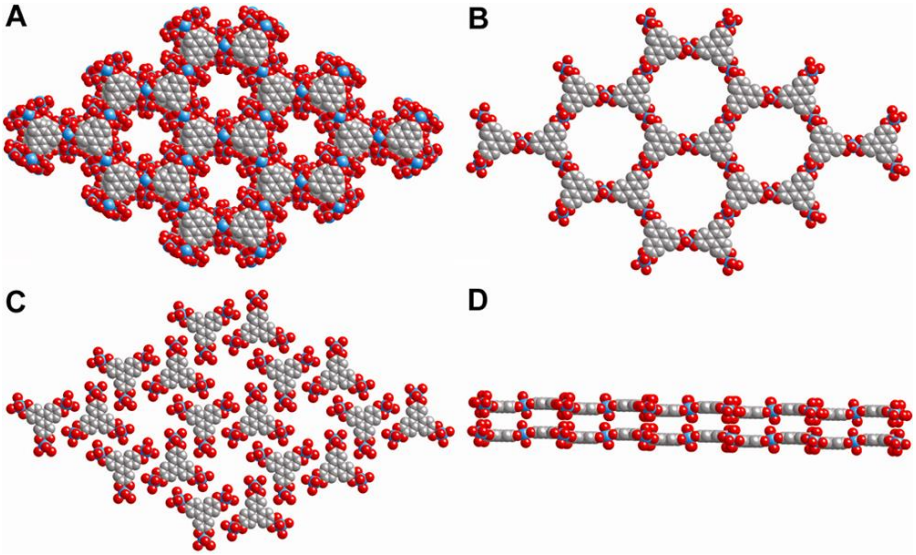

Figure 7: (A & B) Drawings of the Co-catecholate structures in two different views. (C) The obtained organic network of trinuclear complexes of Co_3(hexahydroxytriphenylene)$(H_2O)_{12}$. (D) A side view of the two extended corrugated layers of the catecholate network. (Reprinted by permission of Ref. 74. Copyright © 2012. The American chemical society.)

In 2015, Zhang *et al.* reported formation of ultrathin 2D MOF nanosheets with thickness of sub-10 nm via a surfactant-assisted synthetic method (Figure 8). The presence of surfactant molecules restricts the growth of the MOF structure in two dimensions. The obtained 2D MOF sheet consists of tetrakis(4-carboxyphenyl)porphyrin ligands linked to four zinc paddle-wheel nodes, *i.e.* $Zn_2(COO)_4$. The synthetic process of the porphyrin-based MOF comprises metalation of the tetrakis(4-carboxyphenyl)porphyrin ligand by Zn^{2+} ions. It was investigated that the MOF sheets are stacked in an AB packing pattern such that the zinc atoms in the centers of porphyrin rings in the layer A are aligned with the zinc atoms in the paddle-wheel metal nodes of the layer B .[75]

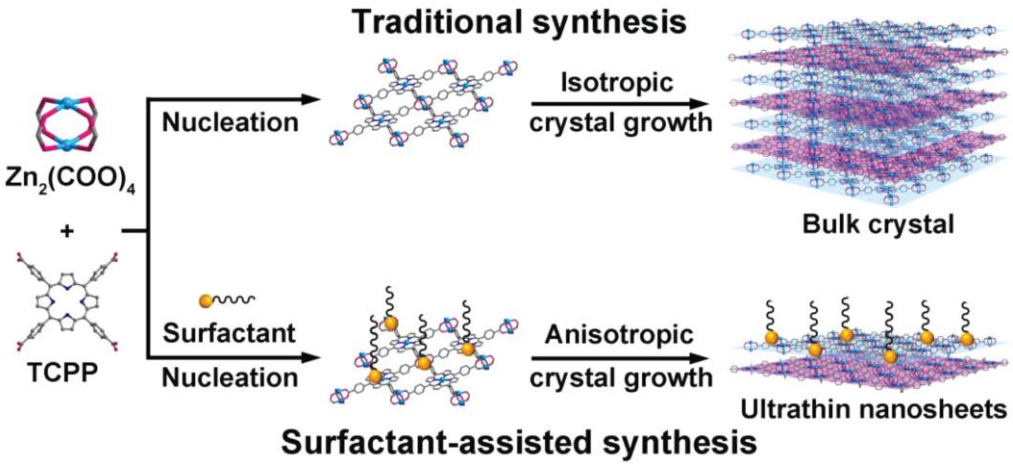

Figure 8: Top: it shows the traditional synthetic method of 2D MOFs with the isotropic growth that forms bulk crystals of MOFs. Bottom: it illustrates the surfactant-assisted fabrication technique that results in formation of a MOF thin film by confining the crystal growth in two dimensions. The selective attachment of surfactant molecules on the surface of MOFs controls their anisotropic growth in two dimensions. (Reprinted from Ref. 75. Copyright © 2015. John Wiley and Sons.)

A semiconducting 2D MOF of planar nickel bis(dithiolene) building components, with a thickness of several micrometers, was synthesized by Nishihara *et al.* (Figure 9). The 2D thiolene-based regulated coordination network was fabricated at the liquid-liquid interface. In this technique, benzenehexathiol and nickel(II) acetate were used as multichalating ligands and node centers, respectively. Using powder *X*-ray diffraction analysis, the crystallinity of the resulted bulk MOFs was investigated. An ordered single-layer nanosheet of the thiolene-based 2D MOF was synthesized by using a gas-liquid interfacial reaction. Atomic force microscopy (AFM) and scanning tunneling microscopy (STM) analysis showed that the π-conjugated coordination nanosheet is a monolayer with a thickness of ~0.6 nm.[76]

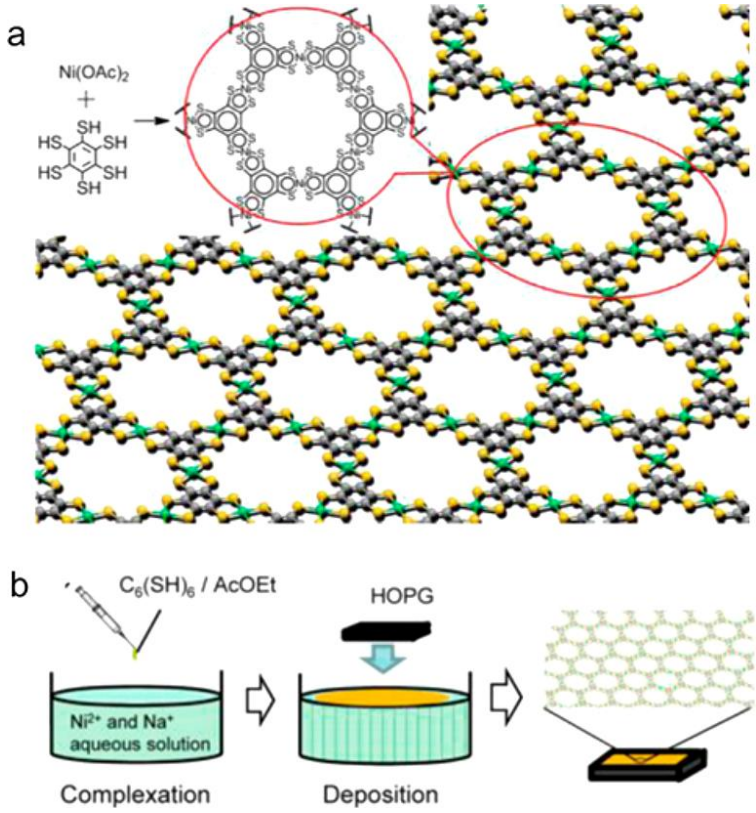

Figure 9: (a) Chemical structure and a drawing of nickel bis(dithiolene) coordination nanosheet fabricated via the interfacial reaction. (b) An illustration of the synthetic route to the 2D thiolene-based monolayer at the gas-liquid interface. (Reprinted with permission from Ref 76. Copyright © 2013. The American chemical society.)

In another paper, Nishihara *et al.* synthesized a series of threefold symmetric terpyridine-based electrochromic metal complexes and their corresponding nanosheets. It was shown that the coordination nanosheets with Fe^{2+} or Co^{2+} ions are functional and porous with several hundreds of nanometers thickness (Figure 10). The liquid-liquid interfacial synthesis, including solutions of the organic ligands and the aqueous metal ions, was used to fabricate multilayered nanosheets. The MOF multilayers were transferred on an indium tin oxide electrode and a reversible and robust redox reaction of the nanosheet was observed. In addition, it was shown that the redux reaction of the transferred nanosheet on the tin oxide electrode is accompanied by a distinctive color change, *i.e.* electrochromic response.[77]

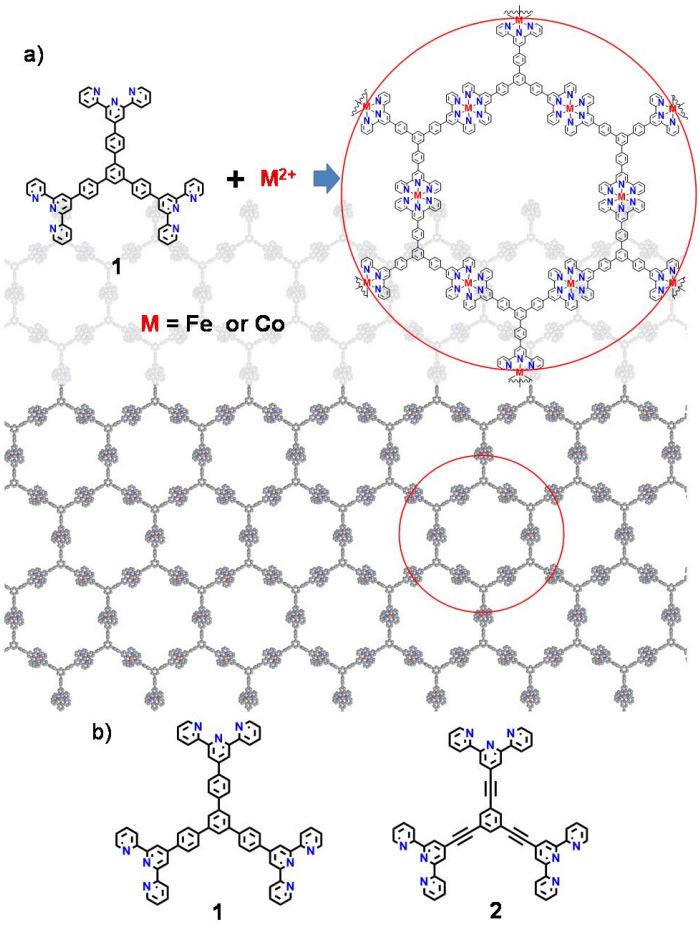

Figure 10: (a) Chemical structure of terpyridine-based coordination nanosheets of **1-Fe** and **1-Co**. (b) Chemical structures of terpyridine-based ligands *i.e.* **1** and **2**. (Reprinted with permission from Ref. 77. Copyright © 2015. The American chemical society.)

The same group published a report on fabrication of polymeric multilayered sheets of photoactive bis(dipyrrinato)zinc(II) complex at the liquid-liquid interface (Figure 11). At the air-liquid interface, a single-layer or few-layers of 2D MOF with domain sizes of more than 10 µm were fabricated. The obtained organic networks were successfully transferred on various solid substrates by the Langmuir-Schaefer (LS) technique. Transmission electron microscopy (TEM) investigations verified that the transferred organic network is crystalline with an hexagonal structure. In this research photofunctionality of bis(dipyrrinato)zinc(II) complex was led to fabrication of the first photofunctional bottom-up nanosheet. Thickness of the pyrrinato-based MOF nanosheet was measured to be in a range of 6 to 800 nm that is tunable by changing the concentration of the dipyrrin ligands. *X*-ray photoelectron spectroscopy (XPS) revealed uncoordinated dipyrrin moieties in the structure obtained via solution-based reaction. This result rules out the possibility to form the 2D MOF in the single-phase reaction and thus a confined platform for the interfacial synthesis is a need.[78]

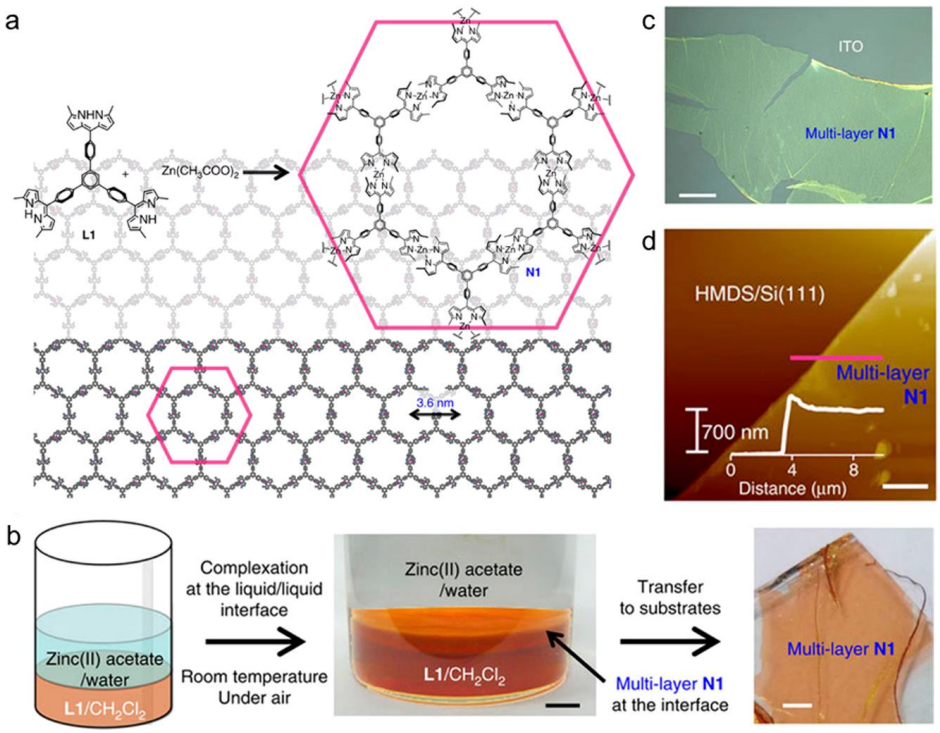

Figure 11: (a) Chemical structures of dipyrrin ligand molecule and the bis(dipyrrinato)zinc(II) complex framework. (b) Schematic illustration and photographs of the liquid-liquid interfacial synthesis and multilayers transferred from the interface onto a solid substrate. Scale bars represent 5 and 1 mm, respectively. (c) Photograph of the multilayers MOF transferred from the interface onto a substrate. Scale bar represents 20 μm. (d) AFM height analysis shows the profile line measuring the layer thickness. Scale bar shows 20 μm. (Reprinted by permission from Macmillan publishers Ltd.: Nat. Commun. Ref 78, copyright 2015.)

Marinescu *et al.* have reported the synthesis of long-range ordered Co-benzenehexathiol and Co-triphenylenehexathiol MOFs, with 2D hexagonal structures (Figure 12). The fabricated 2D thiolate-based MOF at the liquid-liquid interface showed high charge carrier mobility, low resistivity and temperature-dependent charge transport properties. Therefore, 2D thiol-based MOFs have potential applications in electronic devices.[79] It was shown that 2D MOFs consisting cobalt dithiolene building units are efficient molecular catalysts for the hydrogen evolution reaction with a high catalyst loadings and stability under acidic aqueous solutions.[80] Additionally, it is confirmed that the cobalt-dithiolene based MOF exhibits a transition behavior from a semiconducting to a metallic phase with decreasing temperature. This behavior is dependent on the film thickness and the amount of solvent molecules trapped in the pores.[79]

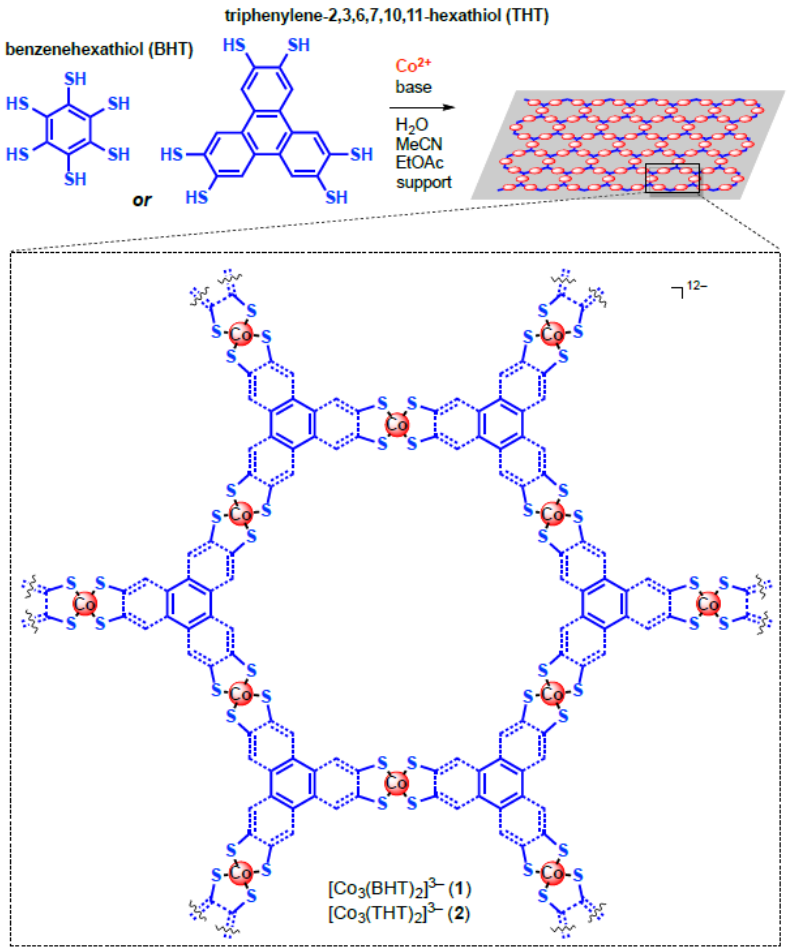

Figure 12: chemical structures and the synthetic procedure of 2D cobalt dithiolen-based MOF. The produced MOF can be transferred from the interface onto various solid substrates in order to be used in different applications. (Reprinted from Ref. 79. Copyright © 2014. The American chemical society.)

2D supramolecular-organic frameworks – This category of 2D materials are monolayers of organic building components held together via non-covalent interactions.[13] It has been shown that 2D SOFs have potentials to be used in self-healing, optoelectronics and environmental fields.[2] Despite many reports on the synthesis of 2D SOFs on solid surfaces,[81] fabrication of stable free-standing 2D SOFs still is a challenge. Free-standing monolayers of 2D SOFs suffer the lack of stability to persist their structures after removal the carrier materials. In order to fabricate stable 2D SOFs, complexation bonds or interactions between the building components and nodes have been widely utilized.

Recently, Stevens *et al.* reported the thermodynamically controlled growth of solution-based free-standing Janus nanosheets of peptide-based bolaamphiphiles (Figure 13).[82] The self-assembly of peptide β-strands and hydrocarbon chains formed a 2D supramolecular structure. Adjusting the intermolecular forces, especially between the aromatic groups, lead to a controlled transition from 2D morphologies to 1D structures. These peptide monolayer sheets were used as substrates for the engineering of guest components such as proteins, nanoparticles, quantum dots and gold nanorods.[82]

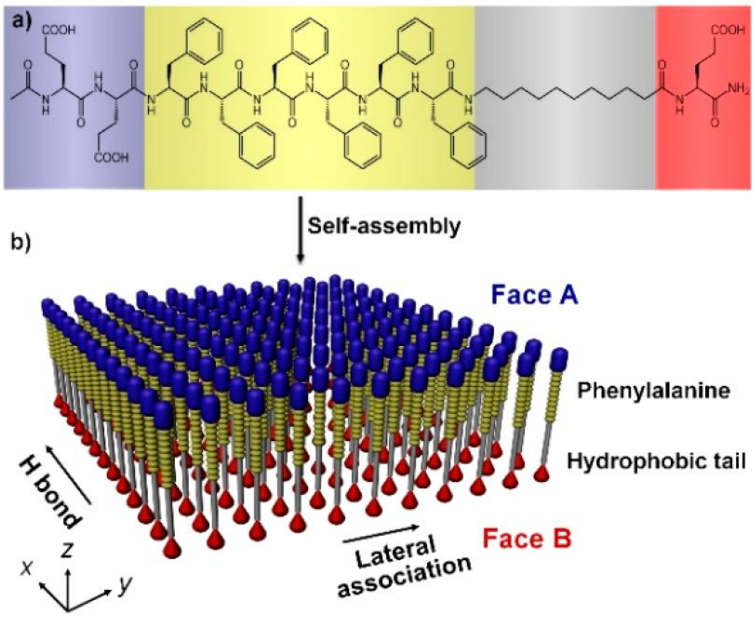

Figure 13: (a) Chemical structure of the peptide-based bolaamphiphile molecules. (b) Schematic of Janus self-assembled nanosheets of peptide bolaamphiphiles upon self-sorting the phenylalanine (blue) and hydrocarbon tails (red). (Reprinted with permission from Ref. 82. Copyright © 2017. The American chemical society.)

In 2013 Li *et al.* synthesized a 2D SOF of triphenylbenzene compound carrying bipyridin units on the peripheral benzene rings upon interaction with cucurbit[8]uril (CB[8]) in water (Figure 14). It is one of the first solution-based self-assembly processes for the fabrication of 2D SOF. The obtained 2D material is stabilized through strong complexation of CB[8] with two bipyridin units of the neighboring molecules forming a monolayer with a thickness of 1.75 nm. The fabricated 2D SOF is a supramolecular polymer, stabilized via non-covalent interactions, which exhibits periodic structural ordering similar to 2D MOFs and COFs.[83]

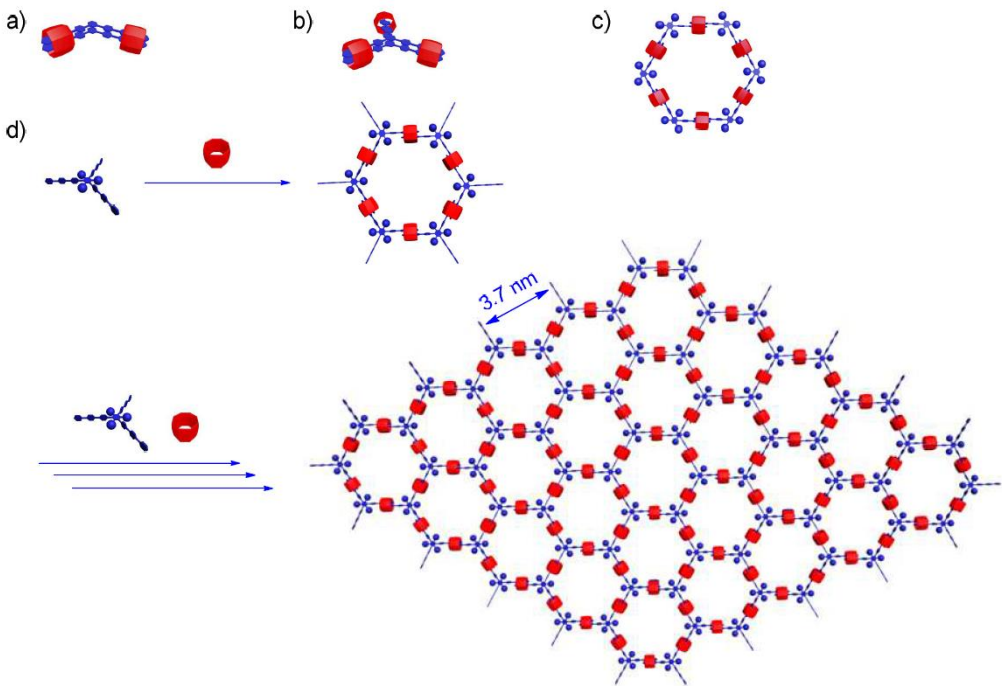

Figure 14: An illustration scheme of the self-assembly process of different bipyridin-based building blocks with CB[8] in water via varying the stoichiometry of reagents. (a) [2+2] complex formation. (b) [2+3] complex synthesis. (c) [6+6] complex formed and (d) fabrication of a 2D honeycomb SOF upon [6+6] complexation reaction. (Reprinted with permission from Ref. 83. Copyright © 2013. The American chemical society.)

Li *et al.* developed a facile and rapid one-pot method to produce free-standing monolayers of organic nanosheets by complexation of CB[8] with small organic molecules such as quinoline (Figure 15).[84] It was observed that the resulting sheets have a well-defined regular square structure, tunable lateral size and a uniform thickness of 1.8 nm. Remarkably, these non-covalent free-standing assemblies reveal sufficient stability for spectroscopic and microscopic characterizations. Indeed, it is shown that CB[8] macrocycle can be used as organic building blocks besides its traditional role as a host. [84]

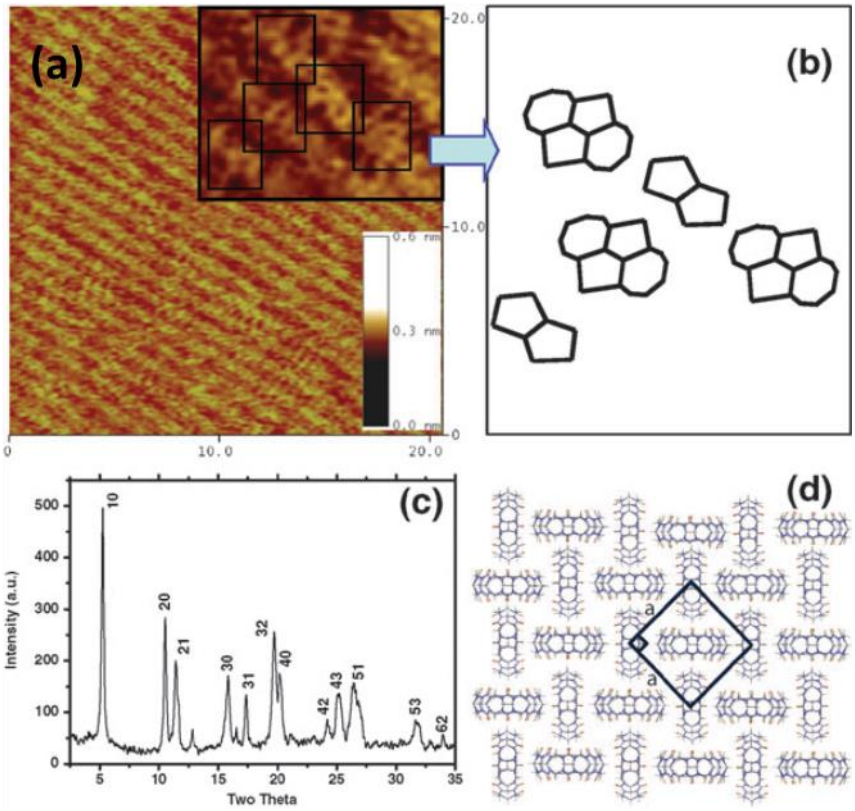

Figure 15: (a) STM image and (b) suggested molecular arrangements of the CB[8] organic building units in the 2D SOF that is recognized from inset in (a). (c) Powder *X*-ray diffraction (XRD) pattern of the complexed CB[8]-quinoline nanosheets. (d) The tentative molecular packing structure of the CB[8]-based nanosheet with a square lattice unit cell. (Reprinted with permission from Ref. 84. Copyright © 2010. The royal society of chemistry.)

In this context, Feng *et al.* fabricated molecularly precise monolayers of 2D SOF with partial internal order. Herein the dynamic self-assembly via a host–guest enhanced donor–acceptor interaction in the cavity of CB[8] macrocycles was used (Figure 16).[85] In this reaction tris(methoxynaphthyl)-substituted truxene spacer (Np-Trx) and naphthalene diimide substituted with N-methyl viologenyl moieties (MV-NDI) were used as donor and acceptor monomers, respectively. The building units self-assemble into a large-area, up to 0.25 cm^2, of an insoluble monolayer with a thickness of 1.8 nm at the liquid-liquid interface. The obtained network features the capability of covering holes of 10 μm^2 as a free-standing layer. In this strategy the planarity of building components was sustained by stacking the guest face inside the cavity of the CB[8] macrocycles in order to suppress the out-of-plane polymerization.[85]

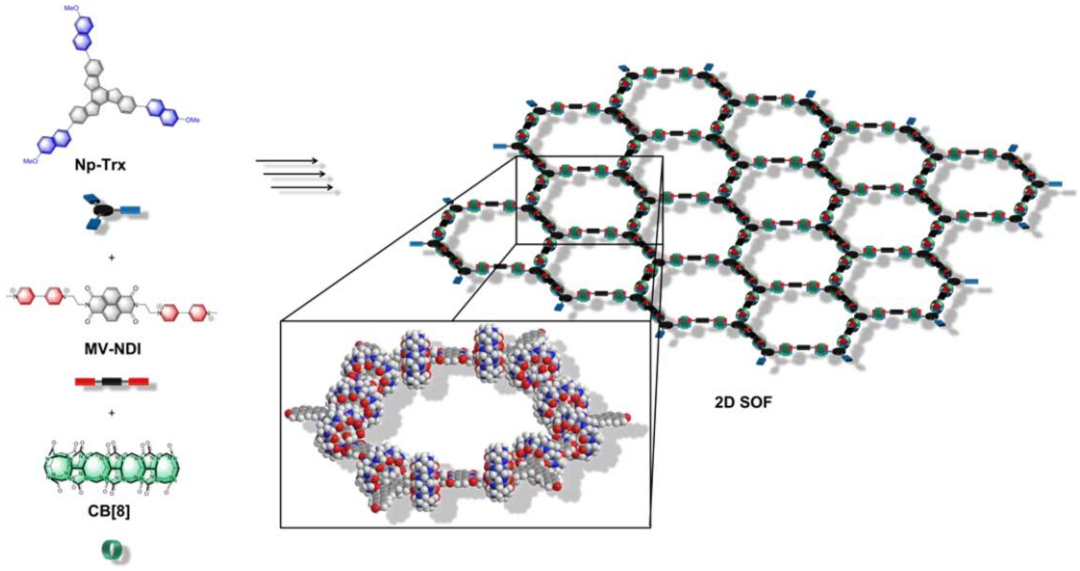

Figure 16: Chemical structures and schematic representations of Np-Trx, MV-NDI, CB[8] molecules and the formed 2D SOF with hexagonal superstructure. The inset shows a tentative molecular model of the 2D structure of CB[8]-based organic network. (Reprinted with permission from Ref. 85. Copyright © 2015. The American chemical society.)

The same group demonstrated the production of triphenylene-fused nickel bis(dithiolene) coordination polymer at the air-water interface (Figure 17). The coordinated polymer can be transferred onto solid substrates as a large area monolayer (mm^2) with a thickness of 0.7 – 0.9 nm. Furthermore, it was proved that the thiolene-based coordination polymer is free-standing and it spans holes with a side length of 18 µm. The high degree of complexation between the Ni ions and the thiol groups plays a key role in the coupling reaction of the triphenylenehexathiol (THT) monomers. It was shown that the transferred nickel bis(dithiolene) coordinated polymer sheets onto electrode surfaces exhibit outstanding electrocatalytic performance for hydrogen generation from water and energy technologies.[86]

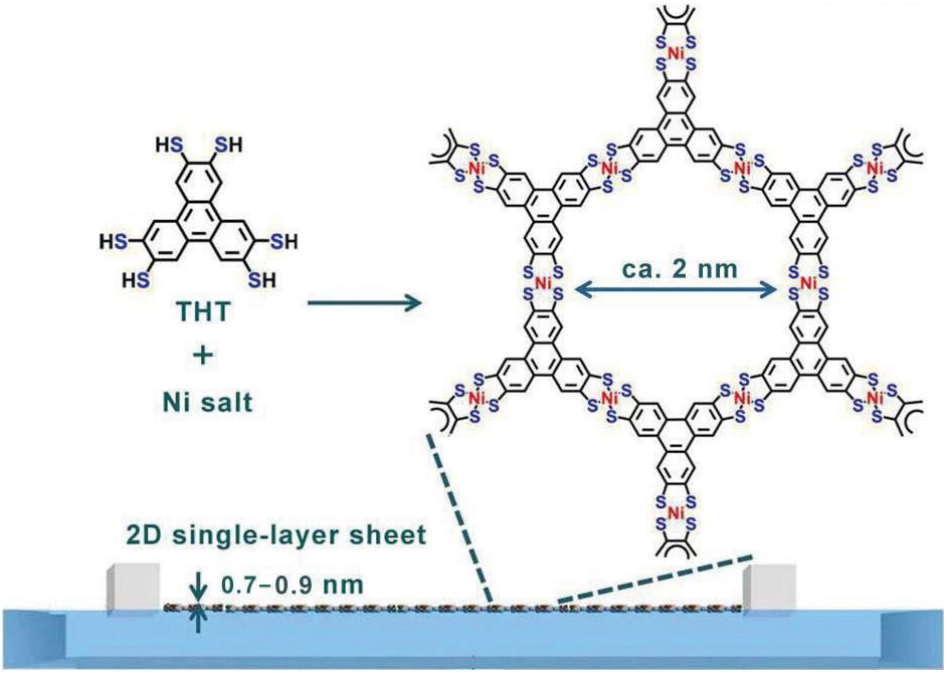

Figure 17: An illustration of the fabrication method of the 2D single-layer supramolecular polymer sheet of triphenylene-fused nickel bis(dithiolene) complexes via the interfacial synthesis technique at the air-water interface. (Reprinted with permission from Ref. 86. Copyright © 2015. John Wiley and Sons.)

Thayumanavan *et al.* developed a bottom-up method to produce smart organic 2D crystalline thin films of bolaamphiphile complexes made of two identical units linked through a biphenyl moiety, in aqueous media (Figure 18).[87] Each unit comprised an ionic headgroup, a urea chemical group and a hydrophobic domain. This strategy is based on exploiting the multiple and synergistic supramolecular interactions including π–π interactions, hydrogen bonds, hydrophobic effect and electrostatic repulsion forces. The thin films produced via this method have mono- or few-layers thickness. It was additionally shown that these structures can be programmed to disassemble upon introduction with a specific protein such that they can release their noncovalently bound guest molecules.[87]

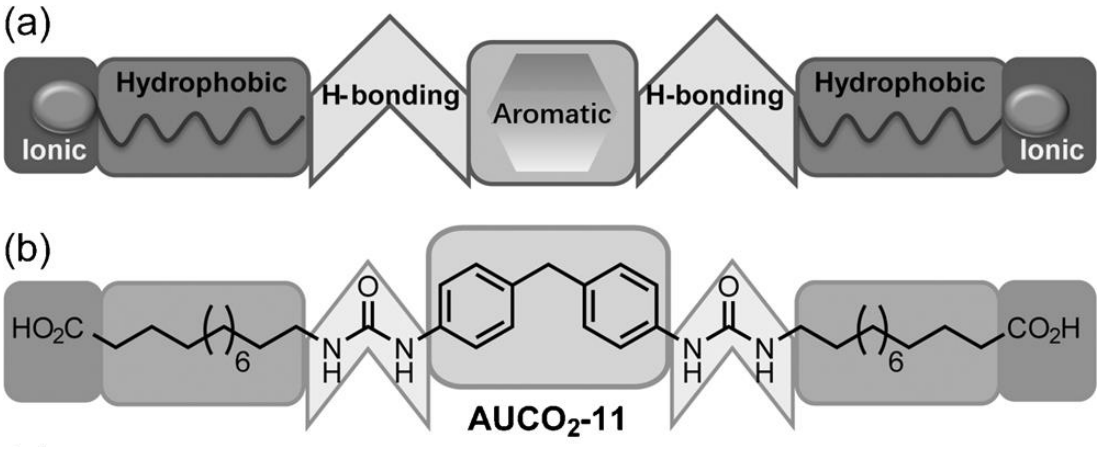

Figure 18: (a) A schematic of the molecular design strategy for fabrication of organic 2D materials using four supramolecular interactions. (b) A representative drawing of a 2D self-assembled structure in an aqueous phase. (Reprinted with permission from Ref. 87. Copyright © 2016. John Wiley and Sons.)

2D polymers **–** Two-dimensional polymers are free-standing monolayers of covalently bonded monomers with well-defined in-plane periodicity.[88] The first reported interfacial polymerization, at the air-water interface, was on elaeostearin and maleic anhydride which goes back to 1935.[89] In 2012 Schlüter *at al.* synthesized a nanometer thick polymer with internal periodicity via exfoliation of anthracene-based lamellar polymer single crystal (Figure 19).[90]

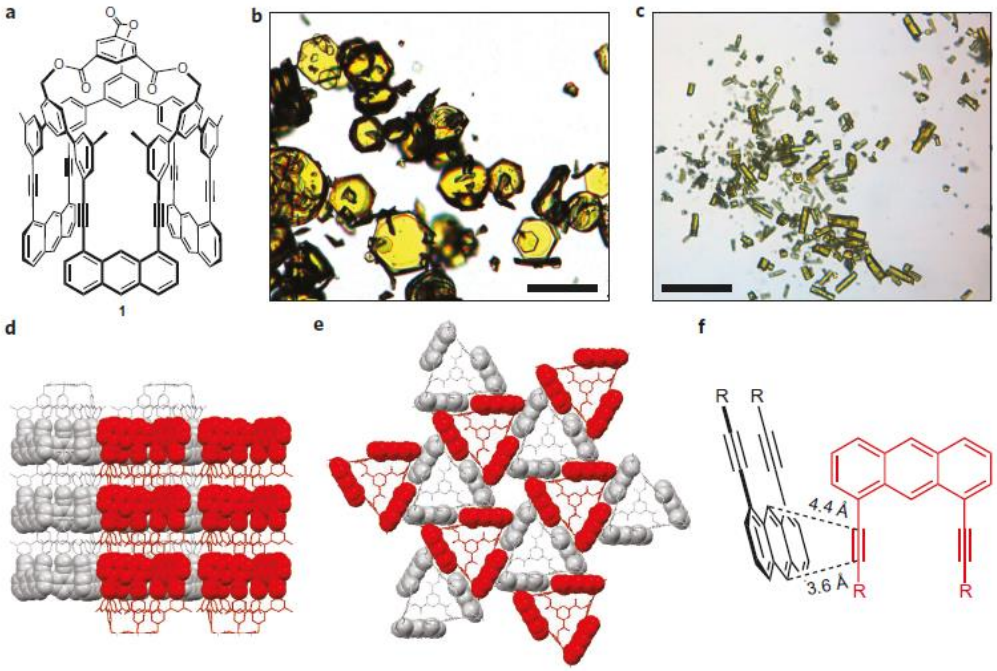

Figure 19: (a) Chemical structure of the anthracene-based monomer. (b & c) Optical microscopy images of the polymer single crystals as plates and rods, respectively. Scale bars represent 100 mm (d) XRD analysis of the laminar crystal structure of the polymer. In the polymer structure, the monomers oriented up and down that are

shown here in red and grey, respectively. (e) Top view of the hexagonally packed monomers in each layer. (f) The distances of the arene rings from the alkynes in each unit cell of the polymer. (Reprinted with permission from Ref. 90. Copyright © 2012. Springer Nature.)

Schlüter *et al.* have published several papers on polymerization of organic building monomers via photoirradiation at the air-water interface using the LB technique.[91,92]
In a collaboration with Prof. Schlüter group we demonstrated a major advance in the field of 2D polymers by introducing the tip-enhanced Raman spectroscopy (TERS) technique to estimate the crystallinity of 2D polymers (Figure 20).[93]

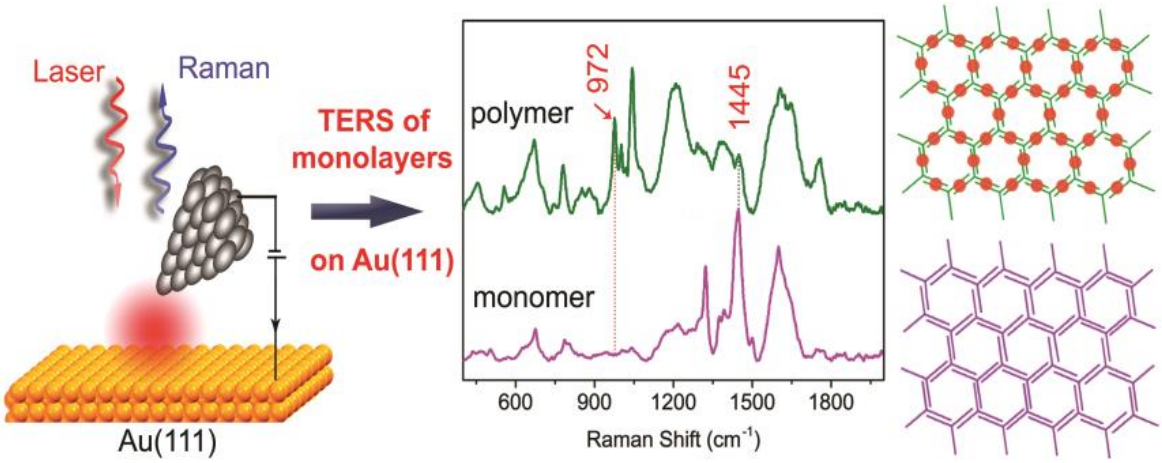

Figure 20: A graphical abstract of the TERS analysis on the polymer monolayer made of partially fluorinated anthracene monomers. This technique can be applied in order to characterize the structure of synthesized polymers and their crystallinity. (Reprinted with permission from Ref. 93. Copyright © 2017. John Wiley and Sons.)

In this work, we described 2D polymerization of partially fluorinated anthracene monomers, functionalized with a carboxylic acid group at one of the bridgehead atoms, at the air-water interface (Figure 21). It is, for the first time, a direct spectroscopic evidence for the kind of crosslinks formed and for the conversion reached in a covalently bonded monolayer sheet. Combination of different characterization analysis on the polymer sheets, before and after transfer from the interface onto solid substrates, confirmed the possibility to estimate the layers crystallinity and the location of regions with defects.[93]

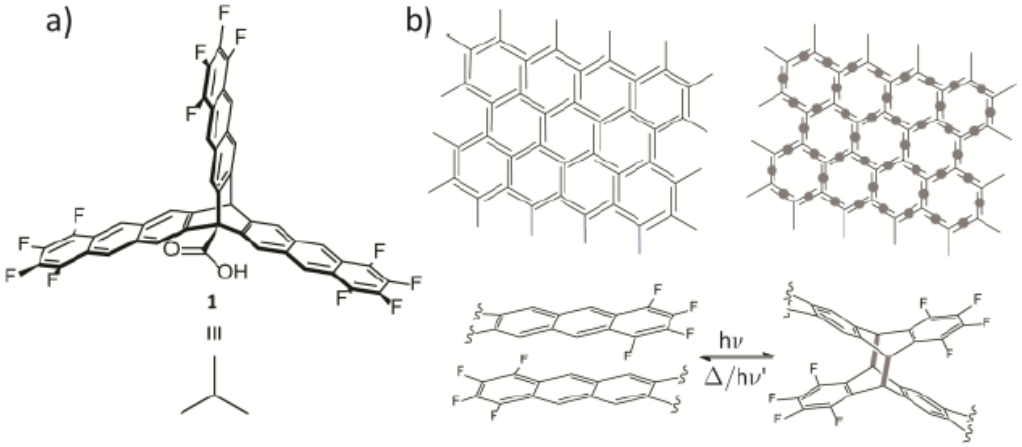

Figure 21: (a) Chemical structure of the C_3-symmetric monomer of anthracene with three partially fluorinated units. (b) Top image shows packing model for the anthracene-based monomers in a monolayer at the air-water interface. Below image represents the 2D photochemically dimerized polymer of anthracene monomer derivatives. The dimerization reaction is triggered by photoirradiation and can be reversed by irradiation at shorter wavelength or by thermal treatment. (Reprinted with permission from Ref. 93. Copyright © 2017. John Wiley and Sons.)

In another collaboration with Prof. Schlüter we reported polymerization of partially fluorinated anthracene-substituted monomers into a 2D ordered monolayer by photoirradiation at the air-water interface. Crystallinity of the polymer layer was studied by Brewster angle microscopy (BAM) directly at the air-water interface. The transferred layer of the polymer from the interface onto solid substrate, *i.e.* highly oriented pyrolytic graphite (HOPG), is analyzed by STM and non-contact AFM measurements (Figure 22). Molecular resolution AFM images of the polymerized anthracene-based monomers were achieved and a long-range ordered monolayer, in an area of 300 × 300 nm with a monodisperse pore size, was shown (Figure 23). Both STM and AFM methods confirm formation of the well-ordered polymer network with unit lattice parameters in a good agreement with an *X*-ray diffractometry structural model of a similar material.[94]

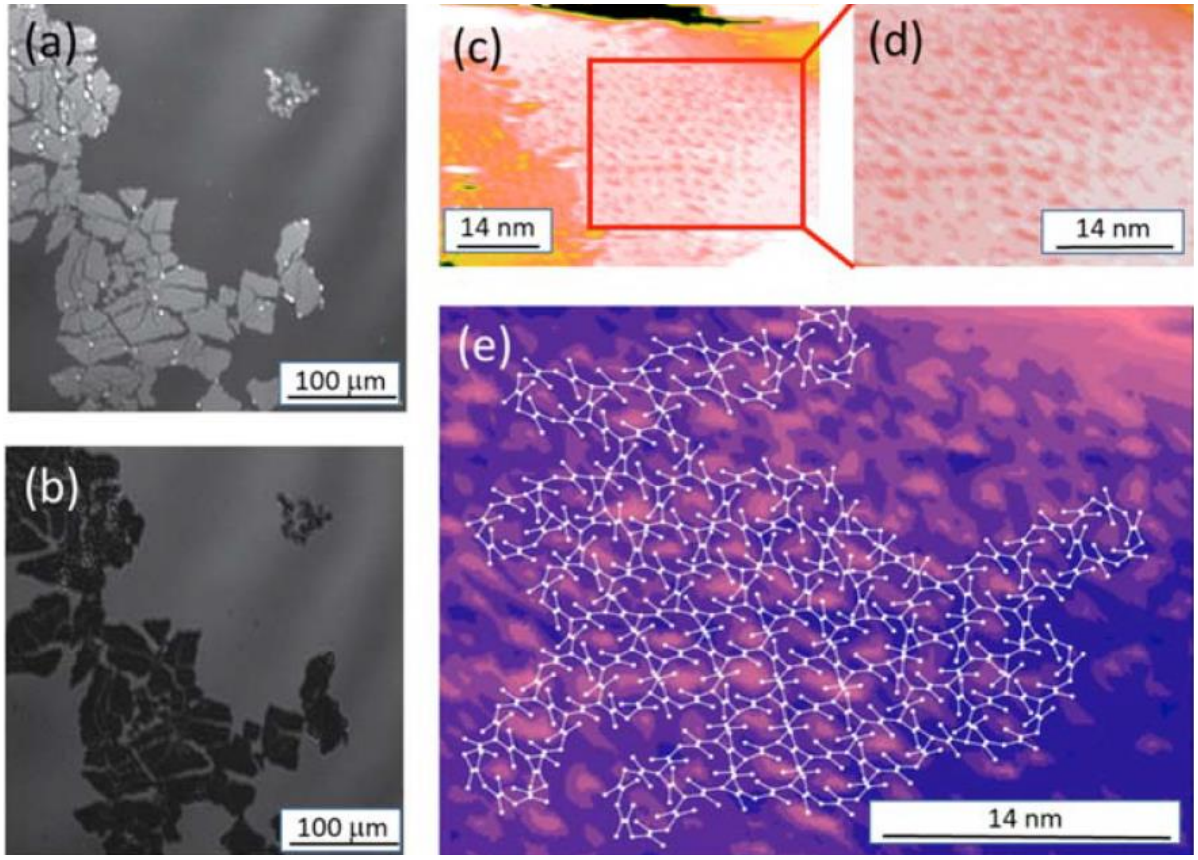

Figure 22: (a & b) BAM and (c - e) STM images of the obtained photoirradiated polymer at the air-water interface and on HOPG, respectively. A change of the polarizer angle from (a) +2° to (b) -2° shows a homogeneous contrast change in the BAM images of the polymerized islands, indicating their crystallinity. (c) The STM image shows a distorted porous film whose pores are partly obscured and partly expanded. (d) A zoomed STM image shows the area of the film with monodisperse pores. (e) It is a polymer model fitted on the STM image in (c). (Taken with permission from Ref. 94. Copyright © 2018. John Wiley and Sons.)

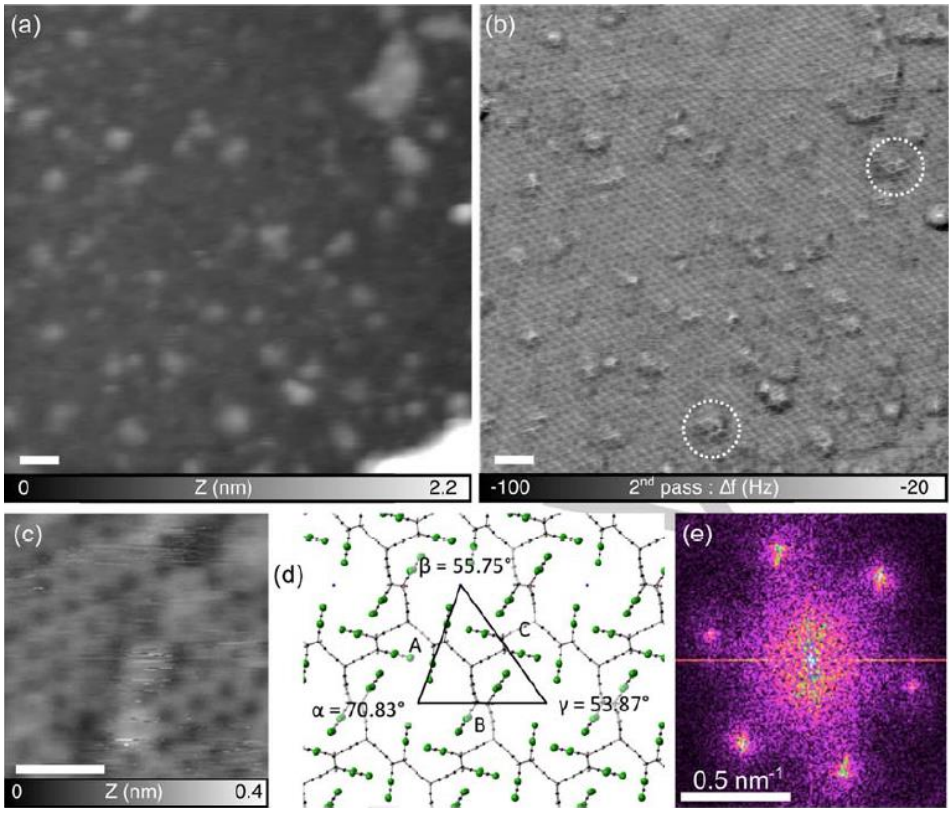

Figure 23: (a - c). Non-contact AFM images of the long-range ordered 2D polymer transferred from the interface onto a HOPG. (d) Single crystal XRD pattern that shows the molecular model of a structure that is closely related to the 2D polymer formed at the interface (A: 1.76 nm; B: 1.80 nm; C: 2.05 nm). (e) The FFT analysis of the AFM image shown in (b). Scale bars of the images are 10 nm. (Taken with permission from Ref. 94. Copyright © 2018. John Wiley and Sons.)

2D covalent organic frameworks – Two-dimensional COFs are a category of crystalline porous polymers consisting atomically precise integration of organic units into ordered structures by using strong covalent bonds. Yaghi *et al.* reported the first example of a layer-stacked crystalline 2D COF of benzene rings and boroxine linkers in 2005 by condensation reactions, named COF-1 and COF-5 (Figure 24).[95]

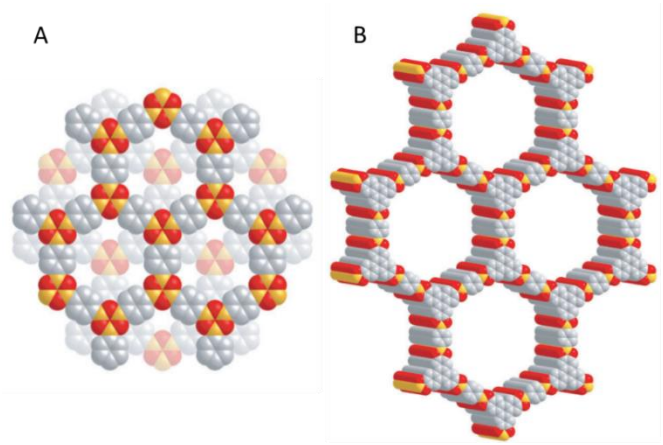

Figure 24: Molecular representations of (A) COF-1 with staggered and (B) COF-5 with eclipsed configuration obtained from XRD analysis and modeling. Carbon, boron, and oxygen are represented as gray, orange and red spheres, respectively and H atoms are omitted. (Reprinted from Ref. 95, copyright © 2005. The American association for the advancement of science.)

Since then plenty of COF structures with different organic building units and likers have been synthesized. For example, in 2011 Dichtel *et al.* used single layer of graphene as a solid substrate to grow a 2D COF of hexahydroxytriphenylene and boronic acid building units through solvothermal condensation reaction (Figure 25). It was shown that the 2D COFs with ordered structures via π-electron systems are ideal candidates for exciton and charge transport. Additionally, they exhibit permanent porosity that is available for subsequent functionalization.[96]

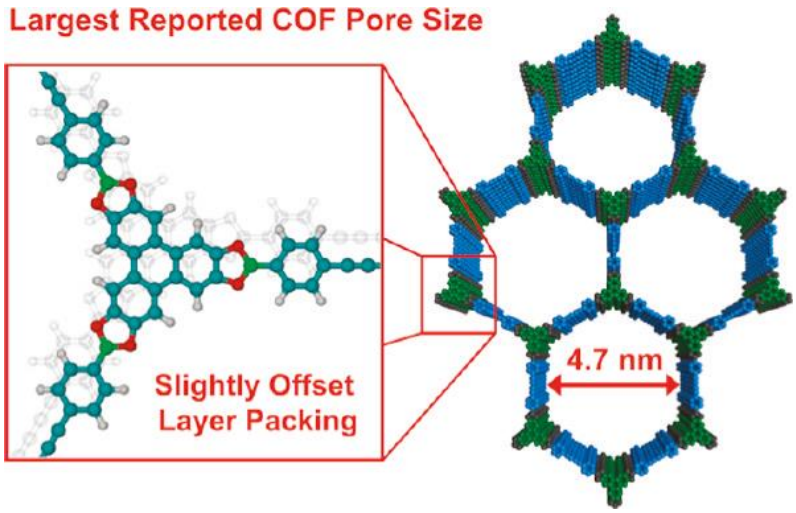

Figure 25: A schematic illustration of the 2D COF synthesized by condensation reaction of hexahydroxytriphenylene and boronic acid with the large pore size of 4.7 nm. (Reprinted from the Ref. 96. Copyright © 2011. The American chemical society.)

As it has been shortly highlighted here, in the past decade the interfacial self-assembly reactions are widely used as the versatile techniques to synthesize 2D organic networks. Among all the interfacial fabrication methods at the air-liquid, liquid-liquid, solid-liquid and gas-solid interfaces, the LB technique is one of the most studied routes for the formation of 2D organic networks of amphiphilic building blocks.

Calix[4]arene Langmuir monolayers – Calixarene amphiphilic macrocycles, in the cone conformation, have been extensively used as promising building blocks for the formation of the Langmuir and the LB mono- and multilayers at the air-water interface. In this field, Shahgaldian *et al.* reported quite large number of self-assembled Langmuir layers based on calixarene amphiphilic macrocycles.[51]

As an example it is demonstrated that *p*-carboxycalix[4]arene derivatives, functionalized with C_{12} alkyl chains at the lower rim, form a very stable monolayer at the interface. It was confirmed that the self-assembly of *p*-carboxycalix[4]arene derivatives at the interface is mainly derived by van der Waals interactions between the aliphatic chains. The interactions of Langmuir monolayers of the *p*-carboxycalix[4]arene derivatives and divalent cations were also studied. It was reported that the self-assembly properties of the calix[4]arenes Langmuir layers are remarkably affected by the presence of Cu^{2+} ions compared to the other cations available in the subphase (Figure 26).[97]

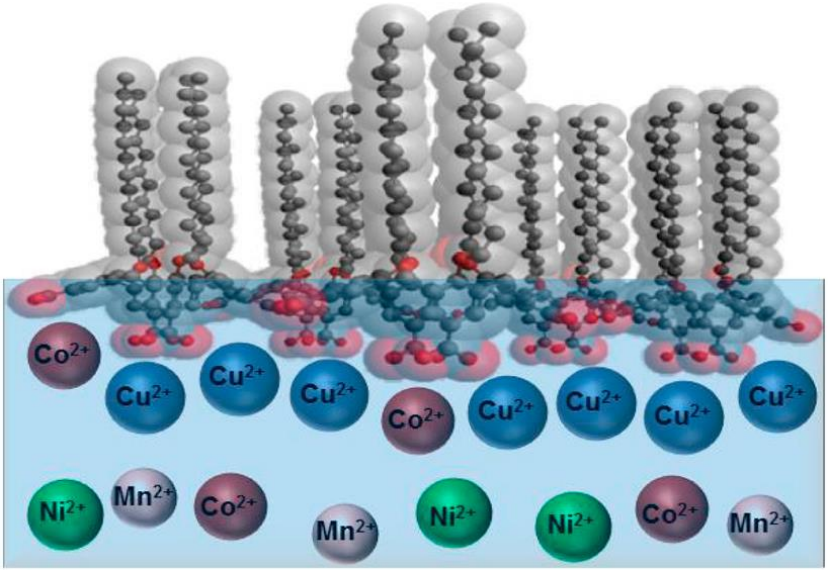

Figure 26: A drawing of the self-assembled *p*-carboxycalix[4]arene-based Langmuir monolayer upon binding to divalent cations. (Reprinted from the Ref. 97. Copyright © 2015. The American chemical society.)

The Langmuir monolayer of the *p*-carboxycalix[4]arene amphiphiles was used as a template for nucleation and growth of different crystalline polymorphic forms of pharmaceutical ingredients by Shahgaldian *et al.* It was shown that the self-assembled monolayer of the calix[4]arene derivative amphiphiles with different packing densities can trigger the crystallization of two polymorphic forms of gabapentin (GBP) (Figure 27).[98]

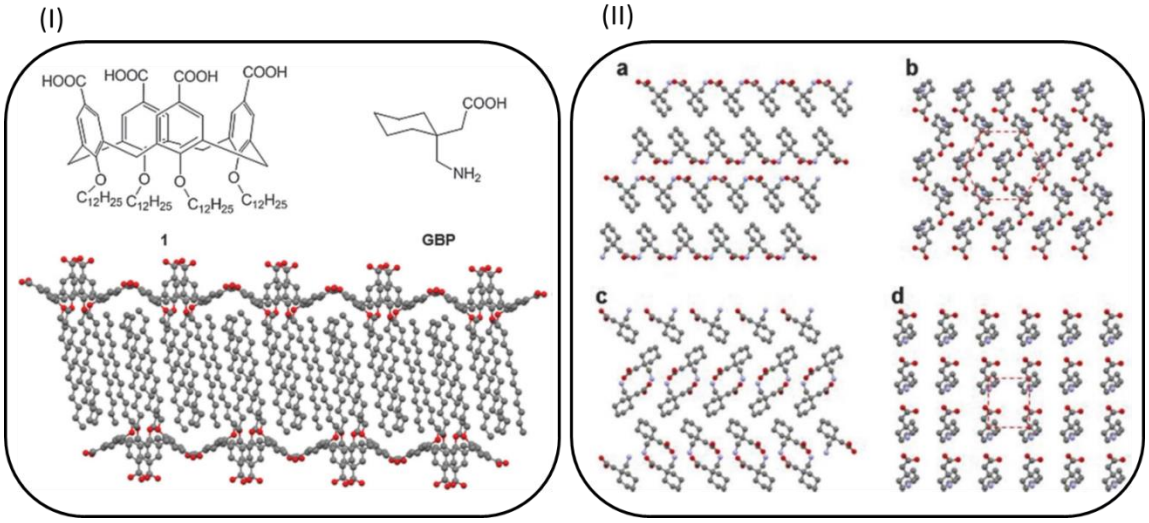

Figure 27: (I) Top: the chemical structure of the calix[4]rene amphiphile and GBP molecule. Bottom: the arrangement of the amphiphilic calix[4]rene derivatives in a bilayer fashion. (II) Packing structures of GBP polymorphic forms (a & c) side view and (b & d) top view. (Reprinted from the Ref. 98. Copyright © 2014. The royal society of chemistry.)

Up to now, plenty reports exist on fabrication of 2D free-standing organic networks stabilized through formation of bonds/interactions between 2D organic building components and organic/inorganic linkers. Planar organic building blocks lay down at the interface/surface providing an easier control over the synthetic reaction and the crystal growth. Subsequently, characterization of the obtained networks is more straightforward. These are reasons that have encouraged scientists to choose 2D organic building units in order to fabricate extended organic networks. However, 2D organic synthons strongly limit the number of potential building blocks and the possibility of post-assembly functionalization.

It is well known that 3D rigid macrocycles have a key role in the synthesis of molecular receptors and they provide great possibilities for post-assembly functionalization. Therefore, the fabrication of stable free-standing and crystalline organic networks comprising 3D building components has a high demand for diverse applications.

The unique approach taken in this PhD project goes one step further to introduce an elegant strategy to mount 3D macrocycles, as organic building blocks, into thin networks through a well-ordered and controllable fashion. The method is based on the self-assembly of inherently 3D multivalent calix[4]arene amphiphiles via coordination bonds with metal ions and supramolecular interactions. This approach allowed us to fabricate first examples of tunable crystalline and free-standing calix[4]arene-based organic networks that can be used as sample supports in structural analysis of biomolecules and magnetic nanoparticles by TEM imaging technique.

OUTLINE

The research contributions to the field of 2D materials presented in this thesis are summarized in three chapters. The ultimate objective of the project was the production and characterization of free-standing and crystalline 2D organic networks of carefully functionalized calix[4]arene macrocycles.

Chapter 1 – The first example of a 2D crystalline metal-organic coordination network (MOCN) of calix[4]arene building blocks, *i.e.* C_3-*p*-carboxy-calix, through coordination bonds with Cu^{2+} ions is reported in the first chapter of this thesis. In order to produce an organic building block with high propensity to self-assemble through strong and directional bonds, we designed calix[4]arene synthons with short propyl chains at the lower rim. Calix[4]arenes functionalized with these short chains still exhibited amphiphilic character, but the presence of the short chains reduced the influence of non-directional van der Waals interactions between the chains during the self-assembly process. Therefore, the directional π-π interactions between the arene rings of calix[4]arenes and coordination bonds between the deprotonated carboxy groups and Cu^{2+} ions drove the self-assembly process and led to the formation of a 2D coordination network.

Brewster angle microscopy (BAM) analysis of the 2D layers formed at the air-water interface revealed various crystalline domains, in which the contrast of the domains was dependent on the orientation of the calix[4]arene molecules within larger self-assembled monolayers. These ordered domains can be attributed to the anisotropic 2D packing of the amphiphiles. We unambiguously demonstrated that the presence of copper ions in the aqueous phase triggered rearrangement of the molecules in the 2D monolayer and led to the formation of large and dendritic crystalline domains. The self-assembled layer can be successfully transferred from the interface onto solid substrates. In spite of the technical challenges related to the imaging of such delicate soft monolayers, high-resolution atomic force microscopy (AFM) images were obtained, and confirmed the crystallinity of the monolayers. Furthermore, the BAM investigation also confirmed that the transferred layer was comprised of crystalline domains with different orientations and stripe morphologies. *X*-ray photoelectron spectroscopy (XPS) analysis confirmed the formation of coordination bonds between the carboxy functional groups of the C_3-*p*-carboxy-calix molecules and Cu^{2+} ions. Based on the AFM and XPS results, we proposed a molecular model describing the structure of the 2D self-assembled MOCN of C_3-*p*-carboxy-calix building blocks and Cu^{2+} ions.[99]

Chapter 2 – Motivated by the insight gained from the coordination-bound calix[4]arenes, we turned our attention to the potential of relatively weak and moderately directional dipole-

dipole intermolecular interactions to stabilize 2D supramolecular organic networks (SONs). For this purpose we designed calix[4]arene synthons bearing methyl cyano functional groups at the upper rim and propyl chains at the lower rim, *i.e.* C_3-*p*-me-cyano-calix amphiphiles. The presence of a methylene bridge between the arene ring and CN group provides rotational freedom for the CN binding moieties to self-assemble in the most energetically favorable fashion.

Very much to our surprise, we found that the limited directionality of the comparably weak dipole-dipole interactions was sufficient to enable the C_3-*p*-me-cyano-calix molecules to assemble into a free-standing and crystalline 2D SON. BAM imaging confirmed the presence of a monocrystalline single layer of C_3-*p*-me-cyano-calix synthons covering the air-water interface. This 2D SON was sufficiently stable to be successfully transferred from the air-water interface onto a solid highly oriented pyrolytic graphite (HOPG) substrate. High molecular resolution AFM analysis of the transferred SON monolayer revealed a crystalline network composed of single C_3-*p*-me-cyano-calix units, with some building blocks missing, in a square packing fashion. Using near-edge *X*-ray absorption fine spectroscopy (NEXAFS), we calculated the angle of the CN functional groups with respect to the normal HOPG surface to be 57°. The molecular model generated using the AFM data and NEXAFS analysis revealed the 2D SON of C_3-*p*-me-cyano-calix amphiphiles is stabilized via dipole-dipole interactions.

The electron diffraction pattern for a free-standing layer of C_3-*p*-me-cyano-calix synthons revealed a square packing structure within the crystalline SON layer, in perfect agreement with the structure determined by AFM analysis. These data further showed that the layer is stable enough to maintain its structure even after removal of the HOPG carrier support.

To the best of our knowledge, this system represents the first example of a self-assembled free-standing monolayer produced in the absence of additional molecular or ionic linkers.[100]

Chapter 3 – The third chapter reports the fabrication of free-standing and crystalline monolayers and bilayers of C_3-*p*-me-carboxy-calix amphiphiles upon coordination with Ni^{2+} or Cu^{2+} divalent ions, respectively.

Building on our previous results, we observed that C_3-*p*-carboxy-calix molecules exhibit a lack of conformational flexibility to adopt different coordination geometries around the ionic centers, even when the ions were changed. This limitation is due to direct attachment of the carboxy functional group to the arene ring of the C_3-*p*-carboxy-calix amphiphile. In order to increase the flexibility of the amphiphile towards the binding moiety, we designed C_3-*p*-me-carboxy-calix, which contains a methylene bridge between the carboxy functional group and arene ring. The presence of the methylene bridge significantly enhances the possibility of conformational adaptation and increases the ability of the COOH-bearing substituents to form coordination bonds via different geometries.

Isotherm experiments and AFM analysis demonstrated that when coordinated with Cu^{2+} ions, the MOCNs monolayer of *C_3-p*-me-carboxy-calix synthons transformed to bilayers during the relaxation time, *i.e.* the time that the layer was kept under constant surface pressure. Changing the relaxation time confirmed that the degree of bilayer formation is kinetically controllable. By integrating the AFM and XPS analysis of bilayered MOCNs of *C_3-p*-me-carboxy-calix building components, we proposed a molecular model based on formation of $\{Cu_2(O_2CR)_4\}$ paddle-wheel coordination motifs. In contrast, *C_3-p*-me-carboxy-calix synthons coordinated Ni^{2+} ions via formation of an octahedral coordination motif of $\{NiO_6\}$. Bilayer and monolayer of the MOCNs of *C_3-p*-me-carboxy-calix amphiphiles exhibited high stability and can cover perforated solid substrates with pore sizes as large as 5 × 5 μm.[101]

Applications of calix[4]arene-based networks in the structural analysis of biomolecules – Having demonstrated that the 2D organic networks of calix[4]arene synthons are stable as free-standing layers, we used these layers as sample carriers to deposit and image single biomolecules/assemblies and nanoparticles by transmission electron microscopy (TEM).

In order to enable the structural analysis of biomolecules via electron diffraction techniques, the sample supports should be:

-highly transparent to *X*-rays/electron beams to ensure a sufficient signal-to-noise ratio,

-highly stable during sample deposition and data acquisition,

-able to withstand vacuum conditions, and be stable at both room temperature and under cryogenic conditions.

The free-standing 2D organic networks of calix[4]arene derivatives meet all of these prerequisites for sample supports, and also offer several other advantages:

-hydrophilicity of the organic network helps to maintain the structure of the biomolecules deposited on the layer,

-the structure and morphology of the networks at the interface can be fine-tuned by adjusting the preparation conditions, such as the concentration of ions (in the case of MOCNs), compression speed, pH and temperature,

-a diverse range of functional groups could be anchored to the calix[4]arene backbone in order to improve the affinity of the layers for biomolecules.

To evaluate the potential of calix[4]arene-based sample supports for TEM imaging, we assessed MOCNs of C_3-*p*-carboxy-calix and C_3-*p*-me-carboxy-calix synthons due to their high stability arising from the strong coordination bonds. We deposited viruses (granulovirus and tobacco mosaic virus), enzymes (catalase nanocrystals and urease solution), protein crystals and single iron nanoparticles on the free-standing MOCNs. TEM analysis confirmed that the free-standing MOCNs of calix[4]arenes could be successfully utilized as sample supports for imaging these molecules.

RESULTS

CHAPTER 1

Two-Dimensional Calix[4]arene-based Metal-Organic Coordination Networks of Tunable Crystallinity

Summary:

In this chapter, a strategy to modulate the in-plane arrangement of *25,26,27,28*-tetrapropoxycalix[4]arene-*5,11,17,23*-tetracarboxylic acid (C_3-*p*-carboxy-calix) building blocks into a crystalline metal-organic coordination network (MOCN) is reported. The crystalline organic network is assembled by interfacial coordination reaction of the amphiphilic C_3-*p*-carboxy-calix synthons and copper ionic connectors at the air-water interface via the versatile Langmuir-Blodgett technique. We have shown that the self-assembly process of C_3-*p*-carboxy-calix molecules and copper ions starts spontaneously after spreading the molecules at the air-water interface *i.e.* before compression. Brewster angle microscopy images confirmed the formation of a multicrystalline monolayer at the air-liquid interface. The layer retains its crystallinity while transferring from the interface onto a highly oriented pyrolytic graphite (HOPG). Atomic force microscopy analysis, on the transferred layer onto HOPG, revealed formation of the crystalline MOCN's stripes comprising three calixarene molecules coordinated with copper ions featuring corrugated/rippled topography. Crystallinity of the MOCN of C_3-*p*-carboxy-calix amphiphiles is tunable via controlling the layer architecture and preparation parameters.

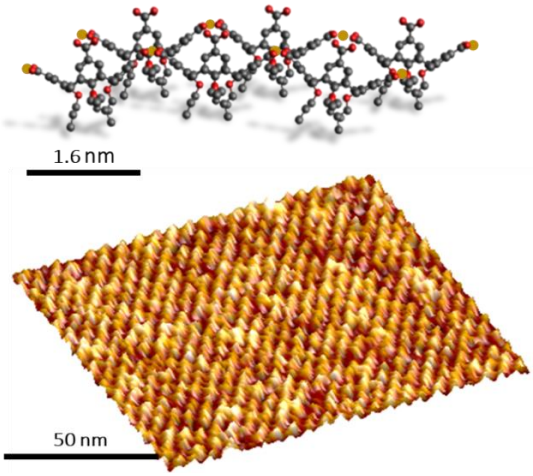

P.S. and T.A.J. conceived the research. M.M. and L.G.T. performed LB, BAM, LS, contact angle, ellipsometry, and AFM experiments and analyzed the data. M.M., J. N. and M.B. conducted XPS experiments and analyzed the data. L.G.T. and M.M. synthesized the molecule. M.M., T.A.J. and P.S. wrote the paper. All authors commented on the manuscript.

Coordination Networks

International Edition: DOI: 10.1002/anie.201703825
German Edition: DOI: 10.1002/ange.201703825

Two-Dimensional Calix[4]arene-based Metal–Organic Coordination Networks of Tunable Crystallinity

Mina Moradi[+], Ludovico G. Tulli[+], Jan Nowakowski, Milos Baljozovic, Thomas A. Jung, and Patrick Shahgaldian**

Abstract: *A flexible and versatile method to fabricate two-dimensional metal–organic coordination networks (MOCNs) by bottom-up self-assembly is described. 2D crystalline layers were formed at the air–water interface, coordinated by ions from the liquid phase, and transferred onto a solid substrate with their crystallinity preserved. By using an inherently three-dimensional amphiphile, namely 25,26,27,28-tetrapropoxycalix[4]arene-5,11,17,23-tetracarboxylic acid, and a copper metal node, large and monocrystalline dendritic MOCN domains were formed. The method described allows for the fabrication of monolayers of tunable crystallinity on liquid and solid substrates. It can be applied to a large range of differently functionalized organic building blocks, also beyond macrocycles, which can be interconnected by diverse metal nodes.*

The discovery of graphene and its unique physical properties combining outstanding mechanical, electronic, and thermal properties has triggered a resurgence of interest of researchers in the design of two-dimensional and highly ordered inorganic films with monoatomic/monomolecular height.[1] Highly organized two-dimensional materials can not only be fabricated from inorganic compounds but also from organic building blocks. For example, covalent organic frameworks (COFs) can be produced as two-dimensional, freestanding, and single-monomer-thick polymers.[2] Grill et al. demonstrated the possibility to produce precisely organized nanoarchitectures through covalent assembly of porphyrin derivatives on surfaces.[3] Lafferentz et al. reported on the design of sophisticated COFs by controlling on-surface polymerization of a porphyrin derivative by hierarchical and substrate-directed growth.[4] Finally, Baek et al. demonstrated that 2D COFs could also be produced without preorganization of the building blocks in a 2D confined space.[5]

Coordination bonds have also been used to link metal atoms to organic building blocks and produce metal–organic coordination networks (MOCNs), two-dimensional analogues of the widely studied metal–organic frameworks (MOFs).[6] This can be achieved on solid substrates as well as at solid–liquid interfaces. Makiura and Konovalov described the formation of two-dimensional MOCNs, generated by the interaction/reaction of metalloporphyrins with Cu^{2+} ions at the air–water interface.[7] The four carboxy groups introduced at the periphery of the porphyrin ring bind cations and drive the formation of two-dimensional crystalline domains. Bauer et al. fabricated freestanding two-dimensional polymers by self-assembly of a large dendrimeric hexakis(terpyridine) derivative at the air–water interface.[6a] This hexakis(terpyridine) assembly coordinates in a linear manner across the surface template, with the phenyl and terpyridine units aligned in out-of-plane direction due to steric constraints. The interfacial coordination reaction of this derivative with Fe^{2+} ions triggered the formation of well-organized assemblies of monomolecular thickness with a characteristic domain size of 500×500 μm. The groups of both Makiura and Schlüter relied on organic building blocks enabling planar ligation also containing out-of-plane components. This strongly limits the number of potential building blocks and the possibility of post-assembly functionalization. The approach taken in this study is more general in that building blocks functionalized with coordination ligands pointing in lower-symmetry directions are used, which are not predetermined to form planar architectures. These "3D" amphiphilic building blocks open up new possibilities for applications in the design of smart functional surfaces and in host–guest chemistry.

Herein the first example of a complex amphiphile, that is, a calix[4]arene derivative, as a representative of a 3D non-planar molecular building block to design MOCNs at the air–liquid interface using the versatile Langmuir balance method is presented. Calix[4]arenes have been widely exploited to design amphiphilic ligands able to self-assemble at the air–water interface as stable Langmuir monolayers.[8] However, amphiphiles based on calix[4]arenes with long alkyl chains have shown a fairly limited 2D crystallization behavior; this is possibly due to the disorder introduced by the thermal motion of these chains. For this reason, we decided to use amphiphiles with shorter chains. As chelating moieties we used carboxylic acid groups directly attached to the phenolic rings.

25,26,27,28-tetrapropoxycalix[4]arene-5,11,17,23-tetracarboxylic acid (**1**; Figure 1), locked in the cone conformation, was produced as previously described.[9] As metal node we used copper(II) because of the well-studied carboxylate–copper coordination.[10] The interfacial properties of **1** have

[*] M. Moradi,[+] Dr. L. G. Tulli,[+] Prof. Dr. P. Shahgaldian
School of Life Science, University of Applied Sciences and Arts Northwestern Switzerland
Gründenstrasse 40, 4132 Muttenz (Switzerland)
E-mail: patrick.shahgaldian@fhnw.ch
Dr. J. Nowakowski, M. Baljozovic, Prof. Dr. T. A. Jung
Laboratory for Micro- and Nanotechnology, Paul Scherrer Institute
5232 Villigen (Switzerland)
E-mail: thomas.jung@psi.ch
[+] These authors contributed equally to this work.

Supporting information and the ORCID identification number for an author of this article can be found under: https://doi.org/10.1002/anie.201703825.

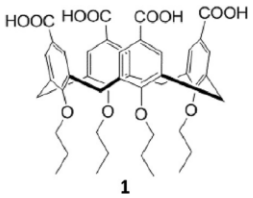

1

Figure 1. Molecular structure of **1**.

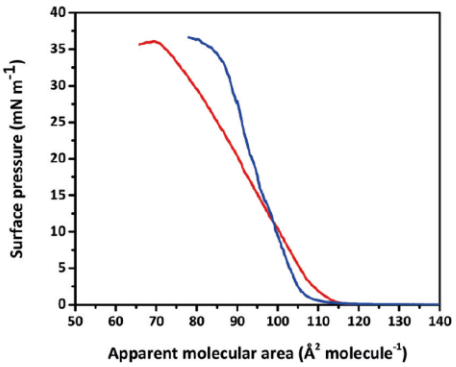

Figure 2. Surface-pressure–area-compression isotherms of **1** on pure water (blue) and on a 10 μM aqueous $CuCl_2$ solution (red). The isotherm is characteristically modified by the presence/absence of Cu ions in, for example, the onset of compression (collapse pressure), the molecular area, and the isotherm slope at takeoff.

been assessed using the Langmuir balance technique (Figure 2).

The surface-pressure–area-compression isotherm shows that **1** can form stable Langmuir monolayers at the air–water interface with a collapse pressure of 34 $mN m^{-1}$. This fairly high value, despite the short aliphatic chains of the amphiphile, can be ascribed to π–π stacking stabilization among the aromatic rings of neighboring amphiphiles. The limiting area (A_{lim}) of 105 $Å^2$ $molecule^{-1}$ is in agreement with the orientation of **1** with the pseudo C_4 axis orthogonal to the air–water interface.[11] At the surface of a solution with a concentration as low as 10 μM $CuCl_2$, the isotherm shows a larger molecular area at takeoff (112 $Å^2$ $molecule^{-1}$) and a slightly increased collapse pressure of 36 $mN m^{-1}$. The shift of the takeoff value is attributed to the interaction of carboxylate groups with Cu^{2+} causing an expansion of the footprint of **1** in the formed monolayer. The rigidity of the Langmuir monolayer of **1** was examined by calculating the isotherm slope, that is, $\delta\pi/\delta A$.[11c] At the takeoff, the surface-pressure isotherm exhibits a higher modulus in the presence of Cu^{2+}, recognized by the higher slope (0.4) compared to the isotherm on pure water (0.2; see Figure S1 in the Supporting Information; SI). This relevant increase indicates, in analogy to an earlier report,[7] a significant modification of the self-assembled monomolecular layer by the interaction of the polar parts of **1** with Cu^{2+}.

The morphology of the self-assembled monolayer of **1**, on pure water and on 10 μM $CuCl_2$ aqueous solutions, was imaged by means of Brewster angle microscopy (BAM; Figure 3).

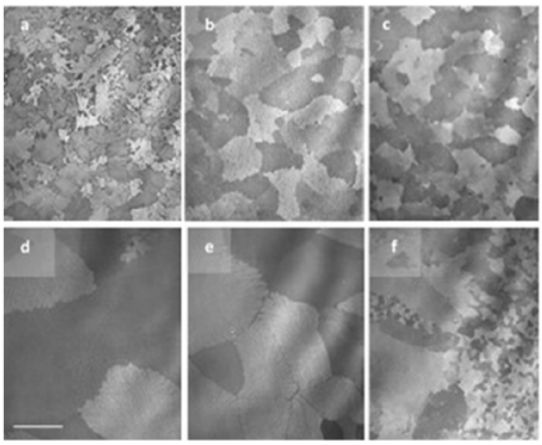

Figure 3. BAM micrographs of a monolayer of **1** on pure water (a–c) and on a 10 μM $CuCl_2$ aqueous solution (d–f), before compression (a, d), at the isotherm takeoff (b, e), and at a surface tension of $\pi = 25$ $mN m^{-1}$ (c, f). Different domains are identified based on their contrast, which depends on the orientation of the sample with respect to the incident polarized light. The domain-size distribution in the layer depends on the architecture of the layer as well as on preparation parameters. The dendritic domains only occur upon Cu coordination and are monocrystalline as identified by BAM (see the SI). Scale bar: 100 μm.

Remarkably, BAM images show in the presence and in the absence of Cu ions in the subphase that, even before compression, the amphiphiles were self-assembled at the interface. Crystalline domains with different polarization-dependent optical contrasts on both pure water and 10 μM $CuCl_2$ subphases were observed. The formation of crystalline domains at the air–water interface, even prior to compression, can be attributed to the directional π–π stacking of the aromatic rings, which is possible with a minor contribution of the short aliphatic chains of **1**. Longer-chain analogues do not show this behavior.[11c] In the presence of $CuCl_2$, however, large domains with a dendritic shape, in coexistence with an amorphous matrix, were observed. The anisotropy of the crystalline structures observed on both pure water and 10 μM $CuCl_2$ subphases is unambiguously evidenced by reflectivity variations observed in BAM (Figure S2).[12] The orientation-dependent contrast provides evidence for monocrystallinity of the single domains in the dendritic networks. The optical contrast in the BAM micrographs can be ascribed to the anisotropy of the arrangement of the molecules in their 2D lattice as well as to the anisotropy of **1**, which may assume a pinched-cone conformation at the interface, as observed in the solid state.[13] By further compression of the layer, smaller, differently oriented crystalline domains reorient and append to larger domains such that a crystalline layer is propagated with a characteristic domain size before the collapse pressure is reached. In addition to the large dendritic crystals, a crystalline layer comprising smaller (< 10 μm) crystalline domains covers a smaller fraction of the surface area in all kinds of orientation, as nucleated during the initial phase of the compression isotherm.

The monomolecular layer of **1** prepared on a 10 μM $CuCl_2$ subphase was transferred by the Langmuir–Schaefer (LS) technique at a surface pressure of 25 mN m^{-1} from the air–liquid interface onto various solid substrates: highly oriented pyrolytic graphite (HOPG), silicon/silicon dioxide (coated with octadecyltrichlorosilane; OTS), and gold (modified with a self-assembled monolayer of 1-dodecanthiol). Surface ellipsometry measurements revealed that for all tested substrates a layer with a thickness of (1.0 ± 0.2) nm was transferred; this value is consistent with a **1**-based monolayer fully covering the substrate. In order to avoid any possible interference of the organic hydrophobic monolayer (i.e., OTS, dodecanethiol) beneath the MOCN, we decided to restrict the next steps of this study to HOPG as a homogeneous and crystalline hydrophobic substrate. Contact-angle measurements further confirmed the successful transfer of the monolayer of **1**; the initial contact angle of HOPG was decreased from 99° to 76° (Table S1).

The change in the chemical environment of the carboxy groups in the presence of Cu^{2+} was assessed by X-ray photoelectron spectroscopy (XPS) for different layers after their transfer onto HOPG (Figure 4). The observed C1s peak position of the carboxy group at a binding energy of 289.3 eV is in good agreement with the values reported in the literature (Table S2).[14] The COOH peak position in the C1s spectrum shifts towards a lower binding energy, by 0.4 eV, upon coordination with the Cu nodes; this shift is in agreement with an earlier report.[15] The average ratio between carboxy groups and Cu nodes in the MOCN of **1** is found to be 4:1. The binding energy and the satellite structure in the Cu2p spectrum indicate that the copper oxidation state is +2.[16] The absence of a Cl2p signal in the XPS results of the MOCN of **1** confirms the balanced charge in the system due to coordination of Cu ions and deprotonated carboxy groups. This all suggests that on average four carboxylate groups of **1** coordinate to one Cu node and rules out the possibility to have a 1:1 complex of **1** and Cu^{2+} (Figure S3 and S4). In this coordination geometry, two water molecules coordinate to the axial sites of the carboxy:Cu unit to complete the coordination sphere.[17]

In order to obtain high-resolution images of the LS layer of **1** on HOPG, we carried out atomic force microscopy (AFM) experiments. By an in-depth comparison of different imaging modes, it became clear that the PeakForce Tapping® mode, operated with carefully optimized parameters, was best suited to avoid the destruction of the delicate monolayer and to provide high-resolution AFM data.

The thickness of the layer transferred onto the substrate was measured to be (1.0 ± 0.3) nm, which is consistent with our ellipsometric data and the expected height of a monomolecular layer of **1** (Figure S5). AFM high-resolution images confirmed that crystalline MOCNs of **1** were successfully transferred onto HOPG. Crystalline domains separated by amorphous zones with different orientations and lateral sizes, up to 200 × 200 nm, were found (Figure 5.) Two-dimensional fast Fourier transform (2D FFT) was applied to the AFM data and resulted in two well-defined first-order peaks with a distance of about 4.6 nm; this value corresponds to the width of the crystalline stripes and is consistent with the dimensions of three calixarene molecules coordinated by copper ions. Additionally, the average height of the crystalline stripes is about 4 Å (Figure S6). This value is lower than expected for a monolayer of **1** (ca. 1 nm) and allows us to rule out 1D crystalline stripes separated by empty spaces. It rather suggests that the crystalline monolayer is two-dimensional and features corrugated/rippled topography.

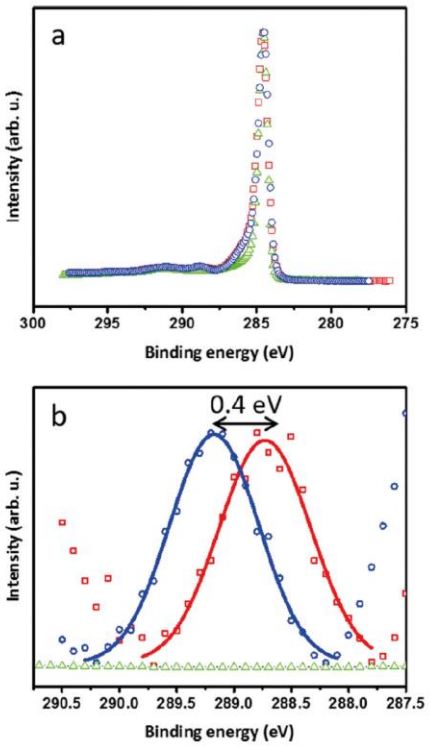

Figure 4. Identification of the carboxy-peak shift in the C1s spectra of the MOCN of **1** after the LS transfer onto HOPG. Data are shown for the initial assembly performed on pure water (○) and on a 10 μM $CuCl_2$ aqueous solution (□). Clean HOPG (△) is shown as reference. a) C1s spectra including the HOPG reference; b) normalized C1s spectra in the carboxylic carbon region after background subtraction.

Combining AFM and XPS results, we propose a packing model for the self-assembled MOCN of **1**, coordinated to Cu nodes (Figure 6). In this model, the geometry of the amphiphile is derived from the XRD single crystal structure of **1**, where the macrocycle is in a pinched-cone conformation.[13] The copper coordination geometry we used to establish our model is similar to that observed for the crystalline structure of a Cu^{II} malonate complex.[18] The molecular organization of the molecules in the monolayer complies with the 4:1 carboxylate:copper stoichiometry measured by XPS. Because of steric hindrance, the most consistent model features one copper ion coordinated by two carboxylate moieties in a flattened orientation with regard to the C_{2v} axis of the macrocycle; the two other arene rings are in close to parallel orientation with regard to the same axis (Figure 6c).

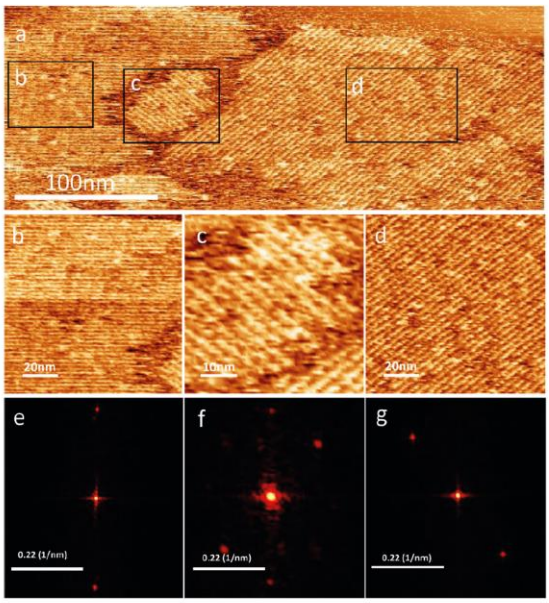

Figure 5. a) High-resolution AFM micrographs of the MOCN of **1** transferred by the LS method; b)–d) zoomed images of the crystalline domains; e)–g) correlated FFT analysis.

The distance between the latter, upright oriented arene rings of two adjacent molecules is 3.9 Å, consistent with a moderate π–π stacking interaction energy.[18,19] This coordination unit also implies that two adjacent calixarene molecules in the flattened-arene–Cu–flattened-arene direction (named *x* direction in Figure 6a) are slightly tilted, with an angle out of the HOPG plan. This is expected to cause the formation of corrugations in the same axis and is consistent with the crystalline stripes shown in the AFM data. The height of those corrugations, from this model, would be about 4.5 Å (Figure 6b), which is also in good agreement with our AFM result (ca. 4 Å; Figure S7).

In conclusion, we report the first example of a metal–organic coordination network based on a complex three-dimensional amphiphile, that is, a calix[4]arene derivative coordinated to copper ions acting as metal nodes. The method developed for this purpose allows for the fabrication of extended crystalline layers at an air–water interface and on solid surfaces and can be adapted to a broad range of macrocycles. The crystallinity of the monolayer can be tuned by adjusting the self-assembly conditions and the inorganic node. The possibility to further functionalize the organic building blocks along with the opportunity to use different metal nodes should open up the way for the design of a large range of tunable crystalline and functional two-dimensional layers on liquid and solid surfaces.

Acknowledgements

The financial support of the Swiss Nanoscience Institute through the ORACLE grant (P1308) is gratefully acknowl-

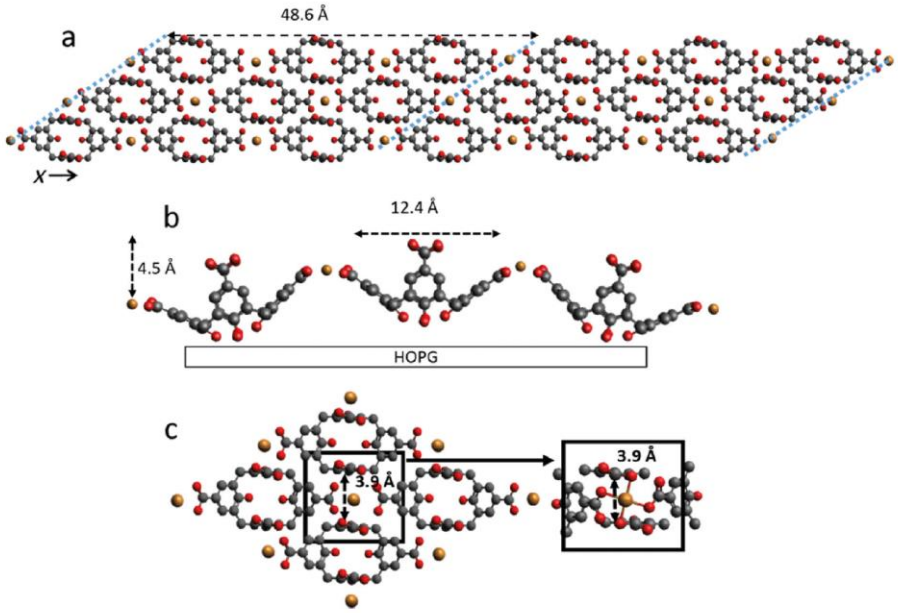

Figure 6. Proposed schematic molecular model for a MOCN of **1**. a,c) top view; 48.6 Å is the width of the crystalline stripes obtained by AFM (a); molecules of **1** interact through π–π stacking (3.9 Å; black dashed line in the black square in c); b) side view. Four carboxylate groups of **1** coordinate to one Cu node in an octahedral geometry (Figure S7). Color code: Cu, yellow; O, red; C, gray. Propyl chains are omitted for clarity.

edged. M.B., J.N., and T.A.J. acknowledge the Swiss Nanoscience Institute (SNI) (Project P1204) and the Swiss National Science Foundation (Grant no. 200020–153549). The authors thank R. Schelldorfer for technical support in the XPS and AFM measurements, as well as H. Stadler (Bruker) for his assistance with the AFM experiments.

Conflict of interest

The authors declare no conflict of interest.

Keywords: calix[4]arenes · Langmuir–Blodgett method · metal–organic coordination networks · self-assembly

How to cite: *Angew. Chem. Int. Ed.* **2017**, *56*, 14395–14399
Angew. Chem. **2017**, *129*, 14587–14591

[1] K. S. Novoselov, A. K. Geim, S. V. Morozov, D. Jiang, Y. Zhang, S. V. Dubonos, I. V. Grigorieva, A. A. Firsov, *Science* **2004**, *306*, 666–669.
[2] P. J. Waller, F. Gandara, O. M. Yaghi, *Acc. Chem. Res.* **2015**, *48*, 3053–3063.
[3] L. Grill, M. Dyer, L. Lafferentz, M. Persson, M. V. Peters, S. Hecht, *Nat. Nanotechnol.* **2007**, *2*, 687–691.
[4] L. Lafferentz, V. Eberhardt, C. Dri, C. Africh, G. Comelli, F. Esch, S. Hecht, L. Grill, *Nat. Chem.* **2012**, *4*, 215–220.
[5] K. Baek, G. Yun, Y. Kim, D. Kim, R. Hota, I. Hwang, D. Xu, Y. H. Ko, G. H. Gu, J. H. Suh, C. G. Park, B. J. Sung, K. Kim, *J. Am. Chem. Soc.* **2013**, *135*, 6523–6528.
[6] a) T. Bauer, Z. K. Zheng, A. Renn, R. Enning, A. Stemmer, J. Sakamoto, A. D. Schlüter, *Angew. Chem. Int. Ed.* **2011**, *50*, 7879–7884; *Angew. Chem.* **2011**, *123*, 8025–8030; b) A. Dmitriev, H. Spillmann, N. Lin, J. V. Barth, K. Kern, *Angew. Chem. Int. Ed.* **2003**, *42*, 2670–2673; *Angew. Chem.* **2003**, *115*, 2774–2777; c) A. Shchyrba, C. Wäckerlin, J. Nowakowski, S. Nowakowska, J. Björk, S. Fatayer, J. Girovsky, T. Nijs, S. C. Martens, A. Kleibert, M. Stöhr, N. Ballav, T. A. Jung, L. H. Gade, *J. Am. Chem. Soc.* **2014**, *136*, 9355–9363; d) S. Stepanow, N. Lin, D. Payer, U. Schlickum, F. Klappenberger, G. Zoppellaro, M. Ruben, H. Brune, J. V. Barth, K. Kern, *Angew. Chem. Int. Ed.* **2007**, *46*, 710–713; *Angew. Chem.* **2007**, *119*, 724–727.
[7] R. Makiura, O. Konovalov, *Sci. Rep.* **2013**, *3*, 2506.
[8] L. G. Tulli, P. Shahgaldian in *Calixarenes and beyond* (Eds.: P. Neri, J. L. Sessler, M.-X. Wang), Springer, Basel, **2016**, pp. 987–1010.
[9] F. Sansone, S. Barboso, A. Casnati, M. Fabbi, A. Pochini, F. Ugozzoli, R. Ungaro, *Eur. J. Org. Chem.* **1998**, 897–905.
[10] a) B. Chen, M. Eddaoudi, T. M. Reineke, J. W. Kampf, M. O'Keeffe, O. M. Yaghi, *J. Am. Chem. Soc.* **2000**, *122*, 11559–11560; b) N. Singh, P. Vishnoi, G. Anantharaman, *CrystEngComm* **2015**, *17*, 2153–2161; c) M. Eddaoudi, D. B. Moler, H. Li, B. Chen, T. M. Reineke, M. O'Keeffe, O. M. Yaghi, *Acc. Chem. Res.* **2001**, *34*, 319–330.
[11] a) L. G. Tulli, N. Moridi, W. Wang, K. Helttunen, M. Neuburger, D. Vaknin, W. Meier, P. Shahgaldian, *Chem. Commun.* **2014**, *50*, 3938–3940; b) P. Shahgaldian, A. W. Coleman, S. S. Kuduva, M. J. Zaworotko, *Chem. Commun.* **2005**, 1968–1970; c) L. G. Tulli, W. Wang, W. R. Lindemann, I. Kuzmenko, W. Meier, D. Vaknin, P. Shahgaldian, *Langmuir* **2015**, *31*, 2351–2359.
[12] "Brewster Angle Microscopy" in K. J. Stine, *Supramolecular Chemistry: From Molecules to Nanomaterials*, Wiley, Hoboken, **2012**.
[13] S. Kennedy, S. J. Teat, S. J. Dalgarno, *Dalton Trans.* **2010**, *39*, 384–387.
[14] a) M. Xu, G. He, Z. Li, F. He, F. Gao, Y. Su, L. Zhang, Z. Yang, Y. Zhang, *Nanoscale* **2014**, *6*, 10307–10315; b) L. Zhang, L. Ji, P.-A. Glans, Y. Zhang, J. Zhu, J. Guo, *Phys. Chem. Chem. Phys.* **2012**, *14*, 13670–13675.
[15] O. Shekhah, N. Roques, V. Mugnaini, C. Munuera, C. Ocal, J. Veciana, C. Wöll, *Langmuir* **2008**, *24*, 6640–6648.
[16] Y. Wang, J. Im, J. W. Soares, D. M. Steeves, J. E. Whitten, *Langmuir* **2016**, *32*, 3848–3857.
[17] S. Motoyama, R. Makiura, O. Sakata, H. Kitagawa, *J. Am. Chem. Soc.* **2011**, *133*, 5640–5643.
[18] M. Mitra, P. Manna, A. Das, S. K. Seth, M. Helliwell, A. Bauzá, S. R. Choudhury, A. Frontera, S. Mukhopadhyay, *J. Phys. Chem. A* **2013**, *117*, 5802–5811.
[19] K. Avasthi, L. Shukla, R. Kant, K. Ravikumar, *Acta Crystallogr. Sect. C* **2014**, *70*, 555–561.

Manuscript received: April 13, 2017
Revised manuscript received: August 22, 2017
Accepted manuscript online: August 28, 2017
Version of record online: October 16, 2017

Angewandte Chemie
Eine Zeitschrift der Gesellschaft Deutscher Chemiker

Supporting Information

Two-Dimensional Calix[4]arene-based Metal–Organic Coordination Networks of Tunable Crystallinity

Mina Moradi[+], Ludovico G. Tulli[+], Jan Nowakowski, Milos Baljozovic, Thomas A. Jung, and Patrick Shahgaldian**

anie_201703825_sm_miscellaneous_information.pdf

Table of Contents

Langmuir monolayer experiment

Surface pressure-area compression isotherms were carried out using a Nima 112D Langmuir trough. For each series of experiments, the trough and barriers were thoroughly cleaned with analytical grade chloroform and nanopure water (resistivity ≥18 MΩ.cm). An aqueous solution of 10 µM $CuCl_2.2H_2O$ in nanopure water was prepared as a subphase extemporaneously. The monolayer was prepared by spreading a solution of **1** (7µL, 1 $mgmL^{-1}$ in chloroform:methanol (95:5, vol:vol) on the liquid subphase using a gastight microsyringe. After solvent evaporation and equilibration of amphiphiles at the interface (15 min), barriers were symmetrically closed at a speed rate of 2 cm^2min^{-1}. The accuracies of π_c and A_0 measurements were of ±1 mNm^{-1} and ±1 $Å^2$ $molecule^{-1}$, respectively.

Langmuir-Schaefer transfer procedure

Langmuir-Schaefer (LS) transfers were carried out using a Nima deposition system. Highly oriented pyrolytic graphite (HOPG), silicon/silicon dioxide substrates coated with octadecyltrichlorosilane (OTS) and gold substrates modified with a self-assembled monolayer of 1-dodecanthiol were used as solid substrates for the LS deposition of MOCN of **1**. Si/SiO_2 substrates were pre-cleaned using detergent, nanopure water, acetone and methanol, respectively. Then, pre-cleaned Si/SiO_2 substrates were placed for 20 min in a UV/ozone chamber and consecutively rinsed with methanol and dried under a nitrogen flow. The cleaned substrates were immersed for 30 min in 3.9 g L^{-1} anhydrous heptane solution of octadecyltrichlorosilane and rinsed using heptane and chloroform, respectively. The SiO_2 and OTS layer thickness values were found to be 3 and 2.8 nm, respectively, measured by ellipsometry. In addition, the hydrophobic substrate of Si/SiO_2 coated with OTS exhibits a contact angle of 110°. [1] Gold slides have been prepared by the evaporation of chromium and gold on glass, were then cleaned by exposure to UV light for 15 min, were rinsed in pure methanol before re-exposure to UV radiation for 15 min and rinsing final rinsing step in pure methanol. Fresh gold slides were immersed in a 1mM solution of 1-dodecanthiol in pure ethanol for 15 hours at room temperature. The slides were rinsed twice with neat methanol, once with neat chloroform and gently dried with N_2. The formation of self-assembled monolayers of 1-dodecanthiol on gold was investigated by contact angle measurement. The measured value was 109°, in agreement with the value of 110° reported for $C_{18}SH$ and 113° reported for $C_{10}SH$. [2]
The substrates were approached toward the interface at a controlled speed of 1 mm/min and touched the monolayer compressed at 25 mN/m. After 15 min, the substrates were slowly removed from the aqueous solution at a constant speed of 1 mm/min.

Brewster angle microscopy

Brewster angle microscopy was performed by using a Nanofilm_ep3 system (Accurion) equipped with an internal solid-state laser at a wavelength of 658 nm. The images were acquired using a CCD camera (768×562 pixels) and a 10X objective, equipped with an automatic focus scanner yielding 1 µm lateral resolution.

Spectroscopic ellipsometry

Ellipsometry measurements were carried out using an imaging and spectroscopic system (EP3 Ellipsometer Accurion) in a nulling PCSA (polarizer-compensator-sample-analyzer) set-up. For all the ellipsometry experiments, OTS-coated silicon wafers were used as substrates as previously described.[1]

Contact angle measurement

Contact angles were measured using a commercial Krüss ®Easy drop optical system (Krüss, GmbH, Germany). Drops of 3µL of nanopure water were used for measuring static water contact angle on samples. To ensure reproducibility, the measurements were repeated at 5 different positions on each sample.

X-ray photoelectron spectroscopy

X-ray photoelectron spectroscopy (XPS) spectra were acquired using monochromatic Al Kα (hv = 1486.7 eV) excitation source (Specs FOCUS 500) in normal emission using a Specs PHOIBOS 150 electron analyzer. The C1s core level of HOPG was used as reference for the binding energies and was assigned to 284.5 eV. The measurements were performed in ultra-high vacuum system with base pressure of 10^{-11} mbar.

Atomic force microscopy

Atomic force microscopy in the PeakForce Tapping® mode using a Multimode 8 instrument (Bruker) equipped with a Nanoscope V controller with a scanasyst-air-HR silicon tip on nitride lever were used.

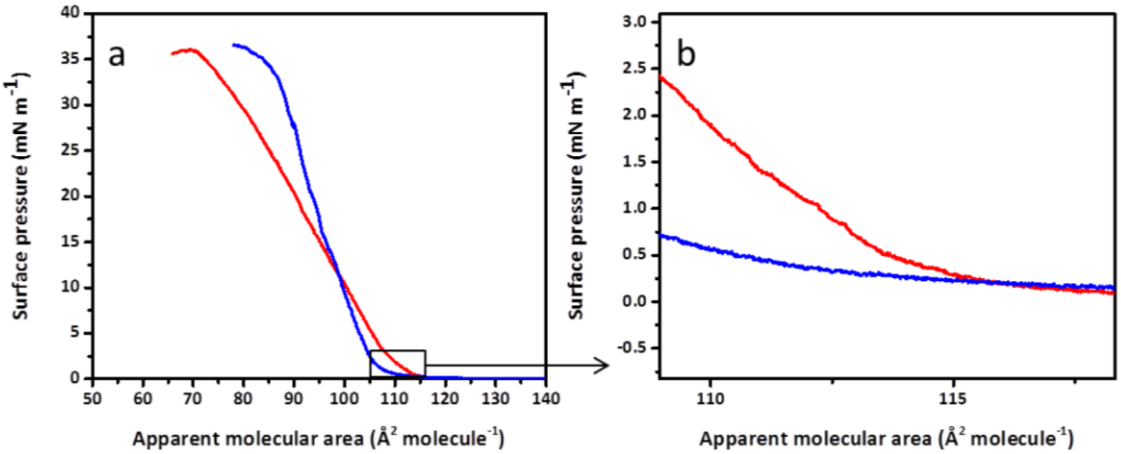

Figure S1. Langmuir compression isotherms of **1** measured on pure water (—) and a 10µM $CuCl_2$ (—) subphases. In order to study the rigidity of the monolayer at surface pressure take-off, the values of the modulus of the isotherm slope |δπ/δA| were calculated.[3] The surface pressure isotherm exhibits a higher modulus, at takeoff, in the presence of Cu^{2+} recognized by a higher slope (|δπ/δA| = 0.4) compared to the isotherm on pure water (|δπ/δA| = 0.2). This relevant increase indicates a significantly modified self-assembled monomolecular layer upon interactions of the carboxylate functions of **1** with Cu^{2+}.

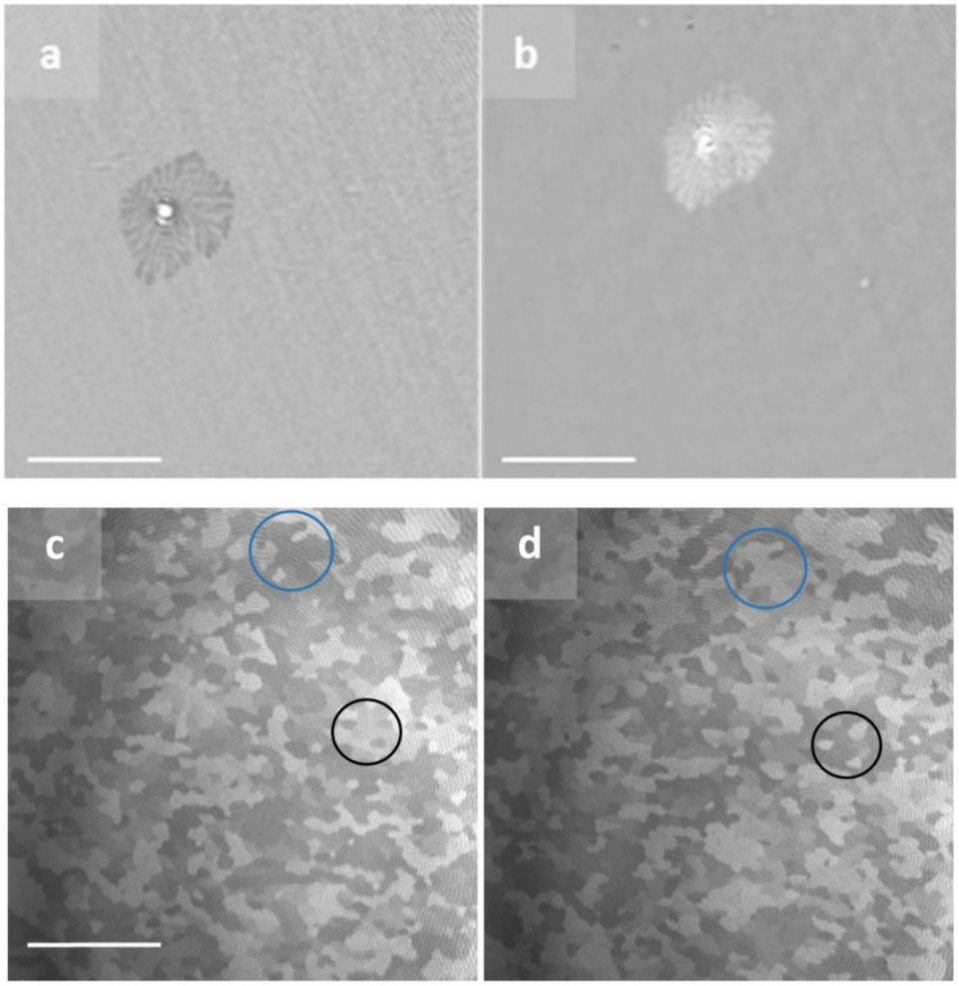

Figure S2. BAM micrographs of the monolayer of **1** on a 10 μM aqueous $CuCl_2$ solution (a and b) and on pure water (c and d) compressed at a surface pressure of 20 mN m^{-1} before (a and c) and after (b and d) rotating the polarizer from a value of 10° to -10°. Scale bar = 100 μm. After rotating the polarizer the contrast of the domain is reversed (b). This result indicates that the crystalline structures of **1** grown at the interface are monocrystalline, where the macrocycles are anisotropically arranged within the single domains. The absence of contrast change of the regular phase after rotation of the polarizer is an indication of its amorphous character.

Table S1. Contact angle measurements on MOCN of **1** and HOPG (reference sample).

Sample	Contact angle(°)
HOPG (reference sample)	98.8±6
Monolayer of **1** transferred from pure water	80.01±8
MOCN of **1** transferred from 10 μM $CuCl_2$	76±5

Table S2. C1s XPS peak assignment for MOCN of **1** transferred on HOPG by the LS method. [4] The derivatives were obtained by fitting the spectra. A precise interpretation of the O1s spectrum is challenging because of multiple peaks overlapping for different O entities of **1** and water molecules.

		Binding energy (eV)
C 1s	π - π*	290.8
	COOH	288.4
	C-O (sp^3)	286.1
	C-C (sp^3)	284.8
	C=C (sp^2)	284.5

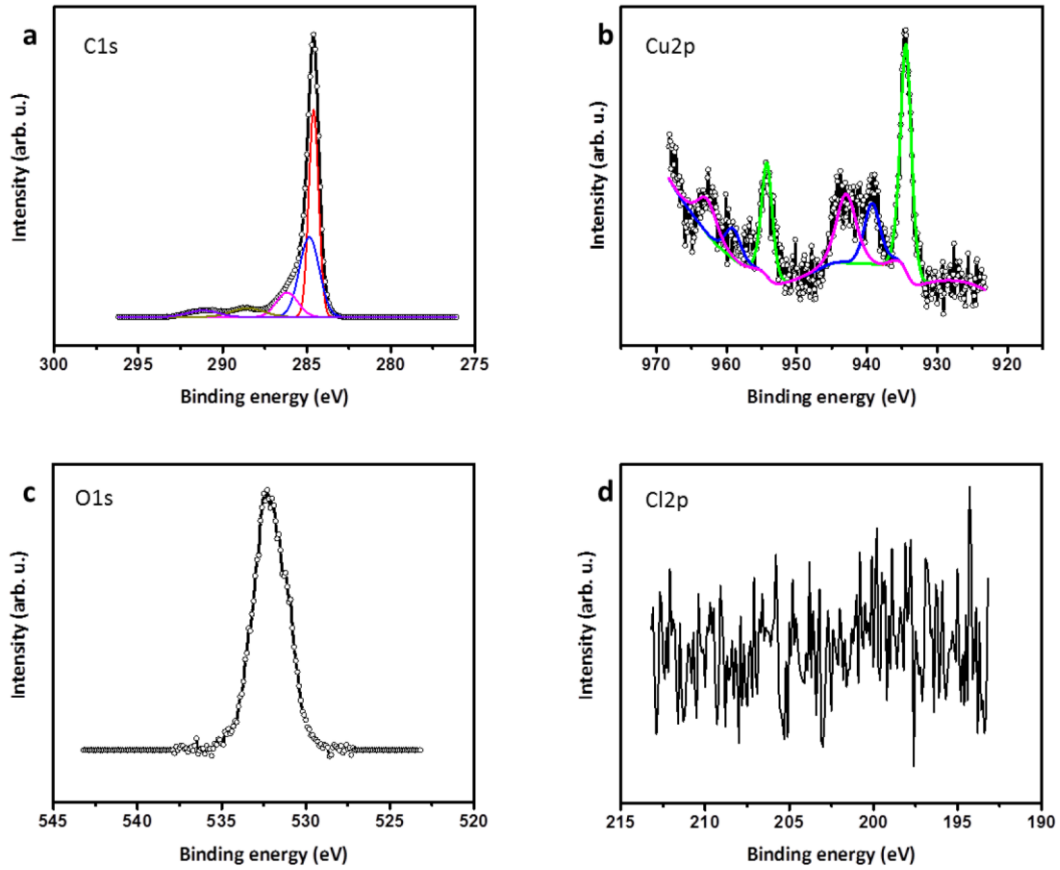

Figure S3. XP spectra of MOCN of **1** transferred on HOPG by the LS method for C1s, Cu2p, O1s and Cl2p peaks, respectively (a-d). Copper XP spectrum in MOCN of **1** shows two satellites peaks in 939.2 and 959.4 eV, characteristic features of Cu in CuO.[5] The binding energy and satellites of the copper XP spectrum indicate the copper oxidation state is +2 for MOCN of **1**.[6] ENREF 2 ENREF 2 The absence of a Cl2p signal in the XPS results of MOCN of **1** evidences the balanced charge in the system without any counter ion, i.e. Cl^-, due to dissociation of $CuCl_2$ and coordination of deprotonated carboxyl groups with Cu nodes. The ratio between carboxyl groups and Cu nodes, presented in MOCN of **1**, has been calculated by integration of the area of carboxyl peak in C1s and Cu in Cu2p spectra.

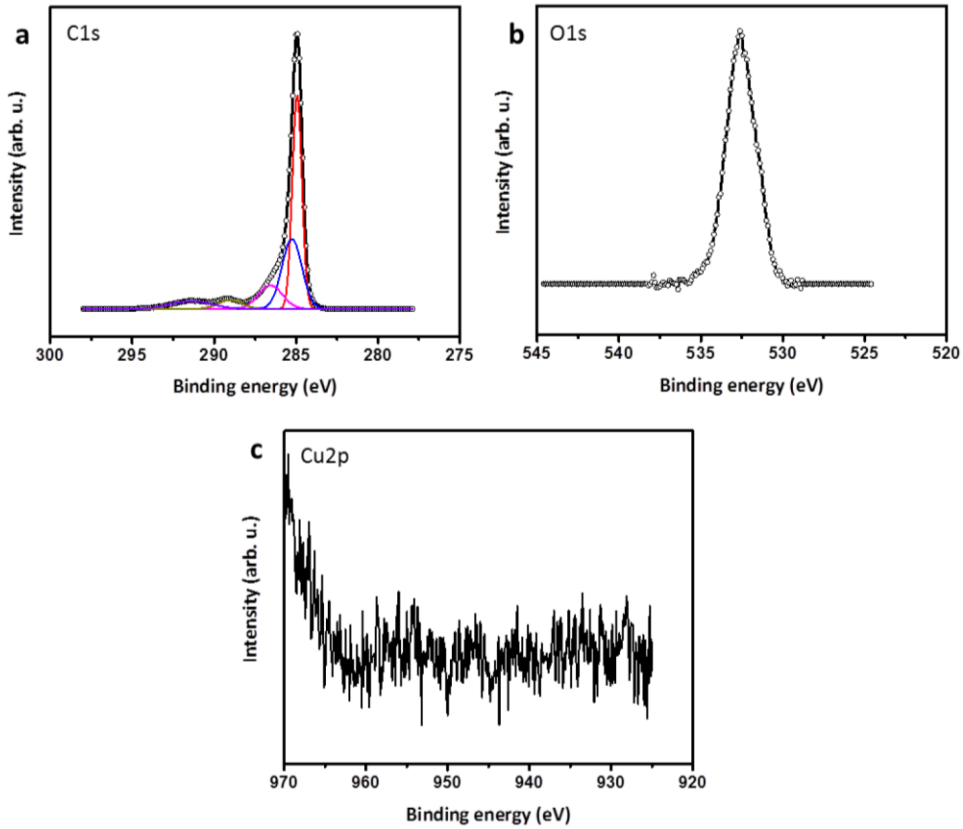

Figure S4. XP spectra of monolayer of **1** transferred on HOPG by the LS method from pure water; i.e. control experiment for C1s, O1s and Cu2p, respectively (a-c). It confirms absence of Cu in the transferred monolayer from pure water. The binding energy of carboxyl functions in C1s spectrum is in agreement with literature.[4]

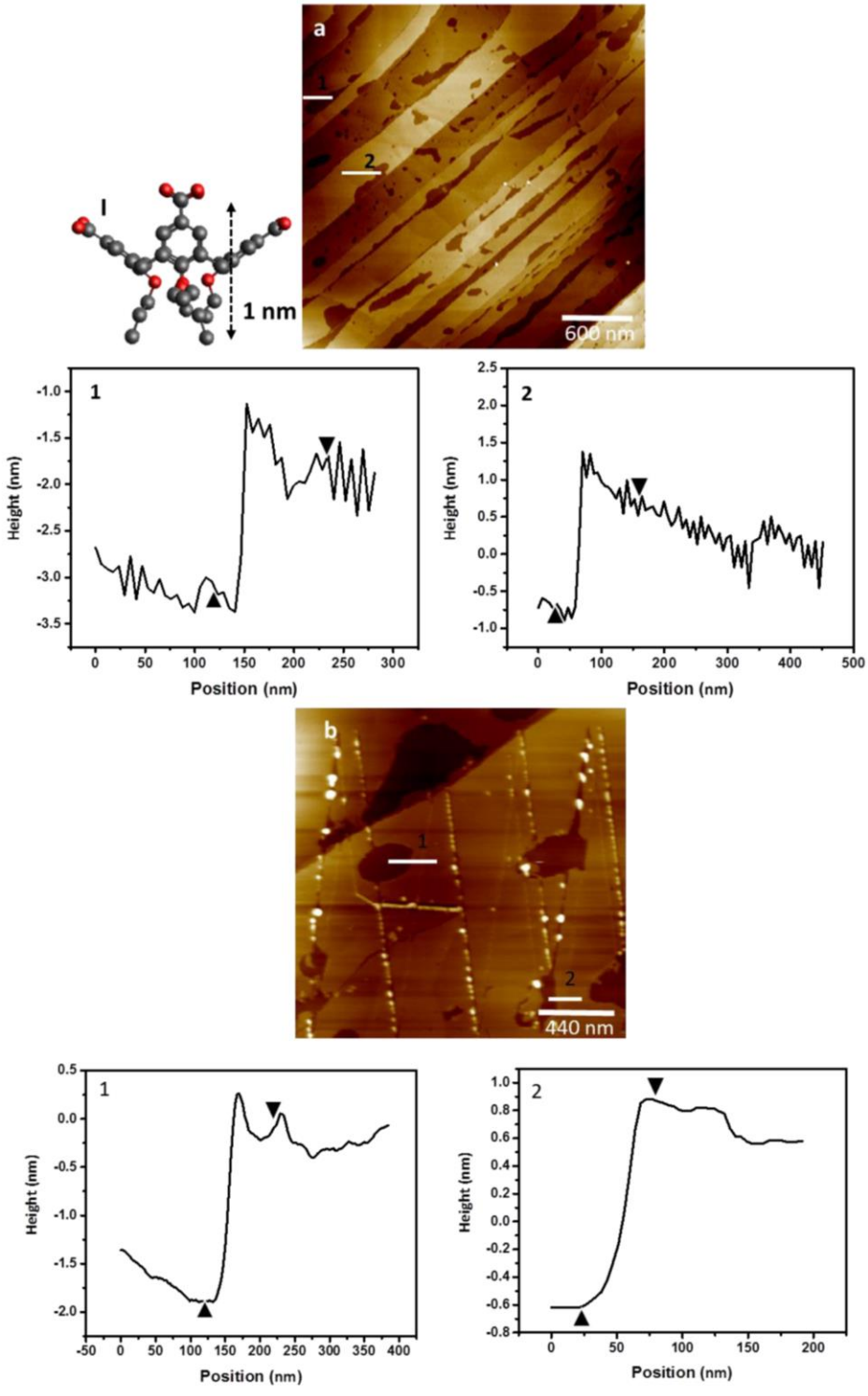
a
1
2
600 nm
I
1 nm
1
Height (nm)
Position (nm)
2
Height (nm)
Position (nm)
b
1
2
440 nm
1
Height (nm)
Position (nm)
2
Height (nm)
Position (nm)

S11

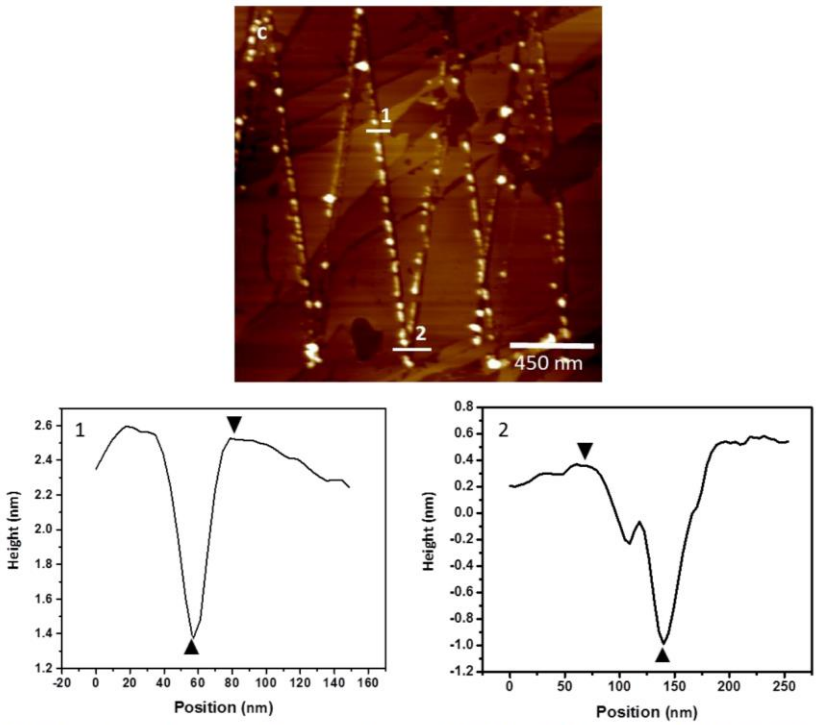

Figure S5. AFM height analyses of the transferred MOCN of **1** from a 10μM $CuCl_2$ subphase on HOPG by the LS method. Height analyses of MOCN of **1** were carried out in partially covered HOPG by monolayer of **1** (a). Scratching experiment on the transferred layer was done intentionally in order to confirm the presence of a MOCN of **1** (b and c). The lines in the images indicate where the height profiles were recorded. The AFM results confirmed the presence of a monomolecular of **1** with a height of 1.0±0.3 nm. The measured height from AFM is in a good agreement with the expected height of **1**, derived from crystalline structure (1 nm) (I).[7] The deviation from 1 nm value could come from the ambient-condition AFM[8] and also partially rearrangement of molecules because of water evaporation.

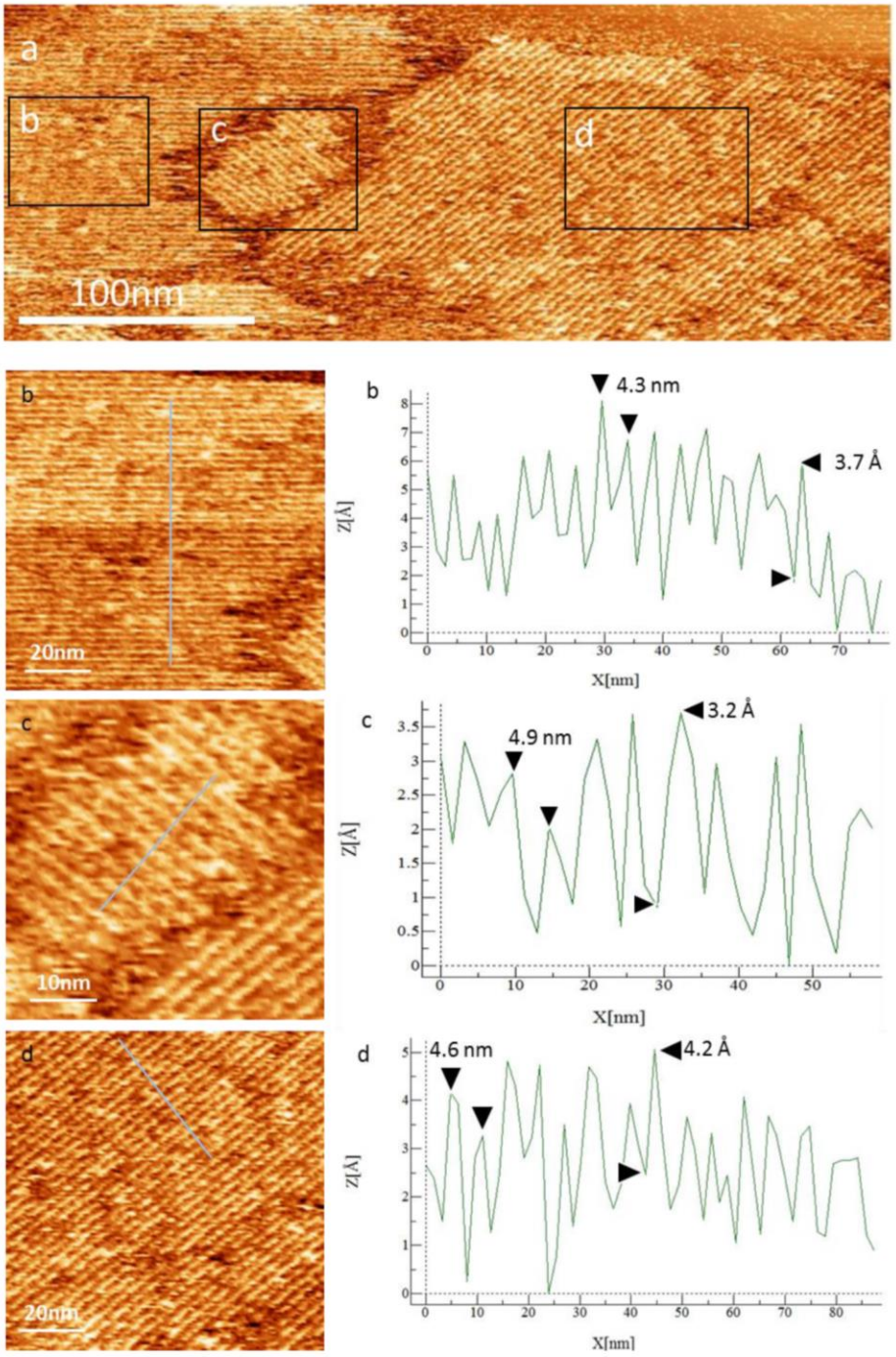

Figure S6. Scan line profiles of the high-resolution AFM images. An overview of crystalline domains of MOCN of **1** with different orientations, transferred from a 10 μM $CuCl_2$ subphase on HOPG (a). Zoomed AFM images of each crystalline domain with their corresponding profile line, the scan line profiles show periodicity of the crystalline domains (b, c and d). An average width and height of the crystalline lines measured in different regions of the AFM images are ~4.6 nm and ~4 Å, respectively.

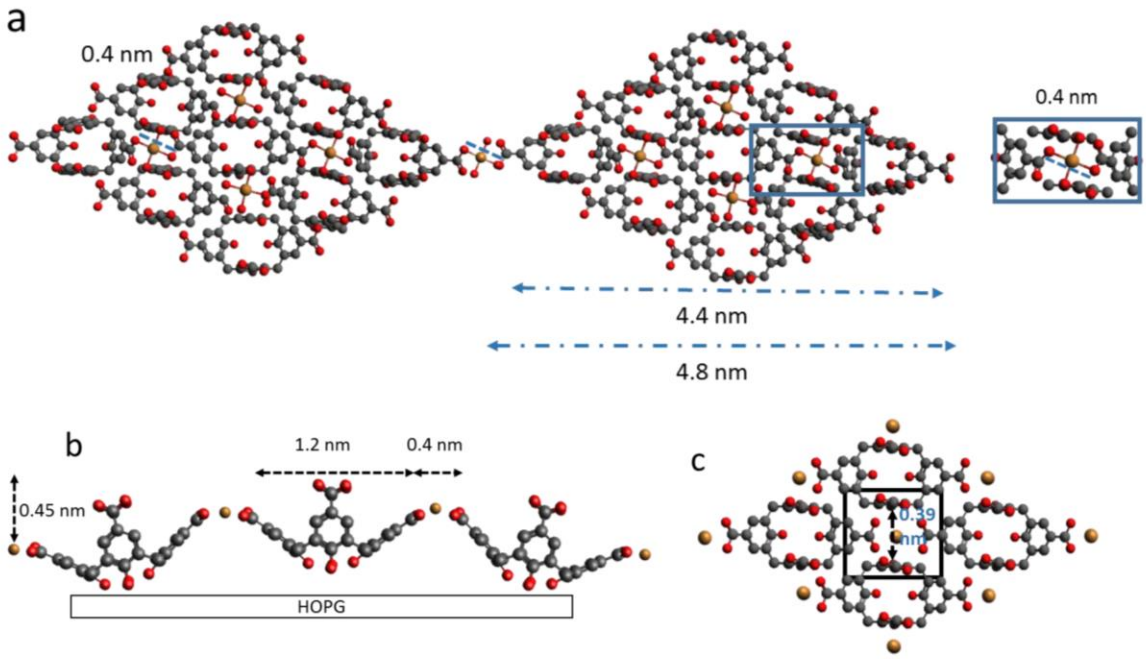

Figure S7. Top (a) and side (b) views of the coordination units of crystalline MOCN of **1** in the proposed molecular model. The model has been drawn by considering the crystalline structure of Cu-carboxylate coordination in a similar crystalline structure i.e. in the Cu(II) malonate complex with **1** (top view of the octahedral geometry has been indicated by the dark blue rectangle in a).[7, 9] The crystal structure of **1** adopting a C_{2v} symmetry has been shown to be more stable than the more symmetrical C_{4v} geometry and is common for *O*-alkyl calixarene derivatives.[10] In this structure, two opposite arene rings are in a close to perpendicular orientation (-11°). Further, the distance between the carbon of these carboxylate functions assumes a value of 4.6 Å. The two other arene rings are flexed down towards the surface and form an opening angle of 104°. The distance between the carboxylate carbons is increased to a value of 12.4 Å. In the Cu(II) malonate complex crystalline structure, copper ions coordinated by 4 carboxylate groups with a Cu-O bond length of 1.9 Å and O-Cu-O angle of 90°, respectively. In our proposed model, 4 molecules of **1** coordinate with one Cu node and form crystalline stripes with a width of ~4.6 nm. The suggested model predicts a periodic corrugated structure with partially tilted orientation of molecules of **1**, with regard to the C_{2v} symmetry axis of the macrocycle of **1** (b). ENREF 7Based on the suggested model two neighboring molecules of **1** interact through π- π stacking (0.39 nm) (indicated by black arrows in c).[9,11] Calculated height of one stripe from the model is 0.45 nm (b) that it is in a good agreement with the measured stripes height from AFM data (~0.4nm). Propyl chains were omitted for the sake of clarity.

References

[1] N. Moridi, C. Wackerlin, V. Rullaud, R. Schelldorfer, T. A. Jung, P. Shahgaldian, *Chem. Commun.* **2013**, *49*, 367-369.

[2] a) H. Ron, S. Matlis, I. Rubinstein, *Langmuir* **1998**, *14*, 1116-1121; b) C. E. D. Chidsey, D. N. Loiacono, *Langmuir* **1990**, *6*, 682-691.

[3] L. G. Tulli, W. Wang, W. R. Lindemann, I. Kuzmenko, W. Meier, D. Vaknin, P. Shahgaldian, *Langmuir* **2015**, *31*, 2351-2359.

[4] L. Zhang, L. Ji, P.-A. Glans, Y. Zhang, J. Zhu, J. Guo, *Phys. Chem. Chem. Phys.* **2012**, *14*, 13670-13675.

[5] J. F. Moulder, W. F. Stickle, Peter E. Sobol, K. D. Bomben, *Handbook of X-ray Photoelectron Spectroscopy*, (Ed: J. Chastain), Perkin-Elmer Corporation, Eden Prairie, **1992**.

[6] a) R. Makiura, S. Motoyama, Y. Umemura, H. Yamanaka, O. Sakata, H. Kitagawa, *Nat. Mater.* **2010**, *9*, 565-571; b) Y. Wang, J. Im, J. W. Soares, D. M. Steeves, J. E. Whitten, *Langmuir.* **2016**, *32*, 3848-3857.

[7] S. Kennedy, S. J. Teat, S. J. Dalgarno, *Dalton Trans.* **2010**, *39*, 384-387.

[8] T. Bauer, Z. Zheng, A. Renn, R. Enning, A. Stemmer, J. Sakamoto, A. D. Schlüter, *Angew. Chem., Int. Ed.* **2011**, *50*, 7879-7884.

[9] M. Mitra, P. Manna, A. Das, S. K. Seth, M. Helliwell, A. Bauzá, S. R. Choudhury, A. Frontera, S. Mukhopadhyay, *J. Phys. Chem. A* **2013**, *117*, 5802-5811.

[10] J. Scheerder, R. H. Vreekamp, J. F. J. Engbersen, W. Verboom, J. P. M. van Duynhoven, D. N. Reinhoudt, *J. Org. Chem.* **1996**, *61*, 3476-3481.

[11] K. Avasthi, L. Shukla, R. Kant, K. Ravikumar, *Acta Crystallogr. C* **2014**, *70*, 555-561.

CHAPTER 2

Supramolecular Architectures of Molecularly Thin Yet Robust Free-standing Layers

Summary:

Self-assembled networks featuring nanometer-sized pores and long-range crystallinity provide configurable templates for host-guest recognition and site-specific chemistry. These crystalline networks impact several technological applications, provided that the resulting material is of sufficient stability. Supramolecular chemistry has now reached maturity, and decades of research allowed formulating a set of basic rules enabling the design of complex molecular architectures. In this context, we demonstrated that slightly directional and weak non-covalent binding such as dipole-dipole interactions can be used, when acting synergistically, to fabricate free-standing and crystalline monomolecular layers. Through the Langmuir-Blodgett technique and at the air-water interface calix[4]arene derivative, *i.e. 25,26,27,28*-tetrapropoxycalix[4]arene-*5,11,17,23*-tetramethylcyano, self-assemble via the dipole-dipole interactions between the cyano binding moieties (-CN· · ·NC-). Surface analysis techniques showed the strong propensity of the calix[4]rene building units to crystallize and form a stable free-standing and crystalline 2D supramolecular organic network in the absence of additional nodes or guest molecules.

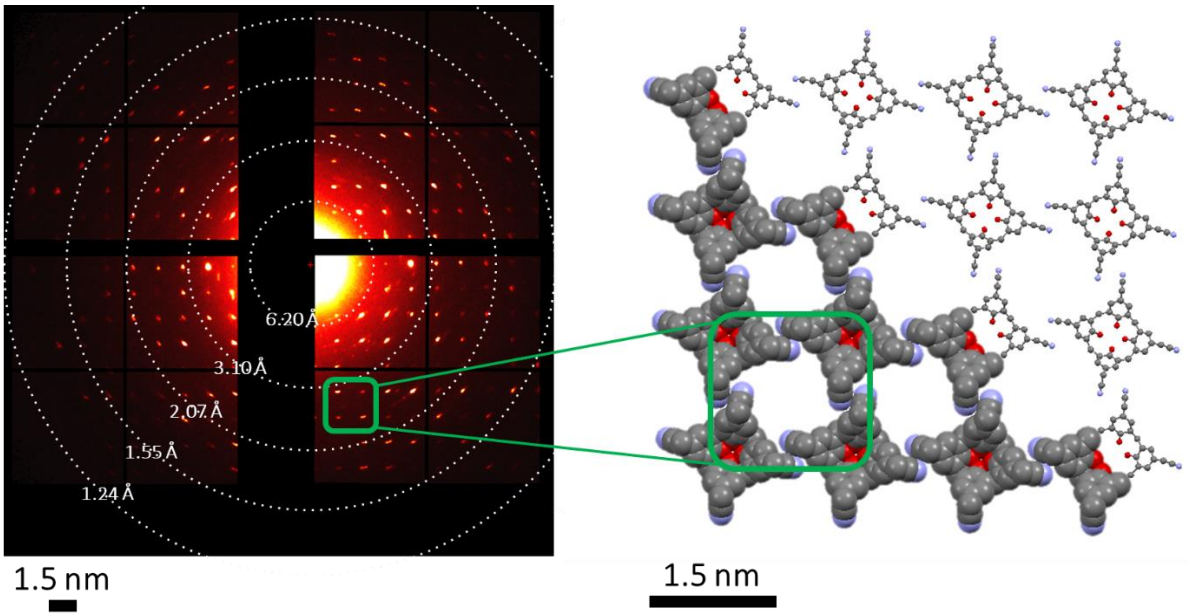

APPLIED SCIENCES AND ENGINEERING

Supramolecular architectures of molecularly thin yet robust free-standing layers

Mina Moradi[1,2], Nadia L. Opara[2,3], Ludovico G. Tulli[1], Christian Wäckerlin[4], Scott J. Dalgarno[5], Simon J. Teat[6], Milos Baljozovic[2], Olha Popova[7], Eric van Genderen[2]*, Armin Kleibert[8], Henning Stahlberg[3], Jan Pieter Abrahams[9,10], Celestino Padeste[2], Philippe F.-X. Corvini[1], Thomas A. Jung[2†], Patrick Shahgaldian[1†]

Stable, single-nanometer thin, and free-standing two-dimensional layers with controlled molecular architectures are desired for several applications ranging from (opto-)electronic devices to nanoparticle and single-biomolecule characterization. It is, however, challenging to construct these stable single molecular layers via self-assembly, as the cohesion of those systems is ensured only by in-plane bonds. We herein demonstrate that relatively weak noncovalent bonds of limited directionality such as dipole-dipole (–CN···NC–) interactions act in a synergistic fashion to stabilize crystalline monomolecular layers of tetrafunctional calixarenes. The monolayers produced, demonstrated to be free-standing, display a well-defined atomic structure on the single-nanometer scale and are robust under a wide range of conditions including photon and electron radiation. This work opens up new avenues for the fabrication of robust, single-component, and free-standing layers via bottom-up self-assembly.

INTRODUCTION

The ambition to produce materials with meticulous control over the organization of molecular building blocks has, for decades, attracted chemists and material scientists and triggered their efforts. This long-standing challenge has been met, to a great extent, with the development of reticular chemistry allowing for the design of complex and chemically programmed crystalline materials, namely, metal-organic and covalent-organic frameworks (MOFs and COFs) (*1*, *2*). The strong resurgence of interest in two-dimensional (2D) materials triggered MOF design strategies to be adapted for the production of 2D networks (*3*–*10*). The 2D nature of this class of materials considerably limits their stability; however, a substrate is required. Thus, the possibility to produce stable and, a fortiori, free-standing monolayers remains a challenge. It is remarkable that currently existing methods do not allow for the fabrication of crystalline and free-standing monolayers of organic building units exclusively via supramolecular interactions between their constituent molecules in the absence of chemical linkers. Here, we challenge the accepted paradigm endorsing strong and directional interactions for the design of stable supramolecular architectures: We report a strategy to construct stable and free-standing monomolecular layers using weak noncovalent bonds of limited directionality (i.e., dipole-dipole interactions).

[1]Institute of Chemistry and Bioanalytics, School of Life Sciences, University of Applied Sciences and Arts Northwestern Switzerland, Hofackerstrasse 35, CH-4132 Muttenz, Switzerland. [2]Laboratory for Micro- and Nano-technology, Paul Scherrer Institute, Villigen CH-5232, Switzerland. [3]Center for Cellular Imaging and NanoAnalytics (C-CINA), Biozentrum, University of Basel, Mattenstrasse 26, CH-4058 Basel, Switzerland. [4]Empa–Swiss Federal Laboratories for Materials Science and Technology, CH-8600 Dübendorf, Switzerland. [5]Institute of Chemical Sciences, Heriot-Watt University, Riccarton, Edinburgh, Scotland EH14 4AS, UK. [6]Advanced Light Source, Lawrence Berkeley National Laboratory, 1 Cyclotron Road, MS6R2100, Berkeley, CA 94720, USA. [7]Department of Physics, University of Basel, Klingelbergstrasse 82, 4056 Basel, Switzerland. [8]Swiss Light Source, Paul Scherrer Institute, CH-5232 Villigen, Switzerland. [9]Biozentrum, University of Basel, Switzerland and Laboratory of Biomolecular Research, Paul Scherrer Institute, Villigen, Switzerland. [10]Institute of Biology Leiden, Leiden University, Sylviusweg 72, 2333 BE Leiden, Netherlands.
*Present address: Center for Cellular Imaging and NanoAnalytics (C-CINA), Biozentrum, University of Basel, Mattenstrasse 26, CH-4058 Basel, Switzerland.
†Corresponding author. Email: patrick.shahgaldian@fhnw.ch (P.S.); thomas.jung@psi.ch (T.A.J.)

RESULTS AND DISCUSSION

The design of the molecular building block chosen for our first demonstration of a free-standing layer architecture has been inspired by our previous work on calixarene macrocycles in their function as an organizing molecular entity (*9*). At the phenolic rim of the parent calix[4]arene macrocycle, short alkyl chains were attached to reinforce the hydrophobic character of the amphiphile while preserving its interfacial crystallization propensity. We decided to restrict the work to four-membered ring macrocycles because of their higher level of symmetry and their relative conformational rigidity. To endow this calixarene derivative with the ability to form 2D supramolecular networks, chemical moieties capable of dipole-dipole interactions have been introduced. Methyl-cyano functional groups have been chosen as they have been widely studied for their ability to establish this type of supramolecular interaction (*11*, *12*). 5,11,17,23-tetra-methylcyano-25,26,27,28-tetrapropoxy-calix[4]arene (**1**) was synthesized and fully characterized (see synthesis section in the Supplementary Materials and fig. S1).

The crystallization of **1** from methanol yielded single crystals suitable for x-ray diffraction studies with synchrotron radiation. Inspection of the structure showed that both molecules of **1** are in the pinched-cone conformation and that all methyl-cyano functionalities point away from the calixarene cavities. Symmetry expansion reveals a bilayer system (fig. S2) akin to those found in the vast majority of structures containing *p*-sulfonatocalix[4]arene (*11*, *12*), with hydrophobic layers alternating within the extended structure. The relative conformational flexibility of **1** is likely to be a contributory factor to bilayer formation; examination of the extended structure shows that the symmetry equivalents of **1** pack in an interdigitated manner, forming a series of identifiable CH· · ·N and CH· · ·π interactions (tables S1 to S8).

The formation of layers of **1** at the air-water interface was studied using the Langmuir balance technique and Brewster angle microscopy (BAM; Fig. 1 and table S9). The compression isotherm shows that **1** here forms stable monolayers characterized by a relatively high collapse pressure of 28 mN m^{-1} and a limiting area of 90 $Å^2$ $molecule^{-1}$. It is noteworthy that, unlike the large majority of amphiphilic calixarenes at the air-water interface, the interfacial behavior of **1** displays two main phase transitions at surface pressure values of 3.4 and 17.9 mN m^{-1}

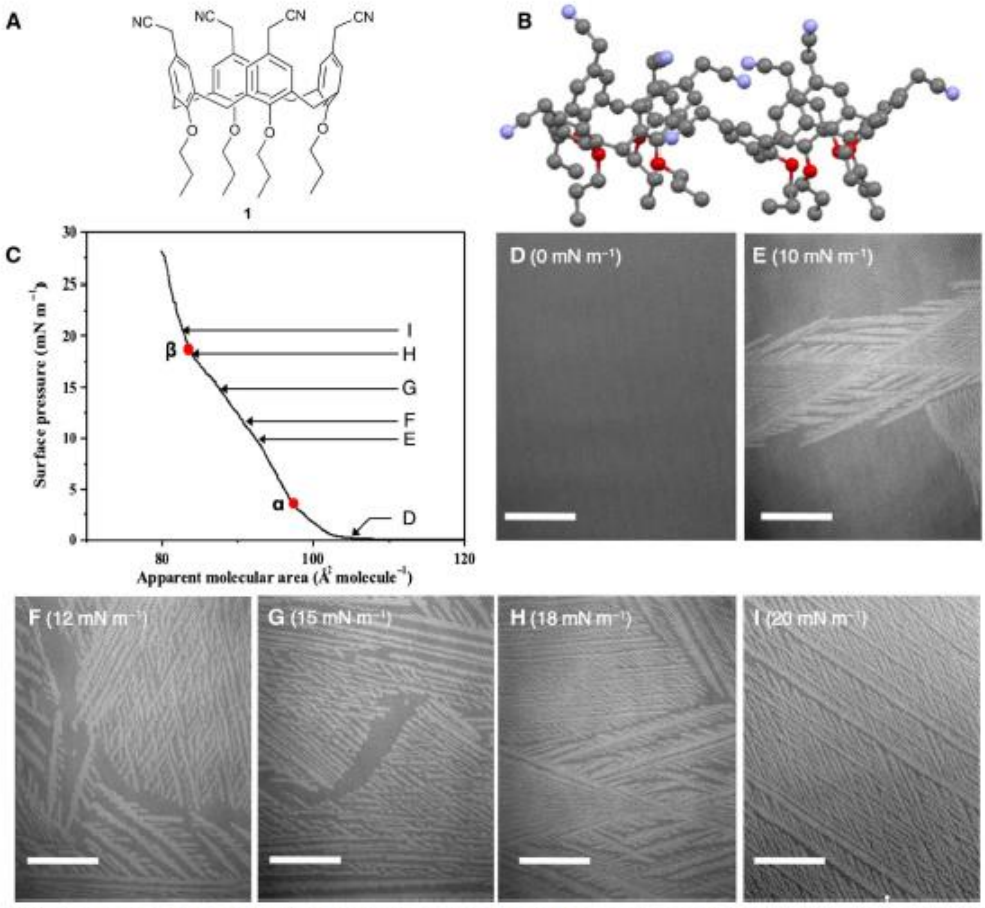

Fig. 1. Chemical structure and interfacial self-assembly characterization of 1. (**A**) Molecular structure of *para*-methyl-cyano-tetra-propoxy-calix[4]arene, **1**. (**B**) Extended structure found in the crystal structure of **1** showing methyl-cyano functionalities pointing away from macrocycle cavities. Color code: C, gray; N, blue; O, red. Hydrogen atoms are omitted for clarity. (**C**) Surface pressure area compression isotherm of **1** on pure water displayed three distinct phases with phase transitions at surface pressure values of 3.4 (α) and 17.9 mN m^{-1} (β), corresponding to molecular area values of 97 and 84 $Å^2$ $molecule^{-1}$, respectively. Letter labels indicate the position on the isotherm where the corresponding BAM micrographs were acquired. (**D** to **I**) BAM micrographs of the monolayer of **1** on pure water. Large crystalline monolayer domains grow after the first phase transition (10 mN m^{-1}). Upon further compression, the crystalline network expands and covers the whole available area at the air-water interface. Scale bar, 100 μm.

(Fig. 1, the points labeled α and β on the isotherm, respectively). Before monolayer compression, BAM analysis of the monolayer of **1** at the air-water interface shows no contrast; this is characteristic of a 2D gas phase (Fig. 1D). At the isotherm takeoff (A_0 = 102 $Å^2$ $molecule^{-1}$), the monolayer exhibits a homogeneous morphology in BAM (Fig. 1D). After the first phase transition observed at 3.4 mN m^{-1}, the morphology of the monolayer changes to yield large needle-like crystalline structures (Fig. 1, E and F). Upon further compression, the second phase transition is reached; large dendritic crystalline structures appear and gradually cover the whole surface available (Fig. 1, G and H). Further compression increases the density of those crystalline domains (Fig. 1I) until the monolayer collapses.

Notably, BAM results confirm that **1** self-assembles as a crystalline layer at the interface in the absence of organic or inorganic nodes. The addition of transition metal salts (i.e., $CuCl_2$, $NiCl_2$, and $CrCl_3$) did not cause any relevant change in the compression isotherm or BAM micrographs. As cyano moieties are known to be capable of metal coordination, this result strongly suggests that in-layer interactions are largely favored (fig. S3) and that the formation of the crystalline network of **1** is due to intermolecular (–CN· ··NC–) dipole-dipole interactions. The influence of van der Waals interactions can be neglected because of the short length of aliphatic chains at the lower rim of the macrocycle. To further verify the nature of the intramolecular interaction stabilizing this layer, compression isotherms were carried out in the presence of a competitor molecule capable of (–CN· · ·NC–) interactions, namely, acetonitrile (ACN), in the subphase (fig. S4). The dissociation constant (K_d) of single dipole-dipole interactions, calculated using reported Gibbs' free energy of interaction values (ΔG_0, ranging from −5 to −20 kJ mol^{-1}) of –CN· ··NC– (*13*), is expected to range from 0.3 to 100 mM. In our experiments, we used ACN concentrations of 10 and 10^{-2} mM. At the lowest tested concentration of 10^{-2} mM (expected to be below K_d), the Langmuir compression isotherm did not reveal any relevant change with regard to that measured on pure water. This confirms that no significant interaction occurred between **1** and ACN. Oppositely, at an ACN concentration of 10 mM, only a very unstable monolayer is formed (with a collapse pressure below 4 mN m^{-1}),

indicating that the interactions of **1** with the cyano group in ACN totally disrupted the self-assembly process. This result further confirms the dipole-dipole nature of the intermolecular forces stabilizing the monolayer of **1**.

The monomolecular layer of **1** was transferred using the Langmuir Schaefer (LS) method at the surface pressure of 20 mN m^{-1} from the air-water interface onto two different solid substrates, i.e., highly oriented pyrolytic graphite (HOPG) and silicon/silicon dioxide coated with octadecyltrichlorosilane (OTS). In both cases, transfer ratio values were close to unity; surface ellipsometry and contact angle measurements confirmed the successful transfer of the monolayer onto the solid substrates tested (table S10). To avoid interferences with the alkyl chains of OTS, HOPG has been chosen as the substrate for surface analytical experiments described hereinafter.

The element-specific chemical analysis of the monolayer of **1** transferred onto HOPG was carried out using x-ray photoelectron spectroscopy (XPS). The N1s spectrum showed only a single peak at 399.7 eV, which is a characteristic value for the cyano CN group attached to carbon (*14*). The single sharp N peak, with a full width at half maximum of 1 eV, provides evidence that all N atoms have the same chemical environment in the monolayer. The O:N ratio, calculated from the O1s and N1s spectra, is ~1, in agreement with the chemical structure of **1**. The amount of water in the transferred monolayer is negligible, as calculated from the O1s spectrum. This provides further counterevidence against H-bonding of **1** with water driving the self-assembly of the monolayer of **1** (Fig. 2, A to C). To further explore whether dipole-dipole interactions between the CN groups are responsible for stabilizing the layer, we transferred the monolayer by LS transfer after assembly on aqueous solutions containing 10 μM $CuCl_2$, $NiCl_2$, or $CrCl_3$ (fig. S3). XPS revealed, in all these cases, the absence of any metal linkers (fig. S5). These results confirm that the CN groups in the calixarene have a higher propensity to interact with one another via dipole-dipole interactions than via coordination bond with metal ion linkers.

To further characterize **1**-based networks transferred on a solid substrate and to establish a molecular model of the monolayer on the surface, near-edge x-ray absorption fine structure (NEXAFS) measurements at the N-K edge were carried out (Fig. 2, D to F). The spectra exhibited a very simple line shape consisting only of the signals of transitions into the π* (400.6 eV) and σ* (approximately 425 eV) molecular orbitals (MOs) of CN (*15*, *16*). Only one peak is observed because the CN MO is not hybridized with the π system of the phenyl group because of the linking sp^3-hybridized carbon (*17*). The linear dichroism (LD) spectrum revealed a slight polarization of the π* signal rising to ~4% at a 70° x-ray incidence angle. The small negative LD implies that, on average, the cyano groups are oriented at an angle γ greater than the magic angle (54.74°) with respect to the surface normal. The angle dependence of the π* LD is modeled as a plane-type orbital (see NEXAFS section in the Supplementary Materials) (*17*, *18*). Also, we find an average angle of the CN group with respect to the surface normal $\langle\gamma\rangle = 57 \pm 1°$.

Atomic force microscopy (AFM) studies of the 2D supramolecular systems provided a substantial challenge; this may be caused by the weak interactions between the short apolar part of **1** (i.e., propyl chains) and the substrate (*19*, *20*). AFM micrographs of the monolayer of **1**, transferred onto HOPG under ambient conditions, were acquired. (Fig. 3). The layer thickness has been determined by measuring the *z* profile after scratching the layer with the AFM at high constant force.

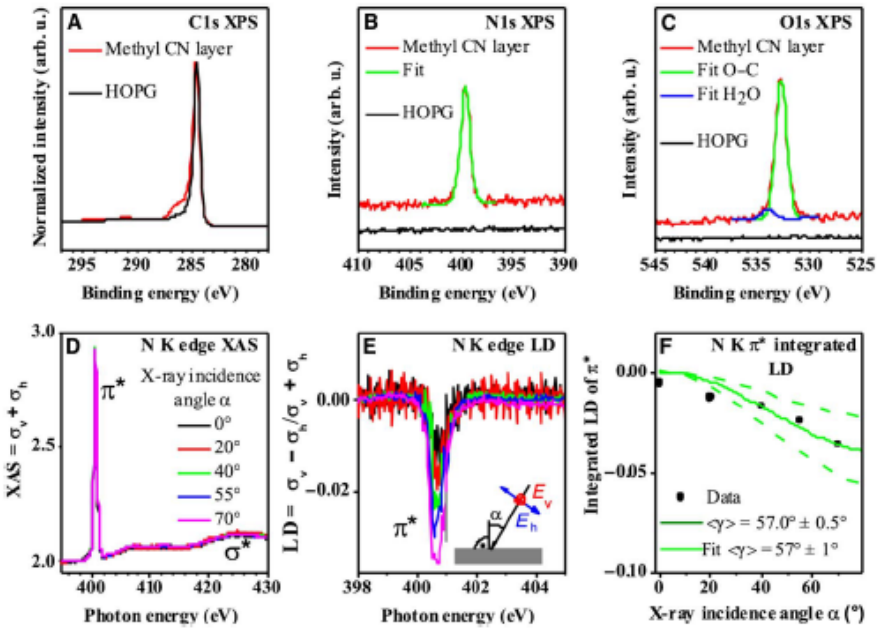

Fig. 2. Surface spectroscopy analysis of 1-based monolayers. (**A** to **C**) X-ray photoelectron spectra of the monolayer of **1** transferred onto HOPG by the LS method for C1s, N1s, and O1s peaks. arb. u., arbitrary units. (C) The O1s spectrum can be fitted with two peaks, 532.5 and 533.2 eV, representing O–C of **1** and an insignificant amount of H_2O (~6% of the O1s spectrum) (*14*). A precise interpretation of the C1s spectrum is challenging because of multiple peaks overlapping for different C entities of **1**. (**D** to **F**) Room temperature N-K edge x-ray absorption spectra ($E_v + E_h$) and LD of the monolayer of **1** on HOPG. (D) The transition into the unoccupied π* MO of the CN groups is visible as a distinct peak at 400.6 eV. (E) Integrated intensity of the LD of the π* signal as a function of the x-ray incidence angle with respect to the surface normal. (F) The data are consistent with an average orientation of $\langle\gamma\rangle = 57°$ of the CN groups. The dashed line corresponds to $\langle\gamma\rangle = 57° \pm 1°$.

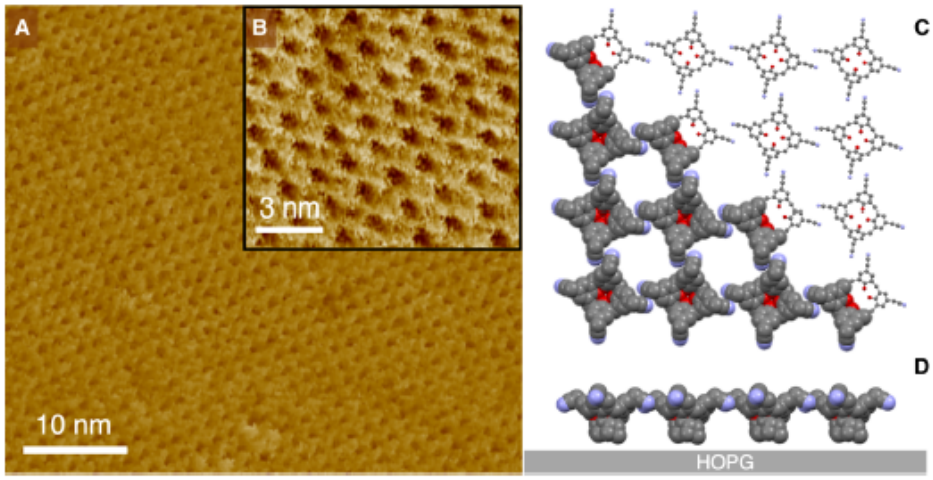

Fig. 3. Molecular resolution AFM imaging of the monolayer of 1. (**A**) AFM images of the monolayer of **1** transferred onto HOPG via the LS method. (**B**) The high-resolution image of the crystalline network of the monolayer shows a highly ordered network formed from the single molecules of **1**. [**C** (top view) and **D** (side view)] Molecular model of the building blocks of **1** interacting via the proposed dipole-dipole interaction in the well-ordered monolayer.

The thereby obtained value of 1.0 ± 0.4 nm further confirms the presence of only a single layer of **1** on HOPG (fig. S6), also consistent with surface ellipsometry measurements that show the value of 1.0 ± 0.2 nm. AFM imaging at molecular resolution revealed large areas covered with molecules of **1** packed in a square fashion with an average lattice constant of 1.5 nm (Fig. 3, A and B). This confirms that the layer is sufficiently stable to be transferred from the liquid to the solid surface without being disrupted by the process despite the above evidenced absence of covalent or coordination bonding.

Combining Langmuir isotherm results, XPS, NEXAFS, and AFM, we propose a model for the molecular packing of **1**-based monolayers (Fig. 3, C and D). In this model, every single building block of **1** interacts with its nearest neighbors via –CN· · ·NC– dipole-dipole interactions. Interatomic distances and angles of the CN groups agree with the values reported by Allen *et al.* (*13*) for dominant antiparallel geometry of dipole-dipole interaction of CN functional groups. The angle of the CN functional groups of **1** with regard to the surface normal, extracted from the molecular model, is 58.4°, which is in agreement with the NEXAFS data.

To further investigate the stability of the layer under different environmental conditions, cryo–transmission electron microscopy (TEM) investigations have been performed on the monolayer of **1** after a successful transfer from the air-water interface onto a lacey carbon copper grid by the LS method (Fig. 4). Lacey carbon grids are hydrophobic by nature and have a mesh structure displaying more than 80% of open areas. The LS transfer was carried out using the same conditions than in the case of HOPG, and the transfer ratio measured was again close to unity. Cryo-TEM investigations of the monolayer of **1**, shown in Fig. 4, revealed the presence of homogeneous free-standing layers across areas as large as 3 μm by 3 μm, without rupturing and shrinking. Thus, the bonding between the molecules in the monolayer is sufficiently stable that it can be transferred as a free-standing film. We attribute this remarkable level of stability to the synergistic action of the dipole-dipole interactions. The diffraction pattern of the free-standing layer shows only one characteristic lattice (Fig. 4B). This, together with the absence of higher-order Laue zones and the high degree of Friedel symmetry in the electron diffraction patterns (also in the shape of the Bragg peaks), confirms that the free-standing layers are indeed monolayers and not ordered or disordered stacks. The electron diffraction patterns of the free-standing monolayer (Fig. 4B) reveal a square lattice with a unit cell size of 15 Å (fig. S7). This result is in agreement with the AFM data and our molecular model.

It has been widely reported that 2D monolayers of organic molecules suffer from decomposition and loss of stability under high electron beam intensity (*21*–*24*). Notably, our results show that the free-standing monolayer of **1** remains intact also during extensive sessions of cryo-TEM imaging.

CONCLUSION

In conclusion, we demonstrated the formation of a crystalline, free-standing supramolecular organic network produced in the absence of coordination or covalent bonds. Thereby, we go beyond the current paradigm endorsing strong and directional interactions for the design of stable supramolecular architectures. The remarkable stability of the layer, despite the absence of covalent bridging of the constitutive building blocks, is reflected in the observation of undistorted free-standing layers and surface-supported layers with the same square crystalline lattice in molecular-resolution AFM and high-resolution TEM, respectively. On the basis of surface chemical analysis and a model, the cohesion between the building blocks of the layer has been attributed to noncovalent dipole-dipole interactions between the functional CN groups of **1**. We expect our chemical design strategy to be versatile so that it could be expanded to a broader range of multivalent building blocks capable of establishing in-plane dipole-dipole interactions. These building blocks should support multiple synergistic dipole-dipole interactions, minimize other less directional interactions such as van der Waals, and form single molecular layers at the solid-liquid interface. The latter is important to gain single molecular layers and not amorphous polymer layers with far less structural and thickness control. The stability of the free-standing layers produced, when exposed to photon-, photoelectron-, and electron irradiations, makes them systems suitable to serve as supporting layers for single-protein and single-nanoparticle analyses and imaging (*25*). Furthermore, the findings reported here pave the way toward the design

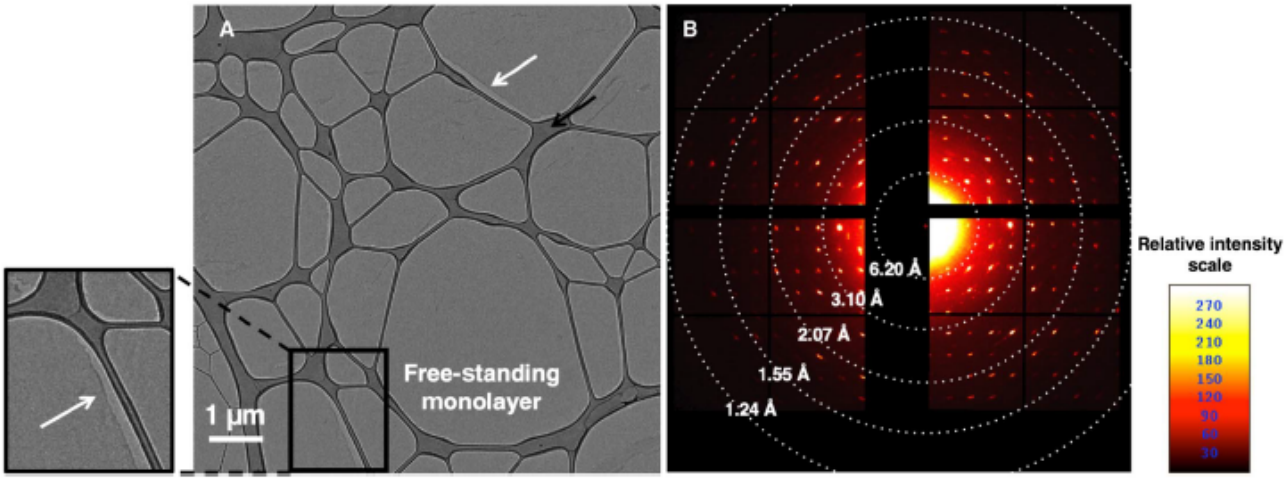

Fig. 4. Cryo-TEM investigation of the free-standing monolayer of 1. (**A**) TEM analysis of the monolayer of **1** transferred via the LS method on a lacey carbon TEM grid [dark areas in the picture are areas of thick carbon from the "lacey carbon" substrate as it is widely used as a TEM substrate for its nonuniform and wide openings (black arrow)]. The layer has fractured and lost contact in some areas with the lacey carbon. In these areas, the free-standing monolayer can be visualized, as shown with white arrows. (**B**) The electron diffraction pattern of the free-standing monolayer of **1** confirms the squarely symmetric packing structure of the crystalline layer. The profile lines across the diffraction pattern (fig. S7) reveal a unit cell size of 15 Å, consistent with the AFM acquired and the molecular model of the self-assembled monolayer of **1**.

of robust 2D layers with molecularly precise architectures and controllable physicochemical properties.

MATERIALS AND METHODS

Synthesis of 5,11,17,23-tetramethylcyano-25,26,27,28-tetrapropoxy calix[4]arene

Compound Cl-C4A-OC_3 (fig. S1) was synthesized as previously described (*26*). 5,11,17,23-tetramethylcyano-25,26,27,28-tetrapropoxy calix[4]arene, **1**, was synthesized using a modified procedure adapted from that described for analogs nonalkylated at phenolic positions (*27*), as follows. Sodium cyanide (0.38 g, 7.63 mmol) was added to a mixture of Cl-C4A-OC_3 (1 g, 1.27 mmol) in dimethyl sulfoxide (150 ml). The reaction mixture was kept under N_2 atmosphere and magnetic stirring at 80°C for 3 hours. The resulting pale yellow solution was cooled down and added to 500 ml of ice/water, yielding a milky solution. This mixture was acidified with an aqueous HCl solution (2 M). The resulting white precipitate was filtered and crystallized from MeOH to yield **1** as white crystals (0.32 g, 34%; mp 200° to 205°C).

^{1}H NMR (nuclear magnetic resonance) (300 MHz, $CDCl_3$): δ 6.62 (s, 2, Ar*H*), 4.45 to 4.41 (d, *J* = 13.3 Hz, 1, Ar-CH_2-Ar), 3.87 to 3.81 (t, *J* = 13.3 Hz, 2, O-CH_2-CH_2-CH_3), 3.50 (s, 2, Ar-CH_2-CN), 3.16 to 3.12 (d, *J* = 13.5 Hz, 1, Ar-CH_2-Ar), 1.98 to 1.86 (m, *J* = 7.5 Hz, 2, O-CH_2-CH_2-CH_3), and 1.02 to 0.97 (t, *J* = 7.4 Hz, 3, O-CH_2-CH_2-CH_3). ^{13}C NMR (75 MHz, $CDCl_3$): δ 156.21, 135.39, 127.81, 123.52, 118.40, 30.87, 23.18, 22.89, 10.26. Mass spectroscopy (electrospray ionization) mass/charge ratio: $[M + Na]^+$, calculated for $[C_{88}H_{52}N_4O_4+Na]^+$ 771.4; found 771.3. Elemental analysis (%) calculated for C, 76.98, H, 7.00; N, 7.48; found, C (76.50, 76.52), H (7.01, 7.05), N (7.42, 7.45).

X-ray crystallography

Data were collected at 100(2) K by shutterless scans using a Bruker D8 diffractometer equipped with a PHOTON 100 detector and operating with a silicon 111 monochromator and synchrotron radiation of wavelength 0.77490 Å. Diffraction data on the crystal powder of **1** were collected using a Bruker D8 Advance powder diffractometer, operating with Ge-monochromated Cu $K_{\alpha 1}$ radiation (wavelength = 1.5406 Å) and a LynxEye linear detector. Data were collected over the angular range of 5° to 85° in 2θ.

Langmuir monolayer, BAM, and LS deposition experiments

Surface pressure area compression isotherms were recorded using a NIMA 112D Langmuir system. For each series of experiments, the trough and barriers were thoroughly cleaned with analytical grade chloroform and nanopure water (resistivity of 18.2 megohm-cm). Nanopure water was used as a subphase. The monolayer was prepared by spreading a solution of **1** (13 μl, 0.5 mg ml^{-1}) in chloroform at the water surface using a gastight microsyringe. After solvent evaporation and equilibration of amphiphiles at the interface (15 min), barriers were symmetrically closed at a speed rate of 5 cm^2 min^{-1}. The accuracies of π_c and A_0 measurements were of ±0.1 mN m^{-1} and ±1 $Å^2$ $molecule^{-1}$, respectively. Each condition was repeated three times to ensure reproducibility of the isotherms.

BAM was performed by using a Nanofilm_ep3 system (Accurion) equipped with an internal solid-state laser at a wavelength of 658 nm. The images were acquired using a charge-coupled device camera (768 × 562 pixels) and a 10× objective, equipped with an automatic focus scanner yielding 1-μm lateral resolution.

LS transfer was carried out using a NIMA deposition system. HOPG and hydrophobic silicon wafers (coated with OTS) (*28*) were used as solid substrates for the LS deposition of the monolayer of **1**. The substrates were brought toward the interface at a controlled speed of 1 mm min^{-1} and touched the monolayer compressed at 20 mN m^{-1}. After 15 min, the substrates were slowly removed from the aqueous solution at a constant speed of 1 mm min^{-1}.

Near-edge x-ray absorption fine spectroscopy

Near edge X-ray absorption fine spectroscopy was measured at the N-K edge at room temperature in a total electron yield mode using linearly

polarized x-rays (E_v and E_h) for different incidence angles α (*18*). α = 0° implies normal incidence, E_v is always parallel to the surface plane, and E_h is perpendicular to E_v. The degree of polarization is 100% (*18*). Each spectrum was divided by a matching (same polarization σ and incidence angle α) spectrum obtained on clean HOPG and normalized to unity at the pre-edge (395 to 398 eV).

The angle dependence of the CN π* signal was modeled according to an established procedure (*17*), assuming a plane-type orbital (suitable for the cyano π* MO) for a threefold or higher substrate symmetry. The equations for the intensities I_p and I_n of the absorption, where the electric field of I_n is normal with respect to the surface normal (i.e., in the surface plane) and where I_p is perpendicular to I_n, are as follows

$$I_p = 1 - \cos^2\theta\cos^2\gamma - \frac{1}{2}\sin^2\theta\sin^2\gamma$$
$$I_n = \frac{1}{2}(1 + \cos^2\gamma)$$

Here, γ is the angle between the plane normal to the plane orbital (i.e., the CN vector) and the surface normal, and θ is the angle between the electric polarization of I_p and the surface normal (*17*). The theoretical LD is then calculated as $(I_n - I_p)/(I_n + I_p)$. Note that the photon energy was not exactly calibrated.

SUPPLEMENTARY MATERIALS

Supplementary material for this article is available at http://advances.sciencemag.org/cgi/content/full/5/2/eaav4489/DC1

Section S1. Materials and methods
Section S2. Contact angle measurement
Section S3. Spectroscopic ellipsometry
Section S4. X-ray photoelectron spectroscopy
Section S5. Atomic force microscopy
Section S6. Transmission electron microscopy
Fig. S1. Synthetic route to 5,11,17,23-tetramethylcyano-25,26,27,28-tetrapropoxy calix[4]arene (**1**) and spectroscopic details of **1**.
Fig. S2. X-ray crystal structure determination details of **1**.
Fig. S3. Interfacial properties of the monolayer of **1** in the presence of transition metal ions in the subphase.
Fig. S4. Interfacial properties of the monolayer of **1** in the presence of ACN molecules as competitors with the CN functional groups of **1** for dipole-dipole interactions.
Fig. S5. Surface analysis of the monolayer of **1** in the presence of transition metal ions in the subphase.
Fig. S6. AFM height analysis of the transferred monolayer of **1** from pure water subphase onto HOPG by the LS method.
Fig. S7. Diffraction analysis of the free-standing monolayer of **1** by means of high-resolution cryo-TEM analysis.
Table S1. X-ray crystal structure determination detail of **1**.
Table S2. X-ray crystal structure determination detail of **1**.
Table S3. X-ray crystal structure determination detail of **1**.
Table S4. X-ray crystal structure determination detail of **1**.
Table S5. X-ray crystal structure determination detail of **1**.
Table S6. X-ray crystal structure determination detail of **1**.
Table S7. X-ray crystal structure determination detail of **1**.
Table S8. X-ray crystal structure determination detail of **1**.
Table S9. Characteristic values of the surface pressure-area compression isotherm of **1**.
Table S10. Contact angle measurements on the monolayer of 1 transferred from the air-water interface onto HOPG.
References (*26*–*32*)

REFERENCES AND NOTES

1. H. M. El-Kaderi, J. R. Hunt, J. L. Mendoza-Cortés, A. P. Côté, R. E. Taylor, M. O'Keeffe, O. M. Yaghi, Designed synthesis of 3D covalent organic frameworks. *Science* **316**, 268–272 (2007).
2. M. Eddaoudi, J. Kim, N. Rosi, D. Vodak, J. Wachter, M. O'Keeffe, O. M. Yaghi, Systematic design of pore size and functionality in isoreticular MOFs and their application in methane storage. *Science* **295**, 469–472 (2002).
3. L. Grill, M. Dyer, L. Lafferentz, M. Persson, M. V. Peters, S. Hecht, Nano-architectures by covalent assembly of molecular building blocks. *Nat. Nano.* **2**, 687–691 (2007).
4. L. Lafferentz, V. Eberhardt, C. Dri, C. Africh, G. Comelli, F. Esch, S. Hecht, L. Grill, Controlling on-surface polymerization by hierarchical and substrate-directed growth. *Nat. Chem.* **4**, 215–220 (2012).
5. N. Zhang, T. Wang, X. Wu, C. Jiang, T. Zhang, B. Jin, H. Ji, W. Bai, R. Bai, From 1D polymers to 2D polymers: Preparation of free-standing single-monomer-thick two-dimensional conjugated polymers in water. *ACS Nano* **11**, 7223–7229 (2017).
6. T. Bauer, Z. Zheng, A. Renn, R. Enning, A. Stemmer, J. Sakamoto, A. D. Schlüter, Synthesis of free-standing, monolayered organometallic sheets at the air/water interface. *Angew. Chem. Int. Ed.* **50**, 7879–7884 (2011).
7. K. Baek, G. Yun, Y. Kim, D. Kim, R. Hota, I. Hwang, D. Xu, Y. H. Ko, G. H. Gu, J. H. Suh, C. G. Park, B. J. Sung, K. Kim, Free-standing, single-monomer-thick two-dimensional polymers through covalent self-assembly in solution. *J. Am. Chem. Soc.* **135**, 6523–6528 (2013).
8. A. Shchyrba, C. Wäckerlin, J. Nowakowski, S. Nowakowska, J. Björk, S. Fatayer, J. Girovsky, T. Nijs, S. C. Martens, A. Kleibert, M. Stöhr, N. Ballav, T. A. Jung, L. H. Gade, Controlling the dimensionality of on-surface coordination polymers via endo- or exoligation. *J. Am. Chem. Soc.* **136**, 9355–9363 (2014).
9. M. Moradi, L. G. Tulli, J. Nowakowski, M. Baljozovic, T. A. Jung, P. Shahgaldian, Two-dimensional calix[4]arene-based metal–organic coordination networks of tunable crystallinity. *Angew. Chem. Int. Ed.* **56**, 14395–14399 (2017).
10. R. Dong, T. Zhang, X. Feng, Interface-assisted synthesis of 2D materials: Trend and challenges. *Chem. Rev.* **118**, 6189–6235 (2018).
11. J. L. Atwood, L. J. Barbour, M. J. Hardie, C. L. Raston, Metal sulfonatocalix[4,5]arene complexes: bi-layers, capsules, spheres, tubular arrays and beyond. *Coord. Chem. Rev.* **222**, 3–32 (2001).
12. S. J. Dalgarno, J. L. Atwood, C. L. Raston, Sulfonatocalixarenes: Molecular capsule and 'Russian doll' arrays to structures mimicking viral geometry. *Chem. Commun.* 4567–4574 (2006).
13. P. A. Wood, S. J. Borwick, D. J. Watkin, W. D. S. Motherwell, F. H. Allen, Dipolar C≡N…C≡N interactions in organic crystal structures: Database analysis and calculation of interaction energies. *Acta Cryst.* **B64**, 393–396 (2008).
14. J. F. Moulder, W. F. Stickle, P. E. Sobol, K. D. Bomben, *Handbook of X-ray Photoelectron Spectroscopy*, J. Chastain, Ed. (Perkin-Elmer Corporation Physical Electronics Division, 1992).
15. A. Chernenkaya, K. Medjanik, P. Nagel, M. Merz, S. Schuppler, E. Canadell, J.-P. Pouget, G. Schönhense, Nature of the empty states and signature of the charge density wave instability and upper Peierls transition of TTF-TCNQ by temperature-dependent NEXAFS spectroscopy. *Eur. Phys. J. B.* **88**, 13 (2015).
16. S. Yu, S. Ahmadi, M. Zuleta, H. Tian, K. Schulte, A. Pietzsch, F. Hennies, J. Weissenrieder, X. Yang, M. Göthelid, Adsorption geometry, molecular interaction, and charge transfer of triphenylamine-based dye on rutile TiO_2(110). *J. Chem. Phys.* **133**, 224704 (2010).
17. J. Stöhr, *NEXAFS Spectroscopy* (Springer Series in Surface Sciences, Springer, ed. 1, 1996).
18. U. Flechsig, F. Nolting, A. Fraile Rodríguez, J. Krempaský, C. Quitmann, T. Schmidt, S. Spielmann, D. Zimoch, Performance measurements at the SLS SIM beamline. *AIP Conf. Proc.* **1234**, 319–322 (2010).
19. M. Pfeffermann, R. Dong, R. Graf, W. Zajaczkowski, T. Gorelik, W. Pisula, A. Narita, K. Müllen, X. Feng, Free-standing monolayer two-dimensional supramolecular organic framework with good internal order. *J. Am. Chem. Soc.* **137**, 14525–14532 (2015).
20. Q. An, Q. Chen, W. Zhu, Y. Li, C.-a. Tao, H. Yang, Z. Li, L. Wan, H. Tian, G. Li, A facile method for preparing one-molecule-thick free-standing organic nanosheets with a regular square shape. *Chem. Commun.* **46**, 725–727 (2010).
21. W. Bai, Z. Jiang, A. E. Ribbe, S. Thayumanavan, Smart organic two-dimensional materials based on a rational combination of non-covalent interactions. *Angew. Chem. Int. Ed.* **55**, 10707–10711 (2016).
22. I. Müllerová, M. Hovorka, L. Frank, A method of imaging ultrathin foils with very low energy electrons. *Ultramicroscopy* **119**, 78–81 (2012).
23. R. Dong, M. Pfeffermann, H. Liang, Z. Zheng, X. Zhu, J. Zhang, X. Feng, Large-area, free-standing, two-dimensional supramolecular polymer single-layer sheets for highly efficient electrocatalytic hydrogen evolution. *Angew. Chem. Int. Ed.* **54**, 12058–12063 (2015).
24. D. Zhang, Y. Zhu, L. Liu, X. Ying, C.-E. Hsiung, R. Sougrat, K. Li, Y. Han, Atomic-resolution transmission electron microscopy of electron beam–sensitive crystalline materials. *Science* **359**, 675–679 (2018).
25. J. Miao, T. Ishikawa, I. K. Robinson, M. M. Murnane, Beyond crystallography: Diffractive imaging using coherent x-ray light sources. *Science* **348**, 530–535 (2015).
26. M. H. Düker, R. Gómez, C. M. L. Vande Velde, V. A. Azov, Upper rim tetrathiafulvalene-bridged calix[4]arenes. *Tetrahedron Lett.* **52**, 2881–2884 (2011).

27. C. D. Gutsche, K. C. Nam, Calixarenes. 22. Synthesis, properties, and metal complexation of aminocalixarenes. *J. Am. Chem. Soc.* **110**, 6153–6162 (1988).
28. N. Moridi, C. Wäckerlin, V. Rullaud, R. Schelldorfer, T. A. Jung, P. Shahgaldian, Langmuir–Blodgett monolayer stabilization using supramolecular clips. *Chem. Commun.* **49**, 367–369 (2013).
29. X. Llopart, R. Ballabriga, M. Campbell, L. Tlustos, W. Wong, Timepix, a 65k programmable pixel readout chip for arrival time, energy and/or photon counting measurements. *Nucl. Instr. Meth. Phys. Res. A* **581**, 485–494 (2007).
30. E. van Genderen, M. T. B. Clabbers, P. P. Das, A. Stewart, I. Nederlof, K. C. Barentsen, Q. Portillo, N. S. Pannu, S. Nicolopoulos, T. Gruene, J. P. Abrahams, Ab initio structure determination of nanocrystals of organic pharmaceutical compounds by electron diffraction at room temperature using a Timepix quantum area direct electron detector. *Acta Cryst. A* **72**, 236–242 (2016).
31. M. T. B. Clabbers, E. van Genderen, W. Wan, E. L. Wiegers, T. Gruene, J. P. Abrahams, Protein structure determination by electron diffraction using a single three-dimensional nanocrystal. *Acta Cryst.* **D73**, 738–748 (2017).
32. K. Suwinska, O. Shkurenko, C. Mbernba, A. Leydier, S. Jebors, A. W. Coleman, R. Matar, P. Falson, Trianionic calix[4]arene monoalkoxy derivatives: Synthesis, solid-state structures and self-assembly properties. *New J. Chem.* **32**, 1988–1998 (2008).

Acknowledgments: We thank R. Schelldorfer for technical support for XPS and AFM measurements and M. Clabbers for the electron diffraction data conversion (from the direct electron detector format). Part of this work was performed at the Surface/Interface: Microscopy (SIM) beamline of the Swiss Light Source, Paul Scherrer Institute, Villigen, Switzerland. **Funding:** The financial support of the Swiss Nanoscience Institute (grant nos. P1305 and P1308) is gratefully acknowledged. C.W. acknowledges financial support by the University Research Priority Program LightChEC of the University of Zürich, Switzerland. M.B. and T.A.J. acknowledge the Swiss National Science Foundation (grant nos. 200020-153549, 200020-175800, and 206021-113149). This research used resources of the Advanced Light Source, which is a DOE Office of Science User Facility under contract no. DE-AC02-05CH11231. This research was in part supported by the SNF [grant no. 5204.23000.160.02; "SwissFEDI, a free electron diffraction instrument for nano-diffraction of biological specimens" (2016–2019) to J.P.A.]. **Author contributions:** P.S. and T.A.J. conceived the research. M.M. and L.G.T. performed LB, BAM, LS, contact angle, ellipsometry, and AFM experiments and analyzed the data. M.M. and M.B. conducted XPS experiments and analyzed the data. N.L.O. and E.v.G. performed EM data collection, with H.S., J.P.A., and C.P. interpreted the data. L.G.T. and M.M. synthesized the molecule. C.W., M.B., O.P., and A.K. acquired the NEXAFS data and analyzed the data. S.J.D. and S.J.T. performed the single-crystal x-ray diffraction work. M.M., T.A.J., P.F.-X.C., and P.S. wrote the paper. All authors commented on the manuscript. **Competing interests:** The authors declare that they have no competing interests. **Data and materials availability:** All data needed to evaluate the conclusions in the paper are present in the paper and/or the Supplementary Materials. Additional data related to this paper may be requested from the authors. Crystallographic data for the structure of compound **1**, reported in the Supplementary Materials, have been deposited at the Cambridge Crystallographic Data Centre under deposition no. CCDC 1586569. Copies of the data can be obtained free of charge at www.ccdc.cam.ac.uk/data_request/cif.

Submitted 17 September 2018
Accepted 11 January 2019
Published 22 February 2019
10.1126/sciadv.aav4489

Citation: M. Moradi, N. L. Opara, L. G. Tulli, C. Wäckerlin, S. J. Dalgarno, S. J. Teat, M. Baljozovic, O. Popova, E. van Genderen, A. Kleibert, H. Stahlberg, J. P. Abrahams, C. Padeste, P. F.-X. Corvini, T. A. Jung, P. Shahgaldian, Supramolecular architectures of molecularly thin yet robust free-standing layers. *Sci. Adv.* **5**, eaav4489 (2019).

ScienceAdvances

Supramolecular architectures of molecularly thin yet robust free-standing layers

Mina Moradi, Nadia L. Opara, Ludovico G. Tulli, Christian Wäckerlin, Scott J. Dalgarno, Simon J. Teat, Milos Baljozovic, Olha Popova, Eric van Genderen, Armin Kleibert, Henning Stahlberg, Jan Pieter Abrahams, Celestino Padeste, Philippe F.-X. Corvini, Thomas A. Jung and Patrick Shahgaldian

Sci Adv 5 (2), eaav4489.
DOI: 10.1126/sciadv.aav4489

Science Advances
AAAS

advances.sciencemag.org/cgi/content/full/5/2/eaav4489/DC1

Supplementary Materials for

Supramolecular architectures of molecularly thin yet robust free-standing layers

Mina Moradi, Nadia L. Opara, Ludovico G. Tulli, Christian Wäckerlin, Scott J. Dalgarno, Simon J. Teat, Milos Baljozovic, Olha Popova, Eric van Genderen, Armin Kleibert, Henning Stahlberg, Jan Pieter Abrahams, Celestino Padeste, Philippe F.-X. Corvini, Thomas A. Jung*, Patrick Shahgaldian*

*Corresponding author. Email: patrick.shahgaldian@fhnw.ch (P.S.); thomas.jung@psi.ch (T.A.J.)

Published 22 February 2019, *Sci. Adv.* **5**, eaav4489 (2019)
DOI: 10.1126/sciadv.aav4489

This PDF file includes:

Section S1. Materials and methods

All chemicals were purchased as reagent grade from Sigma-Aldrich (Switzerland) and used without further purification. Solvents (analytical grade) were used without any further purification. 5,11,17,23-tetrakis(chloromethyl)-25,26,27,28-tetrapropoxy calix[4]arene (Cl-C4A-OC_3) was synthesized as previously reported (*26*).

Synthesis of 5,11,17,23-tetramethylcyano-25,26,27,28-tetrapropoxy calix[4]arene (**1**) was achieved by following a modified literature procedure (*27*).

A Millipore Synergy purification system was used to produce nanopure water with resistivity of 18.2 MΩ.cm. Deuterated solvents for NMR spectroscopic analyses were used as received from Arma AG (Switzerland). ^{1}H and ^{13}C NMR spectra were recorded with a Bruker spectrometer 300 and 75 MHz, respectively. All NMR peaks are reported as chemical shift in parts per million (ppm) using tetramethylsilane as internal standard. All coupling constants (*J*) are quoted in Hertz (Hz). The abbreviations s (singlet), d (doublet), t (triplet) and m (multiplet) are used to describe multiplicities. Electrospray ionization mass spectra were recorded in positive ion mode on a thermoquest LCQ Deca instrument. Elemental analysis was measured on a Leco CHN900 microanalyser. Melting points were measured using a Büchi 530 apparatus as triplicates to ensure the reproducibility of the result.

Section S2. Contact angle measurement

Contact angles were measured using a commercial Krüss ®Easy drop optical system (Krüss, GmbH, Germany). Drops of 3 µL of nanopure water were used for measuring static water contact angle on samples. To ensure reproducibility, the measurements were repeated at five different positions on each sample.

Section S3. Spectroscopic ellipsometry

Ellipsometry measurements were carried out using an imaging and spectroscopic system (EP3 Ellipsometer Accurion) in a nulling PCSA (polarizer-compensator-sample-analyzer) set-up. For all the ellipsometry experiments, OTS-coated silicon wafers were used (*28*).

Section S4. X-ray photoelectron spectroscopy

X-ray photoelectron spectroscopy (XPS) spectra were acquired using Specs FOCUS 500 monochromatic Al K_α ($h\nu$ = 1486.7 eV) with XR 50 M excitation source in normal emission using a Specs PHOIBOS 150 electron analyzer. The C1s core level of HOPG was used as reference for the binding energies and was assigned to 284.5 eV. The measurements were performed in ultra-high vacuum system with base pressure of 10^{-11} mbar.

Section S5. Atomic force microscopy

Atomic force microscopy experiments were carried out in the PeakForce Tapping® mode using a Multimode 8 instrument (Bruker) equipped with a Nanoscope V controller with a scanasyst-air-HR silicon tip on silicon nitride lever.

Section S6. Transmission electron microscopy

The monolayer of **1**, prepared as detailed above, was transferred via the LS method on an electron microscopy grid (copper grid with lacey carbon, Ted Pella Inc., USA) placed on the designed and fabricated polydimethylsiloxane support of required geometry. The TEM imaging and diffraction data collection were done with a TEM system equipped with CCD camera Ceta (16M Pixel CMOS) and Timepix direct electron detector (*29-31*). The images were collected in cryo-conditions (sample placed on the cryoholder, inserted to the

microscope and cooled down with liquid nitrogen before illumination by the electrons) with Talos (FEI) machine operating at 200 keV accelerating voltage (high accelerating voltages are necessary to reduce melting of the material in the electron beam and enable the imaging) and vacuum of 3.5×10^{-8} Torr. The exposure parameters were adjusted to achieve sufficient visibility of the ultrathin material: to increase the contrast image was strongly defocused (>100 μm); gun lens set to the level 5; spot size set to the level 5; electron beam intensity 63.1% and objective lens: 82.1%. Additionally, SA and objective apertures were retracted. The diffraction image shows a stack of the 300 frames. Each frame was an exposure to the electrons of the $\lambda = 2.51$ pm for 0.5 s. The detector distance was calibrated with aluminum grid and theoretical camera length was determined to be 1890 mm.

Supplementary materials

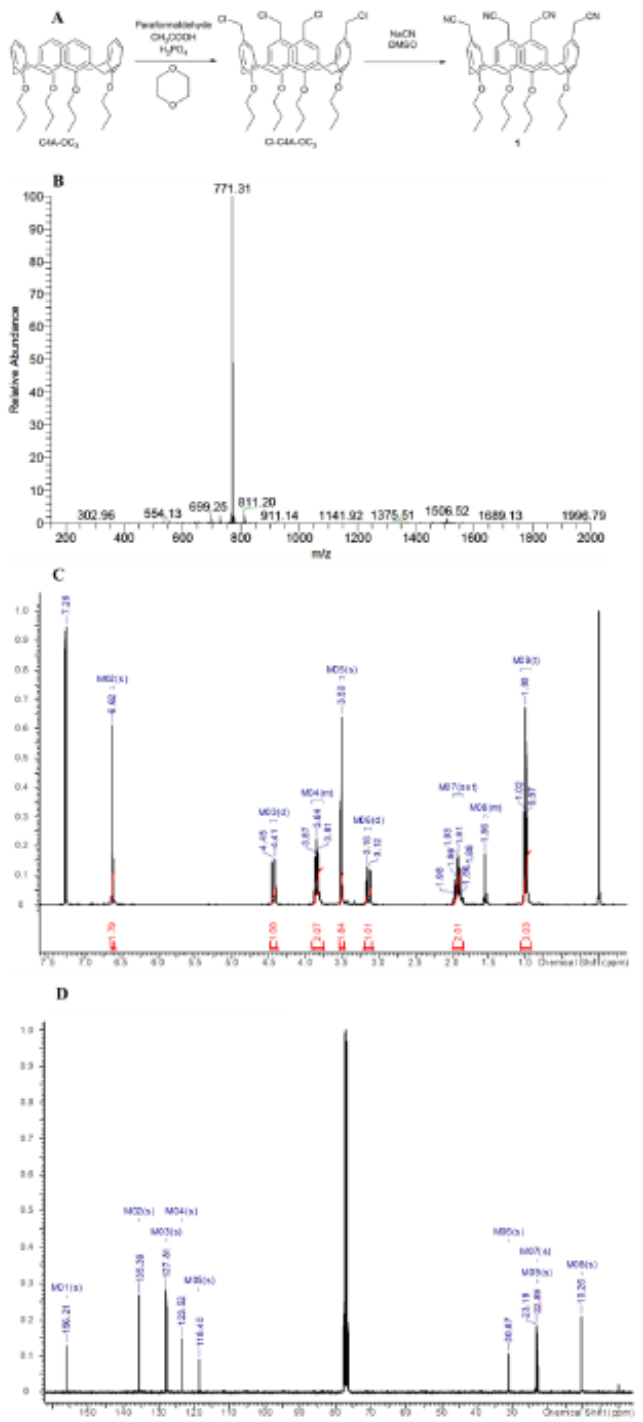

Fig. S1. Synthetic route to 5,11,17,23-tetramethylcyano-25,26,27,28-tetrapropoxy calix[4]arene (1) and spectroscopic details of 1. (**A**) Synthetic route to **1** through the chloro-methlyation of the parent tetra-propyloxy-calix[4]arene ($C4A\text{-}OC_3$), locked in the cone conformation, to yield the tetra-chloromethyl derivative ($Cl\text{-}C4A\text{-}OC_3$) followed by the nucleophilic substitution of chlorine atoms using NaCN to yield **1**. (**B**) ESI mass chromatogram of **1**. (**C**) ^{1}H NMR spectrum of **1**. (**D**) ^{13}C NMR spectrum of **1**.

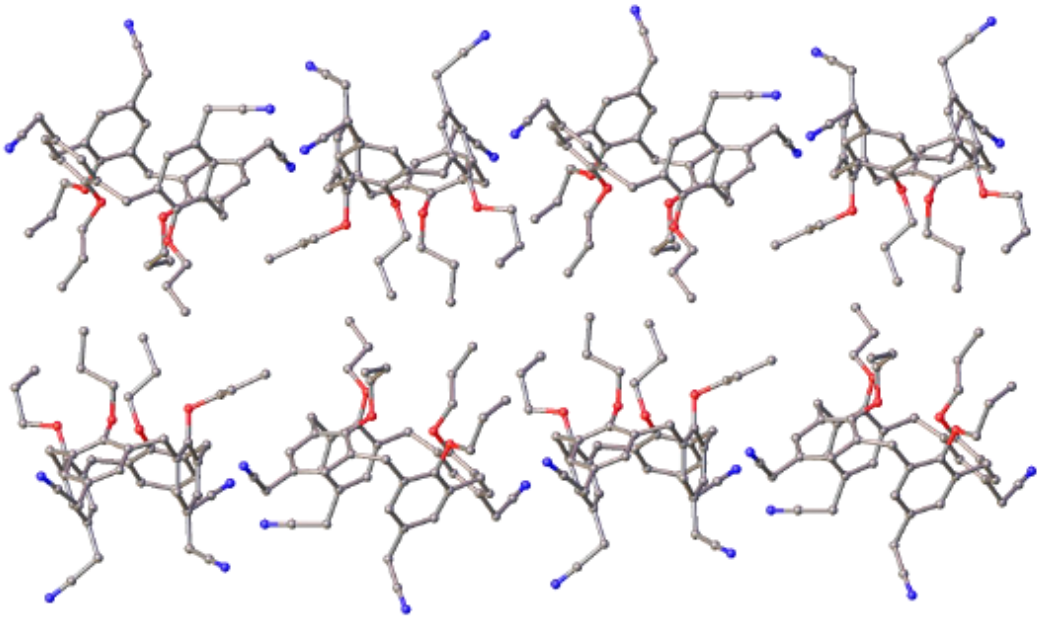

Fig. S2. X-ray crystal structure determination details of 1. Crystal data for **1** (CCDC 1586569): $C_{96}H_{104}N_8O_8$, M =1497.87 g/mol, triclinic, space group P-1 (no. 2), a = 14.6702(7) Å, b = 14.7632(7) Å, c = 20.0756(9) Å, α = 82.227(3)°, β = 76.317(2)°, γ = 89.982(3)°, V = 4183.5(3) Å^3, Z = 2, T = 100(2) K, 34673 reflections measured (4.28° ≤ 2Θ ≤ 57.33°), 16006 unique (R_{int} = 0.0659, R_{sigma} = 0.0909) which were used in all calculations. The final R_1 was 0.0799 ($I > 2\sigma(I)$) and wR_2 was 0.1982 (all data). Symmetry expanded structure of **1** bilayer formation by association of hydrophobic chains at the macrocycle lower-rim.

The asymmetric unit contains two molecules of **1**, as well as diffuse density associated with badly disordered solvent of crystallization; this was removed during refinement using a solvent mask, greatly improving the agreement indices. The density associated with the disordered solvent of crystallization occupies space within the hydrophobic layer of the extended structure, generated by the packing of symmetry equivalents (s.e.) of **1**. There is no indication of the presence of significant intermolecular interactions between the peaks in the density map and atoms of neighboring *s.e.* of **1**, so one may assume that the presence of the solvent is very unlikely to influence bilayer assembly; this lack of interactions likely promotes the severe disorder that in fact compromises modelling. We identified two crystallographically unique CH· · · N interactions with distances of 2.612 and 2.664 Å, and one CH· · · π interaction with a CH· · · aromatic centroid distance of 2.611 Å. It is noteworthy that a search of the Cambridge structural database for upper-rim methyl-cyano functionalized calix[4]arenes returned just 6 hits, and these structures display similar intermolecular interactions as those observed in the present case (*32*).

Table S1. *X*-ray crystal structure determination detail of 1. Crystal data and structure refinement for compound **1** (CCDC 1586569).

Empirical formula	$C_{96}H_{104}N_8O_8$
Formula weight	1497.87
Temperature/K	100(2)
Crystal system	triclinic
Space group	P-1
a/Å	14.6702(7)
b/Å	14.7632(7)
c/Å	20.0756(9)
α/°	82.227(3)
β/°	76.317(2)
γ/°	89.982(3)
Volume/Å^3	4183.5(3)
Z	2
ρ_{calc}g/cm^3	1.189
μ/mm^{-1}	0.090
F(000)	1600.0
Crystal size/mm^3	0.08 × 0.06 × 0.05
Radiation	synchrotron (λ = 0.7749)
2Θ range for data collection/°	4.28 to 57.33
Index ranges	$-18 \leq h \leq 18$, $-18 \leq k \leq 18$, $-24 \leq l \leq 24$
Reflections collected	34673
Independent reflections	16006 [R_{int} = 0.0659, R_{sigma} = 0.0909]
Data/restraints/parameters	16006/0/1017
Goodness-of-fit on F^2	1.055
Final R indexes [I>=2σ (I)]	R_1 = 0.0799, wR_2 = 0.1818
Final R indexes [all data]	R_1 = 0.1132, wR_2 = 0.1982
Largest diff. peak/hole / e Å^{-3}	0.56/-0.48

Table S2. *X*-ray crystal structure determination detail of 1. Fractional atomic coordinates ($\times 10^4$) and equivalent isotropic displacement parameters ($Å^2 \times 10^3$) for **1** (CCDC 1586569). U_{eq} is defined as 1/3 of the trace of the orthogonalised U_{IJ} tensor.

Atom	*x*	*y*	*z*	U(eq)
O7	-1473.9(14)	3841.3(14)	2219.1(11)	19.9(5)
O1	8339.2(14)	8842.2(14)	2215.0(11)	20.1(5)
O8	945.7(15)	4481.6(14)	1785.4(11)	20.7(5)
O6	170.1(15)	2305.5(14)	2341.3(12)	21.8(5)
O5	2391.7(15)	2832.6(14)	1659.7(11)	21.4(5)
O3	4859.7(15)	7834.2(14)	1584.8(11)	20.5(5)
O2	6607.1(15)	7306.5(14)	2316.1(11)	20.3(5)
O4	6220.0(15)	9458.6(14)	1752.6(12)	21.1(5)
N2	6038(2)	2722(2)	4075.4(16)	31.6(7)
N6	-449(2)	-2261(2)	4098.5(16)	30.6(7)
N4	5073(2)	14024(2)	2190.1(18)	35.5(8)
N8	1727(2)	9042(2)	2306.9(18)	36.4(8)
C54	2307(2)	2919(2)	2349.6(16)	17.6(6)
C13	6517(2)	6567(2)	2828.7(16)	18.5(6)
C25	5923(2)	11494(2)	2623.6(17)	21.4(7)
N3	1547(2)	8738(2)	4535.3(16)	36.9(8)
N5	3828(2)	3778(2)	4571.9(17)	37.9(8)
C68	-1268(2)	3855(2)	2856.6(17)	18.3(6)
C75	1165(2)	5209(2)	2086.4(16)	18.1(6)
C6	7697(2)	8854(2)	2842.4(16)	17.9(6)
C9	7058(2)	5698(2)	3748.0(17)	20.2(7)
C66	-631(2)	4636(2)	3622.4(18)	21.7(7)
C10	6273(2)	5111(2)	3889.7(17)	20.4(7)
C4	6867(2)	8075(2)	3942.8(17)	20.8(7)
C5	7516(2)	8060(2)	3324.2(17)	18.5(7)
C49	2532(2)	3759(2)	2534.5(17)	19.1(7)
C70	435(2)	5750(2)	2370.3(16)	18.2(6)
C26	6342(2)	10758(2)	2324.7(16)	18.5(7)
C53	1965(2)	2168(2)	2858.3(18)	20.6(7)
C14	4929(2)	6261(2)	2612.7(17)	21.5(7)
C1	7197(2)	9646(2)	2967.6(17)	18.9(7)
C8	7183(2)	6442(2)	3226.0(17)	18.7(7)
C59	-1238(2)	703(2)	3771.9(17)	21.6(7)
C11	5593(2)	5286(2)	3515.6(17)	20.5(7)
C22	4850(2)	10330(2)	2099.1(17)	19.9(7)
C63	-1418(2)	3061(2)	3338.3(17)	19.0(7)
C57	383(2)	306(2)	3570.0(17)	22.3(7)
C71	642(2)	6488(2)	2682.0(17)	20.1(7)
C56	629(2)	1032(2)	3037.2(17)	20.0(7)
C27	5809(2)	10206(2)	2039.0(17)	19.1(7)
C2	6555(2)	9640(2)	3598.2(17)	22.0(7)
C16	4097(2)	7254(2)	3473.3(17)	21.9(7)
C24	4984(2)	11670(2)	2657.2(17)	21.7(7)
C74	2077(2)	5336(2)	2171.5(16)	18.6(7)
C15	4488(2)	7153(2)	2787.9(17)	19.4(7)

C20	4495(2)	7910(2)	2275.5(17)	19.6(7)
C92	-605(2)	-1562(2)	4275.0(18)	23.4(7)
C28	7303(2)	10458(2)	2400.4(18)	21.0(7)
C72	1558(2)	6667(2)	2727.8(17)	20.3(7)
C51	2198(2)	3066(2)	3732.7(17)	21.7(7)
C19	4171(2)	8753(2)	2455.6(17)	19.3(7)
C73	2253(2)	6073(2)	2493.8(17)	20.9(7)
C23	4451(2)	11073(2)	2410.5(18)	21.4(7)
C67	-841(2)	4639(2)	2978.8(17)	19.1(7)
C62	-1736(2)	2170(2)	3159.0(18)	21.6(7)
C76	2805(2)	4615(2)	2009.6(17)	20.0(7)
C12	5699(2)	6015(2)	2987.1(17)	18.8(7)
C58	-546(2)	125(2)	3929.3(17)	22.2(7)
C21	4248(2)	9605(2)	1923.4(18)	21.4(7)
C7	7954(2)	7166(2)	3150.0(18)	20.7(7)
C65	-810(2)	3864(2)	4118.3(17)	22.4(7)
C44	6086(2)	3425(2)	4247.8(18)	24.7(7)
C17	3728(2)	8076(2)	3660.4(17)	22.6(7)
C48	4835(2)	13349(2)	2543.4(19)	26.0(8)
C52	1923(2)	2257(2)	3544.6(18)	21.9(7)
C55	1644(2)	1277(2)	2672.3(18)	22.3(7)
C61	-85(2)	1579(2)	2858.7(17)	18.5(6)
C3	6390(2)	8871(2)	4092.7(17)	20.7(7)
C69	-564(2)	5453(2)	2418.3(17)	19.9(7)
C18	3789(2)	8820(2)	3148.9(17)	20.6(7)
C50	2474(2)	3817(2)	3225.8(17)	21.0(7)
C89	2211(2)	3145(2)	4476.8(18)	27.7(8)
C43	6144(2)	4318(2)	4479.1(18)	25.0(7)
C60	-1016(2)	1440(2)	3247.3(17)	20.3(7)
C64	-1195(2)	3079(2)	3969.5(18)	22.0(7)
C29	9279(2)	9150(2)	2220.6(18)	23.8(7)
C95	1765(2)	7468(2)	3071.0(19)	25.6(7)
C93	-591(3)	3861(2)	4821.7(18)	28.9(8)
C35	4252(2)	7361(2)	1267.7(18)	25.8(7)
C90	3117(2)	3507(2)	4529.1(18)	26.6(8)
C46	2301(3)	8497(2)	4478.6(18)	27.4(8)
C96	1739(2)	8356(2)	2641(2)	26.9(8)
C80	-135(2)	2230(2)	1719.6(18)	25.8(7)
C83	-2401(2)	4164(2)	2197.2(19)	24.9(7)
C81	520(2)	1704(2)	1225.8(18)	27.2(8)
N1	6527(3)	9435(3)	5673.9(19)	52.3(10)
C38	6447(2)	9550(2)	1012.8(18)	27.0(8)
C32	7321(2)	7242(2)	1694.4(18)	24.9(7)
C41	5695(2)	8869(2)	4784.7(18)	27.9(8)
C30	9888(2)	9157(2)	1503.9(18)	26.4(7)
C45	3258(2)	8161(3)	4405.7(18)	29.8(8)
C91	-803(2)	-671(2)	4513.2(18)	26.6(8)
C47	4542(2)	12478(2)	2990.7(18)	23.8(7)
N7	-2040(3)	4448(3)	5664(2)	56(1)
C86	1312(2)	4524(2)	1051.0(17)	26.1(7)

C31	10023(3)	8212(2)	1276.6(19)	29.5(8)
C36	3557(3)	7979(3)	1008(2)	31.5(8)
C42	6144(3)	9187(3)	5292(2)	33.7(9)
C39	7402(3)	9993(2)	681.6(19)	33.1(8)
C84	-2517(3)	4183(2)	1471.6(19)	30.6(8)
C33	6965(2)	6765(2)	1176.2(18)	29.0(8)
C87	650(3)	4956(2)	633.3(19)	29.2(8)
C82	148(3)	1632(3)	589(2)	35.2(9)
C88	627(3)	5995(2)	572(2)	33.7(9)
C85	-2483(3)	3245(3)	1228(2)	34.8(9)
C94	-1388(3)	4190(3)	5309(2)	35.7(9)
C37	2934(3)	7456(3)	666(2)	42.3(10)
C34	7744(3)	6731(3)	529(2)	45.2(10)
C40	7665(3)	9995(3)	-98(2)	42(1)
C77	3329(3)	2687(3)	1283(2)	40.5(10)
C79	4359(3)	1724(3)	506(2)	52.1(12)
C78	3399(3)	1887(3)	932(3)	55.3(13)

Table S3. *X*-ray crystal structure determination detail of 1. Anisotropic displacement parameters ($Å^2 \times 10^3$) for **1**. The anisotropic displacement factor exponent takes the form: $-2\pi^2[h^2a^{*2}U_{11}+2hka^*b^*U_{12}+\ldots]$.

Atom	U_{11}	U_{22}	U_{33}	U_{23}	U_{13}	U_{12}
O7	16.2(11)	21.8(11)	25.5(12)	-7.4(9)	-10.1(9)	5.6(9)
O1	15.1(11)	21.7(11)	25.0(12)	-7.0(9)	-5.5(9)	3.4(9)
O8	21.5(11)	18.0(11)	24.8(12)	-5.8(9)	-8.1(10)	2.9(9)
O6	22.4(11)	16.2(11)	25.3(12)	0.6(9)	-4.9(10)	-0.9(9)
O5	20.0(11)	20.4(11)	24.3(12)	-5.4(9)	-4.9(10)	5.1(9)
O3	20.2(11)	19.4(11)	23.3(12)	-3.4(9)	-7.7(9)	-0.2(9)
O2	21.2(11)	16.8(11)	22.5(12)	-0.5(9)	-5.9(9)	2.1(9)
O4	21.7(11)	16.0(11)	26.5(13)	-5.8(9)	-6(1)	4.5(9)
N2	32.2(17)	26.1(16)	37.6(18)	-0.7(14)	-12.6(14)	2.7(13)
N6	28.3(16)	25.5(16)	36.8(18)	-1.2(14)	-7.3(14)	2.6(13)
N4	30.8(17)	20.6(16)	55(2)	-5.4(15)	-9.7(16)	5.8(13)
N8	33.8(17)	23.9(16)	55(2)	-7.2(15)	-16.4(16)	2.0(13)
C54	13.4(14)	19.7(15)	21.4(17)	-3.2(13)	-6.9(13)	6.1(12)
C13	21.1(16)	12.3(14)	21.9(17)	-3.1(12)	-4.1(13)	5.4(12)
C25	18.4(15)	16.8(15)	30.3(19)	-4.2(13)	-7.7(14)	1.7(12)
N3	31.5(18)	48(2)	29.5(18)	-2.0(15)	-5.6(14)	9.2(15)
N5	32.2(18)	49(2)	31.3(18)	-0.1(15)	-8.6(15)	-6.0(15)
C68	12.4(14)	17.5(15)	26.4(18)	-6.4(13)	-5.4(13)	5.0(12)
C75	21.4(16)	13.5(14)	20.6(17)	-2.4(12)	-7.4(13)	0.5(12)
C6	16.1(15)	17.7(15)	23.0(17)	-7.6(13)	-7.9(13)	1.6(12)
C9	20.3(16)	17.7(15)	26.4(18)	-7.5(13)	-10.8(14)	7.1(13)
C66	18.5(16)	16.9(15)	31.4(19)	-7.6(14)	-7.2(14)	3.3(12)
C10	24.4(17)	15.4(15)	21.9(17)	-3.1(13)	-6.1(14)	4.8(13)
C4	20.4(16)	17.8(15)	26.5(18)	-3.5(13)	-9.7(14)	3.9(13)
C5	14.7(15)	19.2(15)	25.4(17)	-7.4(13)	-9.8(13)	4.5(12)
C49	13.6(14)	18.1(15)	26.0(18)	-2.2(13)	-6.1(13)	6.2(12)
C70	17.7(15)	14.9(15)	22.0(17)	-0.4(13)	-6.1(13)	1.4(12)
C26	17.9(15)	13.5(14)	23.6(17)	-0.6(13)	-5.0(13)	2.4(12)
C53	13.9(15)	18.6(15)	31.9(19)	-4.9(14)	-9.9(14)	6.2(12)
C14	21.2(16)	20.1(16)	24.6(18)	-4.2(13)	-7.7(14)	3.4(13)
C1	15.2(15)	17.3(15)	27.0(18)	-4.9(13)	-9.7(13)	-0.1(12)
C8	17.6(15)	13.7(14)	26.2(18)	-5.9(13)	-6.3(13)	6.6(12)
C59	19.9(16)	17.4(15)	27.5(18)	-6.4(13)	-4.0(14)	-2.8(13)
C11	18.6(15)	15.5(15)	28.1(18)	-4.7(13)	-5.7(14)	1.4(12)
C22	18.4(15)	15.9(15)	25.8(18)	1.4(13)	-8.4(14)	0.8(12)
C63	10.4(14)	18.2(15)	28.9(18)	-6.6(13)	-3.8(13)	1.8(12)
C57	23.5(17)	16.6(15)	28.4(19)	-5.0(13)	-8.1(14)	3.5(13)
C71	19.3(16)	15.3(15)	25.9(18)	-3.5(13)	-5.6(14)	1.5(12)
C56	18.8(16)	17.4(15)	26.1(18)	-6.5(13)	-7.7(14)	0.8(12)
C27	19.7(16)	11.5(14)	25.5(18)	-0.7(13)	-5.2(13)	2.1(12)
C2	19.9(16)	18.6(16)	29.1(19)	-8.5(14)	-6.0(14)	3.8(13)
C16	16.9(15)	23.1(16)	27.2(18)	0.1(14)	-10.4(14)	3.2(13)
C24	22.1(16)	16.2(15)	26.9(18)	-3.0(13)	-5.8(14)	4.1(13)
C74	18.4(15)	15.1(15)	20.5(17)	0.9(12)	-3.0(13)	-0.4(12)
C15	13.0(14)	18.2(15)	28.3(18)	-3.2(13)	-7.6(13)	2.0(12)

C20	16.0(15)	19.1(15)	23.7(17)	-1.1(13)	-5.9(13)	-0.5(12)
C92	20.0(16)	23.3(18)	25.2(18)	3.1(14)	-5.4(14)	0.8(13)
C28	17.2(15)	15.2(15)	32.1(19)	-4.6(13)	-8.5(14)	3.0(12)
C72	22.6(16)	14.9(15)	24.7(18)	-3.5(13)	-7.5(14)	0.6(13)
C51	13.0(15)	25.2(17)	27.0(18)	-4.9(14)	-4.6(13)	3.1(13)
C19	14.7(15)	17.6(15)	29.0(18)	-1.9(13)	-12.8(14)	2.0(12)
C73	18.0(15)	18.6(15)	27.6(18)	-1.8(13)	-9.4(14)	-1.7(13)
C23	15.4(15)	17.4(15)	31.8(19)	-2.2(14)	-7.1(14)	4.7(12)
C67	13.1(14)	15.6(15)	30.0(18)	-5.7(13)	-6.6(13)	5.6(12)
C62	18.3(15)	17.6(15)	30.9(19)	-5.3(14)	-8.6(14)	1.6(13)
C76	16.9(15)	18.7(15)	24.1(17)	-3.7(13)	-4.2(13)	1.1(12)
C12	17.7(15)	14.7(14)	25.0(17)	-4.3(13)	-6.4(13)	5.7(12)
C58	24.1(17)	17.5(16)	25.2(18)	-3.8(13)	-5.6(14)	0.4(13)
C21	20.1(16)	16.7(15)	29.9(19)	-3.3(13)	-10.8(14)	1.2(13)
C7	14.0(15)	19.3(16)	30.4(19)	-5.3(14)	-7.5(14)	4.0(12)
C65	22.0(16)	22.4(16)	24.8(18)	-6.9(14)	-7.5(14)	2.5(13)
C44	24.4(17)	20.8(17)	28.8(19)	4.2(14)	-10.5(15)	3.1(14)
C17	19.3(16)	25.3(17)	27.3(18)	-4.6(14)	-12.9(14)	3.3(13)
C48	18.8(16)	22.3(18)	42(2)	-12.7(16)	-12.0(15)	8.2(14)
C52	15.2(15)	20.5(16)	27.9(18)	1.1(14)	-3.5(13)	1.5(12)
C55	17.2(15)	17.5(15)	32.0(19)	-3.9(14)	-5.1(14)	4.3(13)
C61	18.2(15)	14.9(15)	22.8(17)	-4.5(13)	-4.6(13)	-1.3(12)
C3	16.0(15)	23.3(16)	24.1(17)	-6.3(14)	-5.2(13)	0.9(13)
C69	16.1(15)	17.1(15)	27.4(18)	-3.3(13)	-6.7(13)	4.2(12)
C18	20.3(16)	17.1(15)	27.8(18)	-5.9(13)	-11.3(14)	5.3(13)
C50	18.1(15)	17.8(15)	28.5(18)	-6.4(13)	-6.2(14)	5.7(12)
C89	23.1(17)	34.6(19)	23.4(18)	-1.0(15)	-3.2(14)	-4.7(15)
C43	29.4(18)	20.9(16)	26.7(19)	-1.6(14)	-12.0(15)	0.9(14)
C60	18.1(15)	18.7(16)	27.3(18)	-8.1(13)	-9.1(14)	1.6(13)
C64	20.2(16)	18.3(16)	26.9(18)	-2.1(13)	-5.2(14)	1.3(13)
C29	14.4(15)	24.8(17)	34(2)	-7.9(15)	-7.0(14)	3.2(13)
C95	24.2(17)	22.6(17)	32(2)	-8.8(15)	-8.7(15)	2.4(14)
C93	32.4(19)	27.2(18)	31(2)	-4.0(15)	-14.7(16)	0.6(15)
C35	28.4(18)	29.2(18)	23.1(18)	-5.6(14)	-11.2(15)	-3.3(15)
C90	27.2(19)	28.7(18)	22.2(18)	1.2(14)	-5.3(15)	0.9(15)
C46	31(2)	27.6(18)	23.5(19)	-1.3(15)	-7.5(15)	1.5(15)
C96	22.2(17)	20.8(18)	42(2)	-12.1(16)	-11.7(16)	0.2(14)
C80	25.0(17)	25.2(17)	25.6(18)	0.3(14)	-5.0(15)	4.7(14)
C83	18.8(16)	23.3(17)	37(2)	-6.3(15)	-13.5(15)	6.6(13)
C81	31.1(19)	21.5(17)	30(2)	-3.9(14)	-8.4(16)	5.6(14)
N1	63(3)	58(2)	35(2)	-12.9(18)	-8.0(19)	-6(2)
C38	29.6(18)	25.4(17)	26.9(19)	-8.1(15)	-6.0(15)	5.6(14)
C32	20.7(16)	25.1(17)	26.6(19)	-0.2(14)	-2.9(14)	1.6(14)
C41	24.8(18)	24.2(17)	34(2)	-5.0(15)	-4.3(15)	4.1(14)
C30	21.7(17)	25.5(17)	29.7(19)	-1.2(15)	-3.1(15)	1.8(14)
C45	29.2(19)	35(2)	28(2)	-7.1(16)	-10.7(16)	8.2(16)
C91	28.9(18)	21.3(17)	28.3(19)	-3.0(14)	-4.6(15)	2.3(14)
C47	20.3(16)	21.2(16)	32.3(19)	-6.6(14)	-9.1(15)	6.7(13)
N7	72(3)	63(3)	37(2)	-14.8(19)	-16(2)	25(2)
C86	28.8(18)	26.9(18)	24.8(19)	-8.2(14)	-8.1(15)	8.7(15)

C31	29.0(19)	29.3(19)	28(2)	-6.8(15)	-1.8(16)	5.0(15)
C36	30.4(19)	39(2)	29(2)	-8.3(16)	-11.3(16)	3.1(16)
C42	40(2)	30.6(19)	28(2)	-5.3(16)	-1.4(17)	2.7(17)
C39	33(2)	27.5(19)	36(2)	-4.3(16)	-4.1(17)	1.9(16)
C84	26.0(18)	32.3(19)	36(2)	0.3(16)	-15.7(16)	0.6(15)
C33	29.5(19)	30.1(19)	28(2)	-7.3(15)	-5.5(15)	4.3(15)
C87	36(2)	30.2(19)	26.3(19)	-8.6(15)	-14.4(16)	7.5(16)
C82	41(2)	35(2)	33(2)	-7.8(17)	-12.9(18)	8.5(17)
C88	41(2)	31.0(19)	32(2)	-3.9(16)	-14.3(17)	6.8(17)
C85	34(2)	42(2)	33(2)	-7.1(17)	-15.6(17)	0.8(17)
C94	52(2)	32(2)	28(2)	-7.3(17)	-17.8(19)	10.1(18)
C37	45(2)	42(2)	48(3)	-6.7(19)	-27(2)	-2.5(19)
C34	44(2)	53(3)	36(2)	-15(2)	-0.6(19)	2(2)
C40	41(2)	41(2)	39(2)	-6.2(19)	0.1(19)	5.9(19)
C77	27(2)	63(3)	32(2)	-16(2)	-2.4(17)	16.2(19)
C79	56(3)	47(3)	41(3)	-1(2)	10(2)	21(2)
C78	42(3)	65(3)	65(3)	-35(3)	-11(2)	13(2)

Table S4. *X*-ray crystal structure determination detail of 1. Bond lengths for **1**.

Atom	Atom	Length/Å	Atom	Atom	Length/Å
O7	C68	1.385(4)	C22	C23	1.396(4)
O7	C83	1.449(4)	C22	C21	1.517(4)
O1	C6	1.385(4)	C63	C62	1.512(4)
O1	C29	1.455(4)	C63	C64	1.386(5)
O8	C75	1.374(4)	C57	C56	1.389(4)
O8	C86	1.437(4)	C57	C58	1.390(5)
O6	C61	1.372(4)	C71	C72	1.396(4)
O6	C80	1.440(4)	C56	C55	1.516(4)
O5	C54	1.384(4)	C56	C61	1.406(4)
O5	C77	1.436(4)	C2	C3	1.384(5)
O3	C20	1.383(4)	C16	C15	1.388(5)
O3	C35	1.441(4)	C16	C17	1.390(5)
O2	C13	1.379(4)	C24	C23	1.391(4)
O2	C32	1.441(4)	C24	C47	1.518(4)
O4	C27	1.386(4)	C74	C73	1.392(4)
O4	C38	1.430(4)	C74	C76	1.520(4)
N2	C44	1.145(4)	C15	C20	1.411(4)
N6	C92	1.142(4)	C20	C19	1.395(4)
N4	C48	1.144(4)	C92	C91	1.465(5)
N8	C96	1.140(4)	C72	C73	1.382(4)
C54	C49	1.403(4)	C72	C95	1.512(4)
C54	C53	1.406(4)	C51	C52	1.387(4)
C13	C8	1.398(4)	C51	C50	1.388(5)
C13	C12	1.399(4)	C51	C89	1.518(5)
C25	C26	1.385(4)	C19	C21	1.522(4)
C25	C24	1.389(4)	C19	C18	1.389(5)
N3	C46	1.145(5)	C67	C69	1.515(4)
N5	C90	1.144(4)	C62	C60	1.532(4)
C68	C63	1.396(4)	C58	C91	1.522(5)
C68	C67	1.394(4)	C65	C64	1.387(4)
C75	C70	1.393(4)	C65	C93	1.520(5)
C75	C74	1.404(4)	C44	C43	1.465(5)
C6	C5	1.397(4)	C17	C18	1.386(4)
C6	C1	1.400(4)	C17	C45	1.514(5)
C9	C10	1.392(4)	C48	C47	1.466(5)
C9	C8	1.392(4)	C61	C60	1.403(4)
C66	C67	1.397(5)	C3	C41	1.516(5)
C66	C65	1.389(5)	C89	C90	1.465(5)
C10	C11	1.388(4)	C29	C30	1.503(5)
C10	C43	1.524(4)	C95	C96	1.474(5)
C4	C5	1.377(5)	C93	C94	1.464(5)
C4	C3	1.400(4)	C35	C36	1.505(5)
C5	C7	1.515(4)	C46	C45	1.470(5)
C49	C76	1.519(4)	C80	C81	1.505(5)
C49	C50	1.384(5)	C83	C84	1.503(5)
C70	C71	1.395(4)	C81	C82	1.521(5)
C70	C69	1.508(4)	N1	C42	1.148(5)

C26	C27	1.394(4)		C38	C39	1.508(5)
C26	C28	1.513(4)		C32	C33	1.518(5)
C53	C52	1.388(5)		C41	C42	1.462(5)
C53	C55	1.520(4)		C30	C31	1.523(5)
C14	C15	1.515(4)		N7	C94	1.150(5)
C14	C12	1.516(4)		C86	C87	1.514(5)
C1	C2	1.387(5)		C36	C37	1.531(5)
C1	C28	1.519(4)		C39	C40	1.520(5)
C8	C7	1.523(4)		C84	C85	1.527(5)
C59	C58	1.392(4)		C33	C34	1.522(5)
C59	C60	1.388(5)		C87	C88	1.524(5)
C11	C12	1.387(4)		C77	C78	1.445(6)
C22	C27	1.397(4)		C79	C78	1.503(6)

Table S5. *X*-ray crystal structure determination detail of 1. Bond angles for **1**.

Atom	Atom	Atom	Angle/°	Atom	Atom	Atom	Angle/°
C68	O7	C83	113.2(2)	O3	C20	C19	118.9(3)
C6	O1	C29	113.1(2)	C19	C20	C15	120.9(3)
C75	O8	C86	116.9(2)	N6	C92	C91	179.0(4)
C61	O6	C80	115.3(2)	C26	C28	C1	109.5(3)
C54	O5	C77	114.6(3)	C71	C72	C95	119.8(3)
C20	O3	C35	114.8(2)	C73	C72	C71	119.1(3)
C13	O2	C32	115.5(2)	C73	C72	C95	121.0(3)
C27	O4	C38	115.7(2)	C52	C51	C50	119.0(3)
O5	C54	C49	119.9(3)	C52	C51	C89	121.5(3)
O5	C54	C53	119.2(3)	C50	C51	C89	119.5(3)
C49	C54	C53	120.8(3)	C20	C19	C21	122.4(3)
O2	C13	C8	119.9(3)	C18	C19	C20	118.6(3)
O2	C13	C12	118.3(3)	C18	C19	C21	119.0(3)
C8	C13	C12	121.4(3)	C72	C73	C74	121.8(3)
C26	C25	C24	121.1(3)	C24	C23	C22	121.5(3)
O7	C68	C63	119.4(3)	C68	C67	C66	118.1(3)
O7	C68	C67	118.9(3)	C68	C67	C69	121.1(3)
C67	C68	C63	121.4(3)	C66	C67	C69	120.7(3)
O8	C75	C70	117.9(3)	C63	C62	C60	109.5(2)
O8	C75	C74	120.5(3)	C49	C76	C74	109.6(3)
C70	C75	C74	121.2(3)	C13	C12	C14	119.6(3)
O1	C6	C5	119.6(3)	C11	C12	C13	118.5(3)
O1	C6	C1	119.4(3)	C11	C12	C14	121.8(3)
C5	C6	C1	120.9(3)	C59	C58	C91	120.0(3)
C8	C9	C10	121.1(3)	C57	C58	C59	119.4(3)
C65	C66	C67	121.1(3)	C57	C58	C91	120.5(3)
C9	C10	C43	119.7(3)	C22	C21	C19	109.3(3)
C11	C10	C9	119.3(3)	C5	C7	C8	109.5(2)
C11	C10	C43	120.9(3)	C66	C65	C93	121.3(3)
C5	C4	C3	120.9(3)	C64	C65	C66	119.5(3)
C6	C5	C7	121.0(3)	C64	C65	C93	119.2(3)
C4	C5	C6	119.2(3)	N2	C44	C43	179.1(4)
C4	C5	C7	119.6(3)	C16	C17	C45	121.1(3)
C54	C49	C76	122.6(3)	C18	C17	C16	118.7(3)
C50	C49	C54	118.6(3)	C18	C17	C45	120.2(3)
C50	C49	C76	118.8(3)	N4	C48	C47	179.1(4)
C75	C70	C71	118.8(3)	C51	C52	C53	121.5(3)
C75	C70	C69	119.3(3)	C56	C55	C53	111.5(3)
C71	C70	C69	121.4(3)	O6	C61	C56	118.0(3)
C25	C26	C27	118.7(3)	O6	C61	C60	121.1(3)
C25	C26	C28	121.3(3)	C60	C61	C56	120.5(3)
C27	C26	C28	119.3(3)	C4	C3	C41	119.5(3)
C54	C53	C55	121.6(3)	C2	C3	C4	118.9(3)
C52	C53	C54	118.3(3)	C2	C3	C41	121.6(3)
C52	C53	C55	120.1(3)	C70	C69	C67	109.2(2)
C15	C14	C12	111.7(3)	C17	C18	C19	121.7(3)
C6	C1	C28	120.2(3)	C49	C50	C51	121.5(3)

C2	C1	C6	118.4(3)		C90	C89	C51	111.7(3)
C2	C1	C28	121.2(3)		C44	C43	C10	112.9(3)
C13	C8	C7	120.6(3)		C59	C60	C62	120.7(3)
C9	C8	C13	118.2(3)		C59	C60	C61	119.0(3)
C9	C8	C7	120.7(3)		C61	C60	C62	119.7(3)
C60	C59	C58	120.9(3)		C63	C64	C65	120.9(3)
C12	C11	C10	121.2(3)		O1	C29	C30	107.7(3)
C27	C22	C21	120.3(3)		C96	C95	C72	112.7(3)
C23	C22	C27	117.7(3)		C94	C93	C65	110.5(3)
C23	C22	C21	121.4(3)		O3	C35	C36	112.8(3)
C68	C63	C62	121.2(3)		N5	C90	C89	179.1(4)
C64	C63	C68	118.9(3)		N3	C46	C45	178.4(4)
C64	C63	C62	119.7(3)		N8	C96	C95	179.4(4)
C56	C57	C58	121.2(3)		O6	C80	C81	113.4(3)
C70	C71	C72	120.8(3)		O7	C83	C84	108.4(3)
C57	C56	C55	121.8(3)		C80	C81	C82	110.8(3)
C57	C56	C61	118.7(3)		O4	C38	C39	113.4(3)
C61	C56	C55	119.4(3)		O2	C32	C33	112.8(3)
O4	C27	C26	118.8(3)		C42	C41	C3	111.2(3)
O4	C27	C22	119.2(3)		C29	C30	C31	113.8(3)
C26	C27	C22	121.7(3)		C46	C45	C17	111.9(3)
C3	C2	C1	121.6(3)		C92	C91	C58	112.8(3)
C15	C16	C17	121.7(3)		C48	C47	C24	111.9(3)
C25	C24	C23	119.1(3)		O8	C86	C87	113.1(3)
C25	C24	C47	120.0(3)		C35	C36	C37	111.2(3)
C23	C24	C47	120.9(3)		N1	C42	C41	177.6(4)
C75	C74	C76	120.4(3)		C38	C39	C40	112.2(3)
C73	C74	C75	118.0(3)		C83	C84	C85	114.1(3)
C73	C74	C76	121.0(3)		C32	C33	C34	110.3(3)
C16	C15	C14	119.8(3)		C86	C87	C88	114.7(3)
C16	C15	C20	118.2(3)		N7	C94	C93	176.3(4)
C20	C15	C14	121.9(3)		O5	C77	C78	113.3(4)
O3	C20	C15	120.1(3)		C77	C78	C79	115.5(4)

Table S6. *X*-ray crystal structure determination detail of 1. Torsion angles for **1**.

A	B	C	D	Angle/°		A	B	C	D	Angle/°
O7	C68	C63	C62	4.3(4)		C71	C72	C73	C74	4.4(5)
O7	C68	C63	C64	178.9(3)		C71	C72	C95	C96	-73.5(4)
O7	C68	C67	C66	-179.4(3)		C56	C57	C58	C59	-2.7(5)
O7	C68	C67	C69	-2.7(4)		C56	C57	C58	C91	-179.8(3)
O7	C83	C84	C85	63.4(4)		C56	C61	C60	C59	-5.7(5)
O1	C6	C5	C4	-179.2(3)		C56	C61	C60	C62	165.6(3)
O1	C6	C5	C7	-4.8(4)		C27	O4	C38	C39	87.0(3)
O1	C6	C1	C2	179.7(3)		C27	C26	C28	C1	-71.0(4)
O1	C6	C1	C28	4.7(4)		C27	C22	C23	C24	-0.3(5)
O1	C29	C30	C31	-64.9(3)		C27	C22	C21	C19	68.0(4)
O8	C75	C70	C71	179.6(3)		C2	C1	C28	C26	-45.7(4)
O8	C75	C70	C69	7.7(4)		C2	C3	C41	C42	-87.8(4)
O8	C75	C74	C73	-178.6(3)		C16	C15	C20	O3	-178.7(3)
O8	C75	C74	C76	-7.1(4)		C16	C15	C20	C19	3.8(4)
O8	C86	C87	C88	77.0(4)		C16	C17	C18	C19	2.9(5)
O6	C61	C60	C59	-179.1(3)		C16	C17	C45	C46	-124.9(3)
O6	C61	C60	C62	-7.8(5)		C24	C25	C26	C27	1.7(5)
O6	C80	C81	C82	178.8(3)		C24	C25	C26	C28	-168.7(3)
O5	C54	C49	C76	4.4(4)		C74	C75	C70	C71	6.6(5)
O5	C54	C49	C50	-177.6(3)		C74	C75	C70	C69	-165.3(3)
O5	C54	C53	C52	177.3(3)		C15	C14	C12	C13	-65.8(4)
O5	C54	C53	C55	-2.9(4)		C15	C14	C12	C11	110.2(3)
O5	C77	C78	C79	177.6(4)		C15	C16	C17	C18	-2.7(5)
O3	C20	C19	C21	-3.1(4)		C15	C16	C17	C45	176.7(3)
O3	C20	C19	C18	178.9(3)		C15	C20	C19	C21	174.4(3)
O3	C35	C36	C37	179.2(3)		C15	C20	C19	C18	-3.7(4)
O2	C13	C8	C9	178.7(3)		C20	O3	C35	C36	84.8(3)
O2	C13	C8	C7	6.3(4)		C20	C19	C21	C22	-118.8(3)
O2	C13	C12	C14	-2.1(4)		C20	C19	C18	C17	0.2(4)
O2	C13	C12	C11	-178.2(3)		C28	C26	C27	O4	-8.1(4)
O2	C32	C33	C34	179.1(3)		C28	C26	C27	C22	165.1(3)
O4	C38	C39	C40	174.2(3)		C28	C1	C2	C3	173.7(3)
C54	O5	C77	C78	126.3(4)		C73	C74	C76	C49	103.0(3)
C54	C49	C76	C74	116.0(3)		C73	C72	C95	C96	110.4(4)
C54	C49	C50	C51	-0.2(4)		C23	C22	C27	O4	178.0(3)
C54	C53	C52	C51	0.8(4)		C23	C22	C27	C26	4.8(5)
C54	C53	C55	C56	-121.4(3)		C23	C22	C21	C19	-103.3(3)
C13	O2	C32	C33	87.5(3)		C23	C24	C47	C48	-107.8(4)
C13	C8	C7	C5	60.0(4)		C67	C68	C63	C62	-170.1(3)
C25	C26	C27	O4	-178.7(3)		C67	C68	C63	C64	4.4(4)
C25	C26	C27	C22	-5.5(5)		C67	C66	C65	C64	0.7(5)
C25	C26	C28	C1	99.4(3)		C67	C66	C65	C93	-179.4(3)
C25	C24	C23	C22	-3.3(5)		C62	C63	C64	C65	173.4(3)
C25	C24	C47	C48	75.1(4)		C76	C49	C50	C51	177.9(3)
C68	O7	C83	C84	175.9(3)		C76	C74	C73	C72	-171.3(3)
C68	C63	C62	C60	121.3(3)		C12	C13	C8	C9	5.9(5)

C68	C63	C64	C65	-1.3(5)		C12	C13	C8	C7	-166.5(3)
C68	C67	C69	C70	-131.0(3)		C12	C14	C15	C16	-56.6(4)
C75	O8	C86	C87	-91.3(3)		C12	C14	C15	C20	120.6(3)
C75	C70	C71	C72	-1.9(5)		C58	C59	C60	C62	-169.1(3)
C75	C70	C69	C67	72.1(4)		C58	C59	C60	C61	2.1(5)
C75	C74	C73	C72	0.1(5)		C58	C57	C56	C55	175.9(3)
C75	C74	C76	C49	-68.2(4)		C58	C57	C56	C61	-0.8(5)
C6	O1	C29	C30	-176.8(2)		C21	C22	C27	O4	6.4(4)
C6	C5	C7	C8	-121.7(3)		C21	C22	C27	C26	-166.8(3)
C6	C1	C2	C3	-1.2(5)		C21	C22	C23	C24	171.2(3)
C6	C1	C28	C26	129.2(3)		C21	C19	C18	C17	-177.9(3)
C9	C10	C11	C12	2.4(5)		C65	C66	C67	C68	2.3(5)
C9	C10	C43	C44	-121.0(3)		C65	C66	C67	C69	-174.5(3)
C9	C8	C7	C5	-112.2(3)		C17	C16	C15	C14	176.7(3)
C66	C67	C69	C70	45.6(4)		C17	C16	C15	C20	-0.6(4)
C66	C65	C64	C63	-1.3(5)		C52	C53	C55	C56	58.4(4)
C66	C65	C93	C94	87.7(4)		C52	C51	C50	C49	-3.7(5)
C10	C9	C8	C13	-2.3(5)		C52	C51	C89	C90	128.1(3)
C10	C9	C8	C7	170.1(3)		C55	C53	C52	C51	-179.0(3)
C10	C11	C12	C13	1.1(5)		C55	C56	C61	O6	1.9(4)
C10	C11	C12	C14	-175.0(3)		C55	C56	C61	C60	-171.7(3)
C4	C5	C7	C8	52.7(4)		C61	O6	C80	C81	-84.9(3)
C4	C3	C41	C42	93.2(4)		C61	C56	C55	C53	67.4(4)
C5	C6	C1	C2	3.6(4)		C3	C4	C5	C6	0.1(5)
C5	C6	C1	C28	-171.4(3)		C3	C4	C5	C7	-174.4(3)
C5	C4	C3	C2	2.2(5)		C69	C70	C71	C72	169.9(3)
C5	C4	C3	C41	-178.7(3)		C18	C19	C21	C22	59.2(4)
C49	C54	C53	C52	-4.8(4)		C18	C17	C45	C46	54.6(4)
C49	C54	C53	C55	175.0(3)		C50	C49	C76	C74	-61.9(4)
C70	C75	C74	C73	-5.7(5)		C50	C51	C52	C53	3.4(5)
C70	C75	C74	C76	165.7(3)		C50	C51	C89	C90	-51.4(4)
C70	C71	C72	C73	-3.5(5)		C89	C51	C52	C53	-176.1(3)
C70	C71	C72	C95	-179.7(3)		C89	C51	C50	C49	175.7(3)
C26	C25	C24	C23	2.6(5)		C43	C10	C11	C12	178.8(3)
C26	C25	C24	C47	179.7(3)		C60	C59	C58	C57	2.0(5)
C53	C54	C49	C76	-173.5(3)		C60	C59	C58	C91	179.1(3)
C53	C54	C49	C50	4.5(4)		C64	C63	C62	C60	-53.2(4)
C14	C15	C20	O3	4.1(4)		C64	C65	C93	C94	-92.4(4)
C14	C15	C20	C19	-173.4(3)		C29	O1	C6	C5	-94.3(3)
C1	C6	C5	C4	-3.0(4)		C29	O1	C6	C1	89.5(3)
C1	C6	C5	C7	171.4(3)		C95	C72	C73	C74	-179.5(3)
C1	C2	C3	C4	-1.6(5)		C93	C65	C64	C63	178.9(3)
C1	C2	C3	C41	179.3(3)		C35	O3	C20	C15	77.5(3)
C8	C13	C12	C14	170.9(3)		C35	O3	C20	C19	-105.0(3)
C8	C13	C12	C11	-5.3(5)		C80	O6	C61	C56	113.2(3)
C8	C9	C10	C11	-1.7(5)		C80	O6	C61	C60	-73.2(4)
C8	C9	C10	C43	-178.2(3)		C83	O7	C68	C63	95.3(3)
C59	C58	C91	C92	118.5(3)		C83	O7	C68	C67	-90.1(3)
C11	C10	C43	C44	62.6(4)		C38	O4	C27	C26	-106.5(3)

C63	C68	C67	C66	-4.9(4)		C38	O4	C27	C22	80.2(4)
C63	C68	C67	C69	171.8(3)		C32	O2	C13	C8	75.0(4)
C63	C62	C60	C59	111.5(3)		C32	O2	C13	C12	-112.0(3)
C63	C62	C60	C61	-59.6(4)		C45	C17	C18	C19	-176.5(3)
C57	C56	C55	C53	-109.2(3)		C47	C24	C23	C22	179.6(3)
C57	C56	C61	O6	178.7(3)		C86	O8	C75	C70	114.3(3)
C57	C56	C61	C60	5.0(5)		C86	O8	C75	C74	-72.6(4)
C57	C58	C91	C92	-64.5(4)		C77	O5	C54	C49	81.0(4)
C71	C70	C69	C67	-99.6(3)		C77	O5	C54	C53	-101.1(3)

Table S7. *X*-ray crystal structure determination detail of 1. Hydrogen atom coordinates ($Å \times 10^4$) and isotropic displacement parameters ($Å^2 \times 10^3$) for **1**.

Atom	x	y	z	U(eq)
H25	6284	11885	2809	26
H9	7515	5589	4012	24
H66	-362	5172	3722	26
H4	6742	7537	4272	25
H14A	5195	6315	2107	26
H14B	4439	5766	2742	26
H59	-1870	592	4027	26
H11	5046	4899	3624	25
H57	859	-74	3691	27
H71	155	6873	2865	24
H2	6221	10178	3693	26
H16	4082	6749	3824	26
H28A	7645	10969	2518	25
H28B	7670	10286	1957	25
H73	2866	6170	2555	25
H23	3801	11174	2455	26
H62A	-1801	2257	2675	26
H62B	-2356	1969	3466	26
H76A	2846	4465	1538	24
H76B	3429	4854	2027	24
H21A	4533	9453	1455	26
H21B	3615	9839	1925	26
H7A	8364	6964	3465	25
H7B	8344	7253	2669	25
H52	1702	1753	3893	26
H55A	1715	1335	2165	27
H55B	2047	779	2804	27
H69A	-621	5285	1969	24
H69B	-987	5963	2529	24
H18	3565	9391	3276	25
H50	2626	4382	3356	25
H89A	1709	3553	4667	33
H89B	2079	2534	4758	33
H43A	6677	4330	4702	30
H43B	5562	4402	4831	30
H64	-1306	2547	4305	26
H29A	9530	8731	2558	29
H29B	9264	9772	2355	29
H95A	1299	7458	3518	31
H95B	2394	7403	3169	31
H93A	-452	3232	5003	35
H93B	-29	4258	4773	35
H35A	3906	6857	1610	31
H35B	4639	7088	876	31
H80A	-194	2852	1481	31

H80B	-765	1924	1848	31
H83A	-2472	4784	2334	30
H83B	-2886	3750	2524	30
H81A	589	1083	1461	33
H81B	1147	2016	1083	33
H38A	5967	9920	840	32
H38B	6424	8937	870	32
H32A	7852	6902	1819	30
H32B	7559	7865	1475	30
H41A	5173	9271	4724	33
H41B	5430	8241	4959	33
H30A	10511	9431	1485	32
H30B	9605	9551	1172	32
H45A	3234	7556	4692	36
H45B	3637	8587	4581	36
H91A	-446	-598	4865	32
H91B	-1479	-655	4738	32
H47A	3850	12403	3093	29
H47B	4722	12490	3435	29
H86A	1442	3897	939	31
H86B	1914	4881	914	31
H31A	10444	8265	814	44
H31B	9414	7950	1265	44
H31C	10296	7814	1605	44
H36A	3898	8488	669	38
H36B	3158	8244	1400	38
H39A	7878	9661	887	40
H39B	7406	10631	782	40
H84A	-2016	4587	1152	37
H84B	-3127	4455	1444	37
H33A	6430	7099	1051	35
H33B	6740	6136	1387	35
H87A	8	4700	849	35
H87B	835	4781	162	35
H82A	574	1272	281	53
H82B	107	2246	344	53
H82C	-477	1331	730	53
H88A	218	6222	269	50
H88B	1263	6257	377	50
H88C	385	6176	1032	50
H85A	-2565	3312	754	52
H85B	-2986	2844	1534	52
H85C	-1874	2978	1240	52
H37A	3329	7168	292	63
H37B	2517	7881	475	63
H37C	2557	6983	1011	63
H34A	7504	6428	197	68
H34B	8267	6389	652	68
H34C	7965	7355	319	68

H40A	8272	10319	-294	63
H40B	7184	10303	-302	63
H40C	7710	9363	-199	63
H77A	3745	2621	1608	49
H77B	3555	3232	937	49
H79A	4537	2216	116	78
H79B	4351	1136	331	78
H79C	4814	1712	794	78
H78A	2957	1944	626	66
H78B	3193	1343	1284	66

Table S8. *X*-ray crystal structure determination detail of 1. Solvent masks information for **1**.

Number	X	Y	Z	Volume	Electron count	Content
1	0.500	0.500	0.000	180.6	43.0	-

Table S9. Characteristic values of the surface pressure-area compression isotherm of **1**.

Sample	A_0 (Å^2 molecule^{-1})	A_{lim} (Å^2 molecule^{-1})	A_c (Å^2 molecule^{-1})	π_c (mN m^{-1})
Monolayer on pure water	103	90	80	28.0

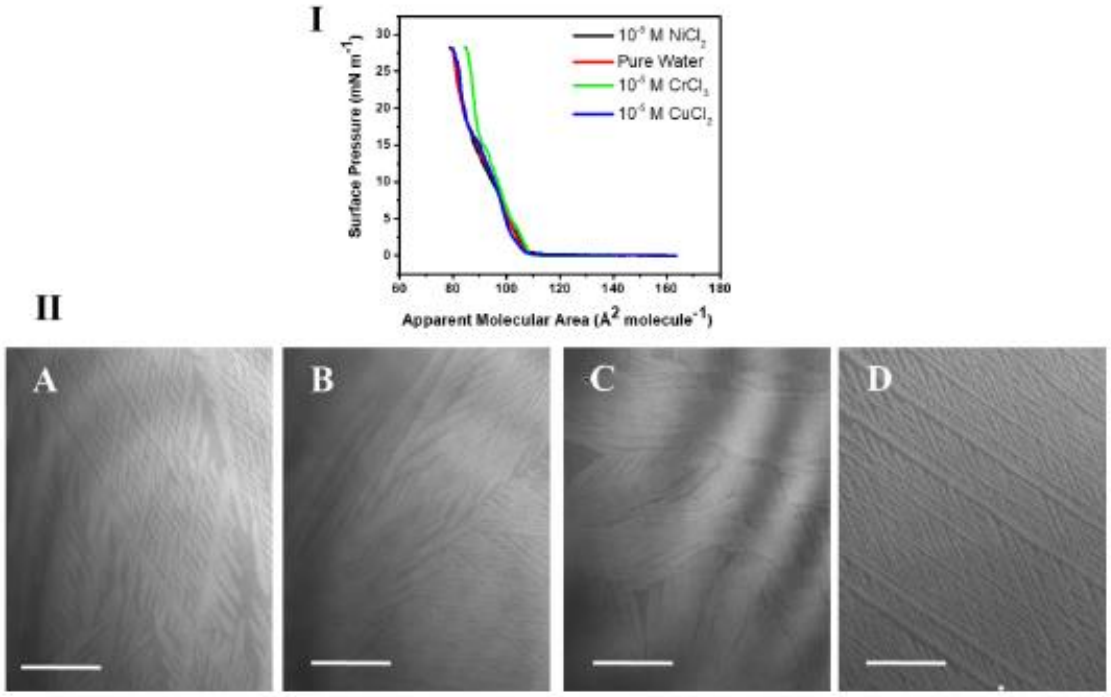

Fig. S3. Interfacial properties of the monolayer of 1 in the presence of transition metal ions in the subphase. (**I**) Surface pressure-area compression isotherms of **1** on a 10 μM $NiCl_2$ (black), $CrCl_3$ (green), $CuCl_2$ (blue) and pure water (red). 10 μM concentration of the salt solutions was chosen based on our recent results on the formation of metal-organic coordination network of calix[4]arene (*9*). The isotherms show no difference in the take-off values of the monolayer of **1** in the presence of ions. (**II**) BAM images of the monolayer of **1** formed at the interface of a 10 μM (**A**) $NiCl_2$, (**B**) $CrCl_3$, (**C**) $CuCl_2$ and (**D**) pure water at π: 20 mN m^{-1} were shown.

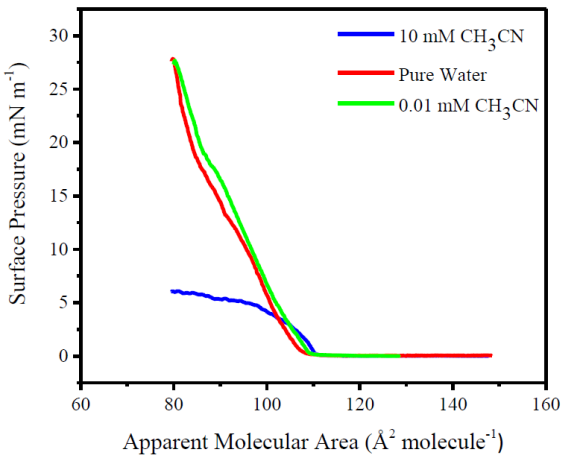

Fig. S4. Interfacial properties of the monolayer of 1 in the presence of acetonitrile molecules, as competitors with the CN functional groups of 1 for dipole-dipole interactions. Surface pressure-area compression isotherms of **1** on 0.01 and 10 mM CH_3CN solutions, compared to pure water subphase.

Table S10. Contact angle measurements on the monolayer of **1** transferred from the air-water interface onto HOPG. HOPG was considered as reference sample.

Sample	Contact Angle (°)
HOPG (reference sample)	98.8 ± 6
Monolayer of **1** transferred from pure water onto HOPG	80 ± 5

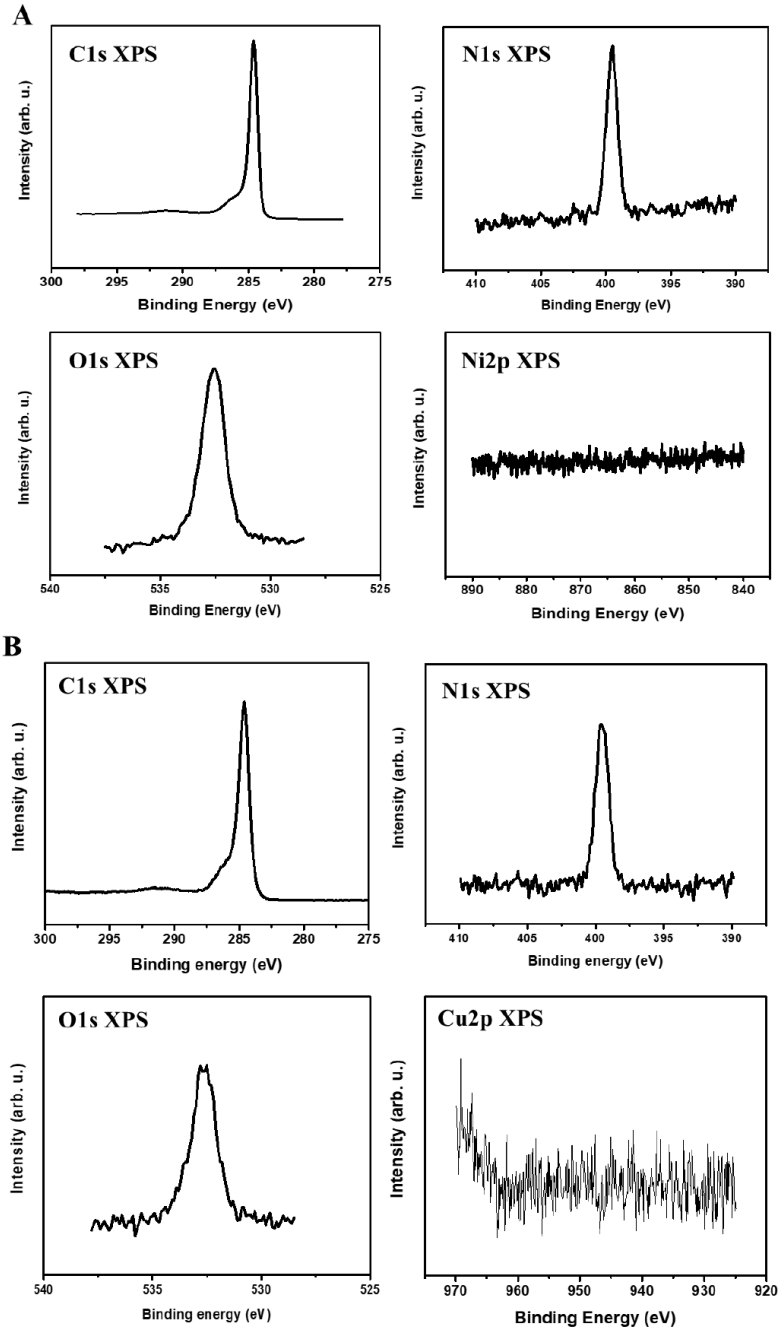
A
C1s XPS
Intensity (arb. u.)
300 295 290 285 280 275
Binding Energy (eV)
N1s XPS
Intensity (arb. u.)
410 405 400 395 390
Binding Energy (eV)
O1s XPS
Intensity (arb. u.)
540 535 530 525
Binding Energy (eV)
Ni2p XPS
Intensity (arb. u.)
890 880 870 860 850 840
Binding Energy (eV)
B
C1s XPS
Intensity (arb. u.)
300 295 290 285 280 275
Binding energy (eV)
N1s XPS
Intensity (arb. u.)
410 405 400 395 390
Binding energy (eV)
O1s XPS
Intensity (arb. u.)
540 535 530 525
Binding energy (eV)
Cu2p XPS
Intensity (arb. u.)
970 960 950 940 930 920
Binding Energy (eV)

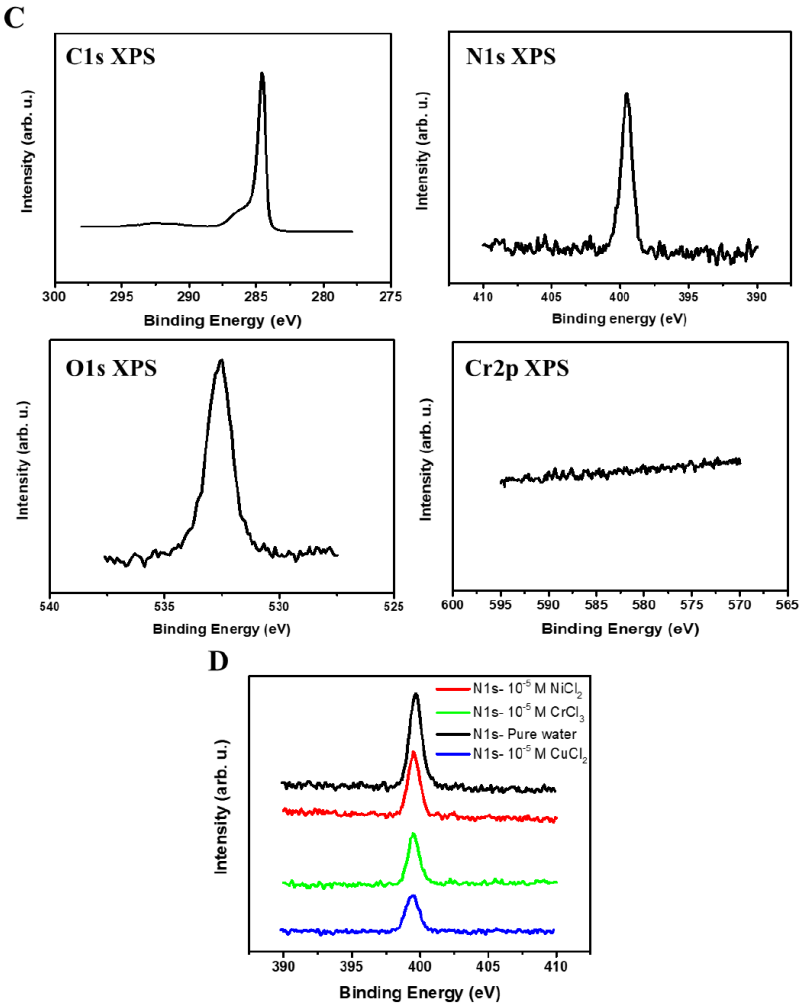

Fig. S5. Surface analysis of the monolayer of 1 in the presence of transition metal ions in the subphase. XP spectra of the monolayer of **1** transferred onto HOPG by the LS method for C1s, N1s and O1s peaks from a 10 µM (**A**) $NiCl_2$, (**B**) $CuCl_2$ and (**C**) $CrCl_3$. Nitrogen XP spectra of the monolayer of **1** show one peak at 399.7 eV that is the characteristic feature of N in the CN functional group (*14*). (**D**) There is no change in the N1s spectra of the transferred layer from different aqueous solutions onto HOPG. The absence of ions *i.e.* Ni^{2+}, Cu^{2+} and Cr^{3+} in the transferred layer confirms that the building units of **1** have a high tendency to interact with one another rather than metal ions. Indeed introducing the ions in the subphase cannot disturb the self-assembled network of **1** through dipole-dipole interaction.

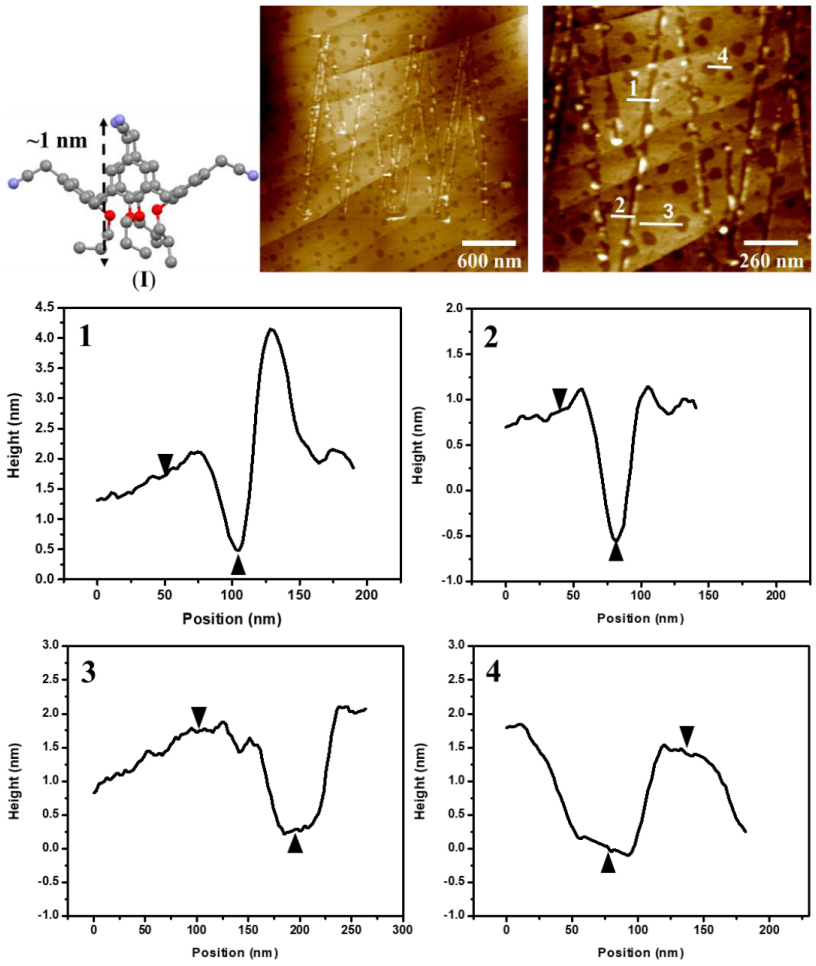

Fig. S6. AFM height analysis of the transferred monolayer of 1 from pure water subphase onto HOPG by the LS method. Height analysis of the monolayer of **1** was carried out in intentionally scratched layer (line profiles of 1 and 2) and on partially covered HOPG by the monolayer of **1** (line profiles of 3 and 4). The lines in the AFM images indicate where the height profiles were recorded. The AFM results confirmed the presence of a monomolecular layer of **1** with a height of 1.0 ± 0.4 nm. The measured height using AFM images is in a good agreement with the expected height of **1**, derived from its crystalline structure (1.1 nm) (**I**). The deviation from 1.1 nm could originate from the ambient-condition AFM experiments (*6*) and also partially rearrangement of molecules because of water evaporation.

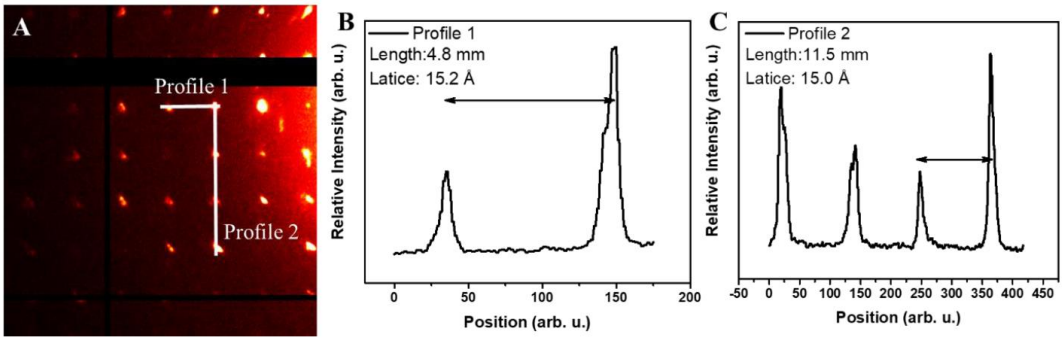

Fig. S7. Diffraction analysis of the free-standing monolayer of 1 by means of high-resolution cryo-TEM analysis. (**A**) Zoomed image of the TEM electron diffraction pattern of the free-standing monolayer of **1**. The diffraction pattern confirms the square packing structure of the crystalline layer. (**B** & **C**) The profile lines across the diffraction pattern, showing a unit cell size of ~15 Å.

CHAPTER 3

Controlling In-situ Formation of Bilayer *vs* Monolayer of Metal-Organic Coordination Networks

Capability to manipulate materials in the atomic scale, aiming properties desirable for specific applications, is an ultimate goal for chemists and material scientists. Herein we report an example of engineering calix[4]arene organic building components in order to synthesize tailorable 2D metal-organic coordination network (MOCN) via interfacial synthesis. The fabrication technique is based on using a calix[4]arene building unit with flexible functional groups at the upper rim, namely *25,26,27,28*-tetrapropoxycalix[4]arene-*5,11,17,23*-tetramethylcarboxylic acid. It is presented that the methylene carboxylic acid linkers at the upper rim of the calix[4]arene backbone lead to in-situ formation of bilayers or monolayers of the MOCN upon coordinating Cu^{2+} or Ni^{2+} transition metal ions, respectively. It is shown that the monolayer of coordinated network with Cu^{2+} ions transform to bilayers over time and the degree of bilayer formation is kinetically controllable. Building upon the Langmuir-Blodgett isotherm experiments and surface analysis on the transferred MOCNs from the interface onto solid substrates, we proposed molecular models of the MOCN monolayers and bilayers of the title compound.

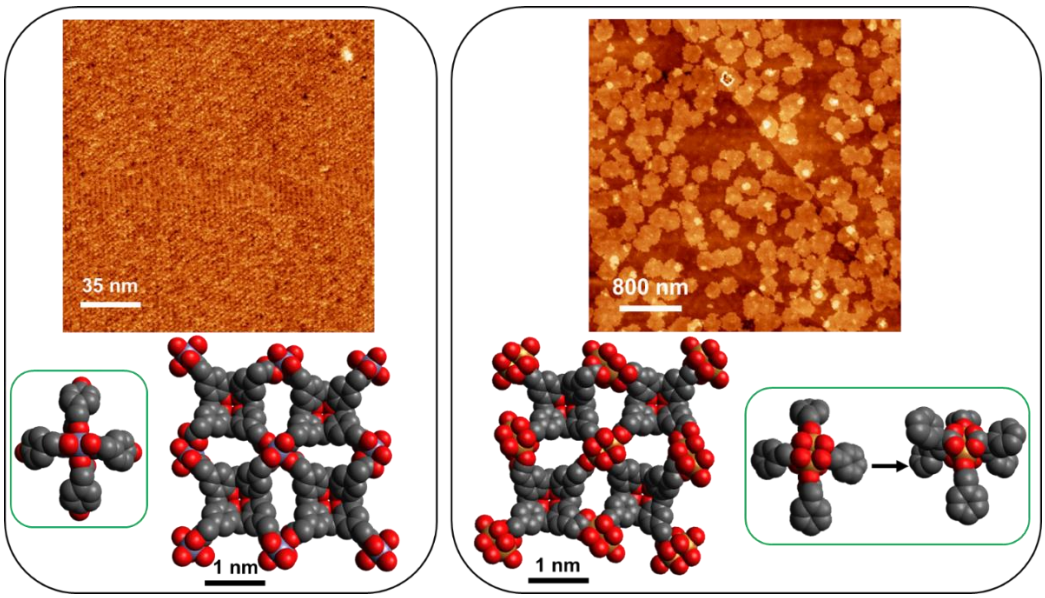

P.S. and T.A.J. conceived the research. M.M. performed LB, BAM, LS, contact angle, ellipsometry, XPS and AFM experiments and analyzed the data. N.L.O. performed EM data collection and with H.S. interpreted the data. M.M. and C. E. Housecraft modeled the crystalline structure of the MOCNs. M.M. and L.G.T. synthesized the molecule. M.M., T.A.J. and P.S. wrote the paper. All authors commented on the manuscript.

COMMUNICATION

Controlling In-situ Formation of Bilayer *vs* Monolayer of Metal-Organic Coordination Networks

Mina Moradi,[a,c] Nadia L. Opara,[b,c] Catherine E. Housecroft,[d] Ludovico G. Tulli,[a] Henning Stahlberg,[b] Thomas A. Jung,[b] and Patrick Shahgaldian[a]**

Abstract: We report on the in-situ fabrication of free-standing and crystalline bilayer of metal-organic coordination networks (MOCNs) of a calix[4]arene derivative, in which the degree of bilayer formation can be kinetically controlled. The methylene bridge linked to the COOH groups in the calixarene body of *5,11,17,23*-tetra-methylcarboxy-*25,26,27,28*-tetrapropoxy calix[4]arene building blocks provides the conformational flexibility for the COOH functions to coordinate with ionic centers through different coordination geometries. Bilayer and monolayer of the MOCNs of the title compound were formed upon coordinating Cu^{2+} or Ni^{2+} ions, respectively, at the air-liquid interface. The assembled layers were transferred from the air-liquid interface onto solid substrates using the Langmuir-Schaeffer method where they – still – exhibited a 2D periodic molecular structure in atomic force microscopy. The molecular design described enables engineering a vast array of organic building blocks for the fabrication of two- and three-dimensional tailor-made structures.

The fabrication of crystalline solids, through the meticulous assembly of polydentate organic linkers and metal clusters, has opened up new perspectives in material sciences.[1] This novel chemical strategy to produce materials, also called reticular chemistry, has allowed the production of a great number of metal-organic frameworks (MOFs) with controlled architectures and properties desired for applications including catalysis,[2] gas storage, purification[3] and electronic devices fabrication.[4] Major milestones in the development of MOFs for various applications have been reached by concomitantly optimizing the molecular design of both organic linkers and secondary building units (SBUs) and production processes.[5]

In a scientific context that witnesses a rejuvenated interest in 2-dimensional (2D) architectures, concepts developed in supramolecular and reticular chemistry may be exploited to design 2D crystalline metal-organic coordination networks (MOCNs).[6] These systems may offer a wealth of opportunities, to develop functional materials and surfaces provided that sufficient stability is reached. In this context, the progress of fabrication methods, characterization and applications of 2D MOFs, *i.e.* MOCNs, have been recently reviewed.[7]

The possibility to produce 2D materials, in the absence of carrier surface, as free-standing systems, may further expand the scope of applications of MOCNs to *e.g.* sample support for single biomolecule and single nanoparticle analysis and imaging. For example, free-standing monomolecular organic nanosheets have been produced via the self-assembly of cucurbit[8]uril and quinoline molecules.[8] Feng et al.reported a free-standing 2D supramolecular organic network (SON) using a host–guest enhanced donor–acceptor interaction in the cavity of the cucurbit[8]uril macrocycle.[9] The same group demonstrated that triphenylene-fused nickel bis(dithiolene) coordination polymers can be produced at the air-water interface and transferred, as free-standing monomolecular layers, onto copper grids.[10] Recently, we fabricated the first free-standing and crystalline linker-free SON of a *para*-methyl cyano-functionalized calix[4]arene derivative stabilized only by weak yet synergistic dipole-dipole interactions between the cyano functional groups.[11]

It is important to note that interfacial self-assembly methods also allow producing bilayers rather than monolayers. In this context, Chevalier et al. reported the transformation of a simple fatty acid -behenic acid- monolayer to bilayer triggered by the presence of Na^+ or K^+ monovalent cations in the aqueous phase.[12] Buzin et al. demonstrated stable multilayer formation of mesomorphic polymer of phosphazene directly at the air-water interface.[13] The same group investigated structure of mono- and multilayers of partially fluorinated poly-dialkoxy-phosphazene under stepwise collapse of the layer at the same interface.[14] Further, Meron at al. reported a reversible transition of a monolayer to a crystalline multilayer stacking of tri-silanobutyl polyhedral oligomeric silsesquioxane dimers, at the air-water interface.[15] It is remarkable, however, that interfacial self-assembly methods are well established for amphiphiles, but have not yet been used to build bilayered MOCN's.

In our efforts to fabricate 2D organic networks, via interfacial coordination, calix[4]arene building components have been selected because of their high symmetry, rigidity and the many possibilities for their modification.[16] Our design strategy includes functionalizing a calix[4]arene synthon with short lipophilic chains at its lower rim (C_3-cal) to minimize the influence of non-directional van der Waals interactions between the chains in the self-assembly process. Thus, the selected compounds are expected to self-assemble via directional and strong bonds between the hydrophilic functional groups at the upper rim of the calix[4]arene amphiphiles.

We reported earlier that functionalized C_3-cal molecule with carboxylic acid groups at the upper rim (C_3-*p*-ccal) coordinates Cu^{2+} ions and forms a tunable crystalline 2D MOCN.[16a] Direct attachment of the carboxy functional groups to the arene rings of C_3-*p*-ccal amphiphiles significantly constrained possible range of coordination geometries at the air-water interface, even if coordinated via different metal ions.[16a] In order to endow the C_3-*p*-ccal building blocks with more conformational mobility, we modified the C_3-*p*-ccal amphiphile by addition of a methylene bridge between the carboxy group and the arene ring at the upper rim. In the present report, we show that the modified C_3-*p*-ccal analogue forms in-situ bilayers of MOCNs upon coordinating Cu^{2+} ions, at the air-water interface, with control over the degree of bilayer formation. Coordinating the same building blocks via Ni^{2+} ions, however, leads to a crystalline monolayer of the MOCN, with a different coordination geometry.

5,11,17,23-tetra-methylcarboxy-*25,26,27,28*-tetrapropoxy calix[4]arene (**1**) (Figure 1, inset), locked in the cone conformation, was synthesized as previously reported.[11;17] The interfacial properties of **1** on pure water, and aqueous solutions containing 10 µM $CuCl_2$ and $NiCl_2$ were studied using the Langmuir balance technique and Brewster angle microscopy (BAM). The surface

pressure-area compression isotherm shows that, unlike analogues C_3-*p*-ccal deprived the methylene bridge at its upper rim, **1** does not form a stable monolayer at the air-water interface, with a pseudo-collapse as low as ~3 mN m^{-1}. The stability of C_3-*p*-ccal monolayer at the air-water interface was attributed to π-π interactions between the arene rings of the neighbouring amphiphiles.[16a] In case of the present system, in contrast, the π-π stacking between the arene rings of **1** are compromised by the presence of the methylene bridge in the head groups. The limiting area (A_{lim}) of 100 Å^2 molecule^{-1} for the layer of **1**, consistent with measurements for other amphiphilic calix[4]arenes. This rules out the hypothesis that the low collapse pressure of the layer of **1** (~3 mN m^{-1}) is due to a partial solubilization of **1** in the subphase.[18] The acquired isotherms on 10 μM $NiCl_2$ and $CuCl_2$ solutions consistent with stable layers are measured with π_c as high as 35 and 42 mN m^{-1}, respectively. We attribute the stabilization of the layer of **1** in the presence of divalent ions to the strong interactions between the carboxylate groups and ions.[16a;19] This is because there is no other considerable interaction mediated by the short aliphatic chains, the low polarity of the head groups and the absence of π-π stacking of **1**. Our BAM investigations showed that the layer of **1** maintains a homogeneous morphology throughout the whole compression experiment, in contrast to the crystalline layer of C_3-*p*-ccal amphiphiles (Figure S1).

The A_{lim} value measured on $NiCl_2$ of 102 Å^2 molecule^{-1} is consistent with the cross-section of **1**, orientated with the C_4 pseudo-symmetry axis orthogonal to the air-water interface. The A_{lim}, measured on $CuCl_2$ (84 Å^2 molecule^{-1}) is below the structural footprint of the molecule.[18] This low A_{lim} value indicates the loss of molecules from the monolayer at the interface. Partial solubility of **1** in the subphase could be held responsible for this low A_{lim} value, but has been ruled out already.

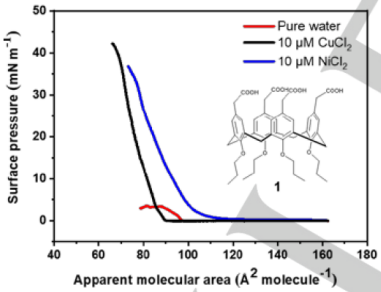

Figure 1. Surface pressure-area compression isotherms of **1** on pure water (—), a 10 μM aqueous $CuCl_2$ solution (—) and a 10 μM aqueous $NiCl_2$ solution (—). Inset is the molecular structure of **1**.

Understanding the high π_c and low A_{lim} values of the monolayer of **1** in the presence of Cu^{2+} ions, motivated further investigations of the monolayer stability and the layer thickness by surface ellipsometry measurements. The stability test was done by keeping the monolayer of **1** at 40 mN m^{-1} compressed and recording the molecular area loss over time (*i.e.* the relaxation time). The data reveals losing and flipping the molecules of **1** into the aqueous solution (Figure S2).

Surface ellipsometry measurements performed on the compressed layer of **1** at 40 mN m^{-1} in 10 μM $CuCl_2$ solution shows a steady increasing the layer thickness with time. The measured thickness at start is ~1.5 nm and it reaches ~3.5 nm after 30 min, representing a monolayer and bilayer of **1**, respectively (Figure 2). These data suggest that amphiphiles of **1** move away from the interface into the subphase or on top of the first layer to form a bilayer, in perfect agreement with the compression isotherms. It is worth to note that the measured monolayer thickness from ellipsometry is slightly higher than the calculated values. In the XRD data of a similar analogue of **1** its height appears as ~1.1 nm [11]

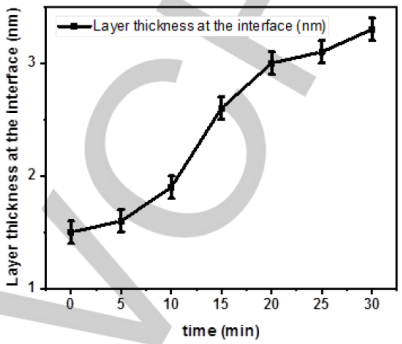

Figure 2. Surface ellipsometry measurement, at the interface, on the layer of **1** formed in the presence of Cu^{2+} ions. The layer was kept under a surface pressure of π: 40 mN m^{-1} for 30 min and the layer thickness was measured every 5 min.

The Langmuir-Schaefer (LS) technique was used to successfully transfer the layers of **1** from $CuCl_2$ and $NiCl_2$ aqueous solutions onto solid substrates with a transfer ratio close to unity. Ellipsometry analysis after transfer of the layer from the $CuCl_2$ and $NiCl_2$ subphases onto solid substrates revealed a layer thickness of 1.4 ± 0.4 and 1 ± 0.2 nm, respectively. These results are in agreement with the above reported interfacial thickness measurements. Atomic force microscopy (AFM) was used to visualize the formation and growth of bilayers of **1** upon interaction with Cu^{2+} ions. Therefore, layers transferred from the air-$CuCl_2$ solution interface onto highly oriented pyrolytic graphite (HOPG) were inspected by AFM. The surface area covered with the bilayer increases linearly with increasing relaxation time (Figure 3A). The AFM micrographs taken of the layers transferred after 0 and 30 min relaxation time, respectively, clearly prove this trend (Figure 3B&C).

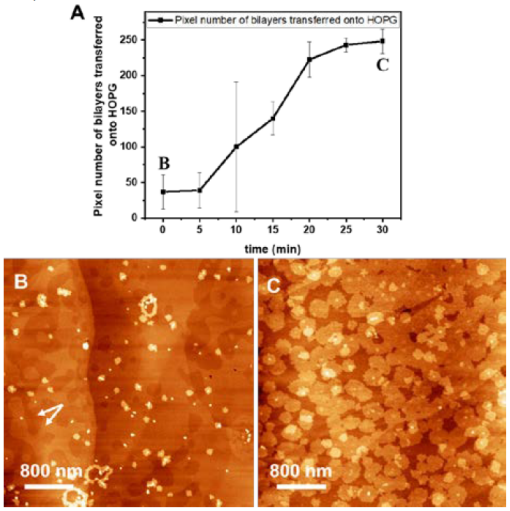

Figure 3. The plot (A) shows the number of pixels (~surface area) of the bilayer domains transferred after different time intervals with the surface pressure set to 40 mN m^{-1}. AFM micrographs of the transferred layer of **1** transferred from the air-$CuCl_2$ solution interface onto HOPG after 0 (B) and 30 min (C). AFM images of the layer transferred after 5, 10, 15, 20 and 25 min relaxation time are available in figure S3.

The transferred layer of **1** from $CuCl_2$ solution comprises islands and vacancy islands with different elevation. The single step height is in the order of ~0.5 nm (white arrows in Figure 3B & Figure S4D). These domains are representing coexistence of liquid-expanded and liquid-condensed phases during layer formation.[20] On the produced layer of **1** transferred after 0 min waiting time some bilayer islands are observed. This morphology explains the difference between the calculated and obtained layer thickness in the ellipsometry results (Figure 3B). In addition, the layer of **1** created at the air-$CuCl_2$ solution interface exhibits coexistence of both crystalline stripes and amorphous domains (Figure 4A-4C). Two-dimensional fast Fourier transform (2D FFT) reveals the width of these crystalline stripes to be ~5 nm (Figure 4D), in line with our earlier report on a similar synthon.[16a] The layer of **1** transferred from the air-$NiCl_2$ solution interface is a crystalline monolayer with no observed multilayer islands (Figure 4E-4G & S4E). 2D FFT analysis on the AFM image of the network of **1** interacted with Ni^{2+} ions measures a rhombohedral unit cell size of ~2 nm, consistent with the expected size of **1** in the cone conformation (Figure 4H).[11] Scratching AFM experiments enabled us to measure the thickness of the layers of **1** from $CuCl_2$ and $NiCl_2$ solutions transferred onto HOPG, *i.e.* 1.3 ± 0.2 nm. AFM height analysis performed on the bilayers of the copper mediated organic layer of **1** shows a height of 3 ± 0.5 nm (Figure S4), consistent with the surface ellipsometry measurements.

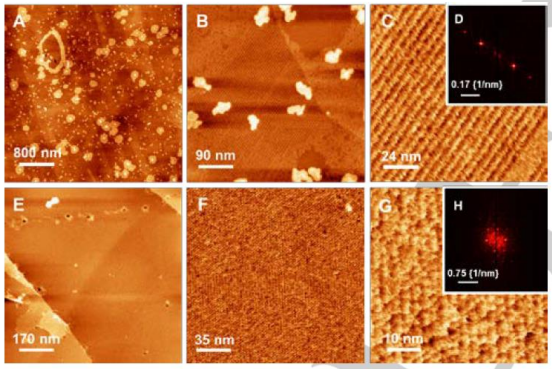

Figure 4. AFM micrographs of the layers of **1** transferred via the LS method from the interface of a 10 µM $CuCl_2$ (A-C) and $NiCl_2$ (E-G) aqueous solutions. The correlated FFT analysis on the crystalline layers of **1** is shown in (D&H). The layer of **1** interacted with Cu^{2+} ions reveals crystalline stripes with the width of ~5 nm (D). While the interaction of **1** with Ni^{2+} ions results in a crystalline monolayer with a rhombohedral unit cell size of ~2 nm.

Contact angle measurements on the layers of **1** transferred from the interface onto HOPG shows that the layer of **1**, interacted with Cu^{2+} ions, is more hydrophobic (~87°) compared to the one interacted with Ni^{2+} ions (~82°) (Table S1). This provides further evidence that the layer transferred from the interface of $CuCl_2$ solution comprises amphiphiles of **1** with the aliphatic chains pointing away from the substrate surface, *i.e.* in-situ formed bilayer domains.

X-ray photoelectron spectroscopy (XPS) has been performed in order to assess the type of interactions between the carboxyl groups and transition metal ions and their stoichiometry (Figure 5). Elemental XPS analysis on the transferred layers of **1** from the interface of $CuCl_2$ and $NiCl_2$ solutions confirmed the formation of coordination bonds between the carboxyl groups of **1** and the divalent ions (Table S2, Figure S5 & S6).[16a] The 0.5 eV chemical shift of the C1s spectra in the carboxylate region provides evidence for different coordination geometries in the MOCNs of **1** with Cu^{2+} and Ni^{2+} ions (Figure 5B). The C1s peak positions of the carboxy groups in the copper- and nickel-coordinated networks of **1** were found to be in 288.8 and 289.2 eV, respectively. The obtained values are in agreement with the paddle-wheel and octahedral coordination geometries for the carboxy-Cu[21] and the carboxy-Ni[22] motifs, respectively. In the MOCN of **1**, the average ratio between the carboxyl groups and copper or nickel centers found to be ~1:1 and 4:1, respectively. The ~1:1 ratio of the COOH functional groups to copper centers is consistent with the bilayer formation of **1** with the paddle-wheel coordination motif (Figure 5C). The obtained 4:1 ratio for the MOCN of **1** coordinated with Ni^{2+} ions suggests an octahedral coordination geometry of nickel and carboxy linkers (Figure 5D).

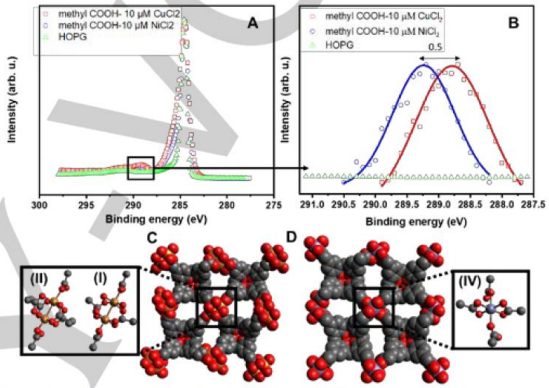

Figure 5. XP spectra of the C1s peak of the MOCNs of **1**. Data is shown for the layer transferred from a 10 µM aqueous solution of $CuCl_2$ (□) and $NiCl_2$ (○). Clean HOPG (Δ) is shown as reference (A). Normalized C1s spectra in the carboxylic region after background subtraction (B). Proposed molecular models of the coordination networks of **1** with copper and nickel centers (J&K). The MOCN of **1** with Cu centers consists of the paddle-wheel coordination motifs (I). The turned molecule of **1**, from the interface into the subphase, completes the coordination positions of the copper in the paddle-wheel motif (II) Octahedral coordination geometry of **1** with Ni, consists of two bidentate and two monodentate carboxyl ligands (III), forms a monolayer of the MOCN of **1**.

Building upon the interfacial studies, AFM and XPS analysis we propose packing models of the MOCNs of **1**, coordinated with Cu^{2+} and Ni^{2+} ions (Figure 5C & 5D). In our tentative model for the bilayer of the MOCNs of **1** every carboxy group coordinates with copper centers of the paddle-wheel coordination geometry. The amphiphiles of **1** flip from the interface into the subphase and complete the coordination positions of the Cu atoms in the paddle-wheel structure. According to this hypothesis, the bilayers are formed through formation of molecular capsules consisting two calix[4]arene synthons linked together from their head groups via the copper atoms (Figure 5CII). The bilayer formation is controlled by the nucleation rate and the growth of the molecular capsules of **1** which is adjustable by the time allocated for the out of plane diffusion process at a given surface pressure. The $\{Cu_2(O_2CR)_4\}$ paddle-wheel motif (Figure 5II) is an extremely common geometry in both discrete and extended coordination assemblies. This is confirmed by a search of the Cambridge Structural Database (CSD) v. 5.39 with update[23] and using Conquest v. 1.20[24] which gives 737 hits for a $\{Cu_2(O_2CC)_4\}$ unit. In contrast, only twelve analogous Ni_2-containing units have been structurally characterized. Instead, octahedral $\{NiO_6\}$ are typical with monodentate *O*- or bidentate *O,O'*-ligands or in multinuclear assemblies. The molecular model of a MOCN monolayer of **1** and Ni^{2+} ions is based on coordination of two bidentate and two

monodentate carboxy ligands with one Ni^{2+} ions, in an octahedral coordination fashion.

CryoTEM investigations on the MOCNs of **1**, transferred from the air-liquid interface onto a lacey copper TEM grid, is shown in Figure 6. The TEM images confirm that the MOCNs of **1** are free-standing over holes as large as 4 × 4 µm. TEM analysis performed on bilayers of the MOCNs of **1** transferred from the air-$CuCl_2$ solution interface after 0 and 30 min relaxation time confirm that the degree of bilayer formation is tunable over time (figure 6B & 6D, respectively).

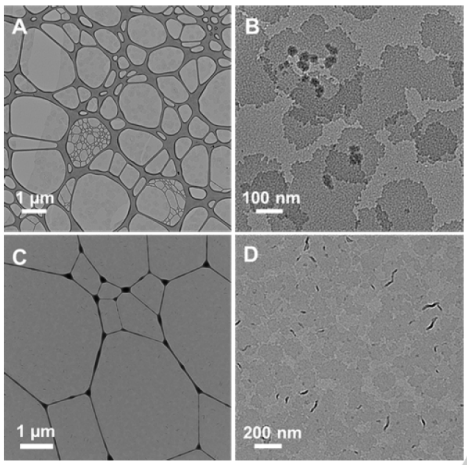

Figure 6. TEM images of the transferred bilayers of the MOCN of **1** via the LS method from a 10 µM aqueous solution of $CuCl_2$ after 0 min (A&B) and 30 min (C&D) relaxation time.

In conclusion, we demonstrate a molecular design strategy to fabricate tailorable MOCNs of calix[4]arene macrocycles upon changing the transition metal ions. The designed organic building blocks of **1**, with the flexible methyl carboxy linkers, coordinate Cu^{2+} ions and form bilayers of MOCNs comprising the paddle-wheel coordination geometry. It is the first example of a bilayered MOCN with a controllable degree of the bilayer formation. In contrast, the calix[4]arene synthons of **1** form a crystalline monolayer of the MOCN through formation of an octahedral coordination geometry with Ni^{2+} ions. This molecular-design strategy paves the way towards fabrication of 2D non-trivial self-assembled networks i.e. of linking 2D MOCN's with 3D MOF's by enabling a layer by layer fabrication mechanism at the solid/liquid interface.

Acknowledgments

The financial support of the Swiss Nanoscience Institute through the grant of P1305 & P1308 are gratefully acknowledged. The authors thank R. Schelldorfer for technical support for XPS and AFM measurements.

Keywords: metal-organic coordination network • amphiphilic bilayer • Calix[4]arene • Langmuir- Blodgett method

[1] M. J. Kalmutzki, N. Hanikel, O. M. Yaghi, *Sci. Adv.* **2018**, *4*.

[2] L. Zhu, X.-Q. Liu, H.-L. Jiang, L.-B. Sun, *Chem. Rev.* **2017**, *117*, 8129-8176.

[3] M. P. Suh, H. J. Park, T. K. Prasad, D.-W. Lim, *Chem. Rev.* **2012**, *112*, 782-835.

[4] I. Stassen, N. Burtch, A. Talin, P. Falcaro, M. Allendorf, R. Ameloot, *Chem. Soc. Rev.* **2017**, *46*, 3185-3241.

[5] O. M. Yaghi, M. O'Keeffe, N. W. Ockwig, H. K. Chae, M. Eddaoudi, J. Kim, *Nature* **2003**, *423*, 705-714.

[6] a) R. Chakrabarty, P. S. Mukherjee, P. J. Stang, *Chem. Rev.* **2011**, *111*, 6810-6918; b) C. Tan, X. Cao, X.-J. Wu, Q. He, J. Yang, X. Zhang, J. Chen, W. Zhao, S. Han, G.-H. Nam, M. Sindoro, H. Zhang, *Chem. Rev.* **2017**, *117*, 6225-6331.

[7] a) M. Zhao, Y. Huang, Y. Peng, Z. Huang, Q. Ma, H. Zhang, *Chem. Soc. Rev.* **2018**, *47*, 6267-6295; b) R. Dong, T. Zhang, X. Feng, *Chem. Rev.* **2018**, *118*, 6189-6235.

[8] Q. An, Q. Chen, W. Zhu, Y. Li, C. A. Tao, H. Yang, Z. Li, L. Wan, H. Tian, G. Li, *Chem. Commun.* **2010**, *46*, 725-727.

[9] M. Pfeffermann, R. Dong, R. Graf, W. Zajaczkowski, T. Gorelik, W. Pisula, A. Narita, K. Mullen, X. Feng, *J. Am. Chem. Soc.* **2015**, *137*, 14525-14532.

[10] R. H. Dong, M. Pfeffermann, H. W. Liang, Z. K. Zheng, X. Zhu, J. Zhang, X. L. Feng, *Angew. Chem. Int. Ed.* **2015**, *54*, 12058-12063.

[11] M. Moradi, N. L. Opara, L. G. Tulli, C. Wäckerlin, S. J. Dalgarno, S. J. Teat, M. Baljozovic, O. Popova, E. v. Genderen, A. Kleibert, H. Stahlberg, J. P. Abrahams, C. Padeste, P. F.-X. Corvini, T. A. Jung, P. Shahgaldian, *Sci. Adv.* **2018**, In press.

[12] N. R. Chevalier, C. Chevallard, P. Guenoun, *Langmuir* **2010**, *26*, 15824-15829.

[13] A. I. Buzin, G. Brezesinski, D. R. Tur, V. S. Papkov, A. V. Bakirov, S. N. Chvalun, *Macromolecules* **2015**, *48*, 3327-3336.

[14] A. I. Buzin, G. Brezesinski, V. S. Papkov, S. N. Chvalun, *MATEC Web Conf.* **2017**, *98*, 01002.

[15] R. Banerjee, M. K. Sanyal, M. K. Bera, A. Gibaud, B. Lin, M. Meron, *Sci Rep-Uk* **2015**, *5*, 8497.

[16] a) M. Moradi, L. G. Tulli, J. Nowakowski, M. Baljozovic, T. A. Jung, P. Shahgaldian, *Angew. Chem. Int. Ed.* **2017**, *56*, 14395–14399 ; b) P. S. L. G. Tulli, (Ed.: J. L. S. P. Neri, M.-X. Wang), Springer, Basel, **2016**, pp. 987 –1010.

[17] S. K. Sharma, S. Kanamathareddy, C. D. Gutsche, *Synthesis* **1997**, *1997*, 1268-1272.

[18] a) L. G. Tulli, N. Moridi, W. Wang, K. Helttunen, M. Neuburger, D. Vaknin, W. Meier, P. Shahgaldian, *Chem. Commun.* **2014**, *50*, 3938-3940; b) P. Shahgaldian, A. W. Coleman, S. S. Kuduva, M. J. Zaworotko, *Chem. Commun.* **2005**, 1968-1970; c) L. G. Tulli, W. Wang, W. R. Lindemann, I. Kuzmenko, W. Meier, D. Vaknin, P. Shahgaldian, *Langmuir* **2015**, *31*, 2351-2359.

[19] R. Makiura, O. Konovalov, *Sci. Rep.* **2013**, *3*, 2506.

[20] F. T. Hane, E. Drolle, Z. Leonenko, *Physical Chemistry Chemical Physics* **2014**, *16*, 15430-15436.

[21] P. Gao, X.-Y. Sun, B. Liu, H.-T. Lian, X.-Q. Liu, J.-S. Shen, *J. Mater. Chem. C* **2018**, *6*, 8105-8114.

[22] a) Y. Wang, C. Zhang, H. Li, G. Zhu, S.-S. Bao, S. Wei, L.-M. Zheng, M. Ren, Z. Xu, *Journal of Materials Chemistry B* **2015**, *3*, 296-305; b) K. Kishi, Y. Ehara, *Surf. Sci.* **1986**, *176*, 567-577.

[23] C. R. Groom, I. J. Bruno, M. P. Lightfoot, S. C. Ward, *Acta Crystallogr. B* **2016**, *72*, 171-179.

[24] I. J. Bruno, J. C. Cole, P. R. Edgington, M. Kessler, C. F. Macrae, P. McCabe, J. Pearson, R. Taylor, *Acta Crystallogr. B* **2002**, *58*, 389-397.

COMMUNICATION

First reported in-situ bilayer formation of metal-organic coordination networks (MOCNs) based on calix[4]arene building blocks upon coordination with copper metal ions at the air-water interface. By changing the copper ionic centers to nickel ions, a crystalline monolayer of the MOCN is fabricated.

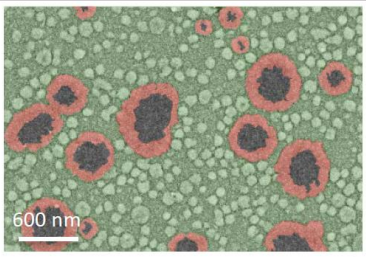

Mina Moradi, Nadia L. Opara, Catherine E. Housecroft, Ludovico G. Tulli, Henning Stahlberg, Thomas A. Jung, and Patrick Shahgaldian**

Page No. – Page No.

Controlling in-situ formation of bilayer vs monolayer of metal-organic coordination networks

Supporting Information

Controlling In-Situ Formation of Bilayer *vs* Monolayer of Metal-Organic Coordination Networks

Mina Moradi, Nadia L. Opara, Catherine E. Housecroft, Ludovico G. Tulli, Henning Stahlberg, Thomas A. Jung,* and Patrick Shahgaldian*

Table of Contents

Langmuir monolayer experiment

Nima 112D Langmuir trough was used to perform surface pressure-area compression isotherms. For all the experiments the trough and barriers were cleaned with analytical grade chloroform and nanopure water (resistivity ≥18 MΩ.cm). Aqueous solutions of 10 μM $CuCl_2.2H_2O$ and 10 μM $NiCl_2.6H_2O$ were used as subphase. A solution of **1** (13 μL, 0.5 mg mL^{-1} in chloroform) was spread on the air-liquid interface using a gastight microsyringe. After 15 min, for solvent evaporation and equilibration of amphiphiles at the interface, barriers were symmetrically closed at a speed rate of 5 cm^2 min^{-1}. The accuracies of π_c and A_0 measurements were of ±1 mN m^{-1} and ±1 $Å^2$ $molecule^{-1}$, respectively.

Langmuir-Schaefer transfer procedure

Highly oriented pyrolytic graphite (HOPG) and hydrophobic silicon wafers (coated with octadecyltrichlorosilane (OTS))[1] were used as solid substrates for the Langmuir-Schaefer (LS) transfers, using a Nima Coventry England deposition system. The speed of substrates approaching the interface was 1 mm min^{-1}. Metal organic coordination networks (MOCNs) of **1**, prepared in a 10 μM $CuCl_2$ and a 10 μM $NiCl_2$ solutions, were transferred onto the solid substrates at 40 and 30 mN m^{-1}, respectively. The substrates were slowly removed from the aqueous solution, after 15 min, at a constant speed of 1 mm min^{-1}.

Brewster angle microscopy

Nanofilm_ep3 system (Accurion) equipped with an internal solid-state laser at a wavelength of 658 nm was used to perform Brewster angle microscopy. The images were acquired using a CCD camera (768 × 562 pixels) and a 10× objective, equipped with an automatic focus scanner yielding 1 μm lateral resolution.

Spectroscopic ellipsometry

Ellipsometry analysis were carried out using an imaging and spectroscopic system (EP3 ellipsometer Accurion) in a nulling polarizer-compensator-sample-analyzer set-up. In the ellipsometry measurements the refractive index of **1** was considered 1.5.[2] OTS-coated silicon wafers were used as solid substrates for the LS transfer in the ellipsometry experiments.

Contact angle measurement

Contact angle experiments were carried out using a commercial Krüss ®Easy drop optical system (Krüss, GmbH, Germany). Static water contact angle was measured on samples with drops of 3 μL of nanopure water. Reproducibility was ensured by repeating the measurements at 5 different positions on each sample.

X-ray photoelectron spectroscopy

Monochromatic Al K_α (hv = 1486.7 eV) excitation source (Specs FOCUS 500) in normal emission using a Specs PHOIBOS 150 electron analyzer was used to perform *X*-ray photoelectron spectroscopy (XPS). The C1s core level of HOPG, 284.5 eV, was used as reference for the binding energies. The measurements were done in ultra-high vacuum system with base pressure of 10^{-11} mbar.

Atomic force microscopy

Atomic force microscopy in the PeakForce Tapping® mode using a Multimode 8 instrument (Bruker) equipped with a Nanoscope V controller was used for imaging and height analysis of the transferred MOCN of **1** from the interface onto a HOPG. The scanasyst-air-HR silicon tip on nitride lever were used for high-resolution AFM imaging.

Transmission electron microscopy

Monolayers of the MOCN of **1** were transferred from the air-solution interface onto a lacey-carbon-covered copper, electron microscopy grid (Ted Pella Inc., USA) via the Langmuir-Schaefer transfer procedure as developed and described before.[3] The transmission electron microscopy (TEM) imaging performed in the low dose mode, at cryo-conditions (the EM grid has been placed onto the cryoholder at room temperature, inserted to the microscope and cooled down with liquid nitrogen before exposure to the electrons) to reduce the electron beam-induced damage to minimum. The Talos (FEI) transmission electron microscope has been used, operating at accelerating voltage of 200 keV (corresponding to the 2.51 pm wavelength) and vacuum of 3.5×10^{-8} Torr. The strongly defocused images have been registered on FEI Ceta 16 MPixel CMOS camera reaching the contrast sufficient for clear observation of the MOCN layers of **1**.

Results

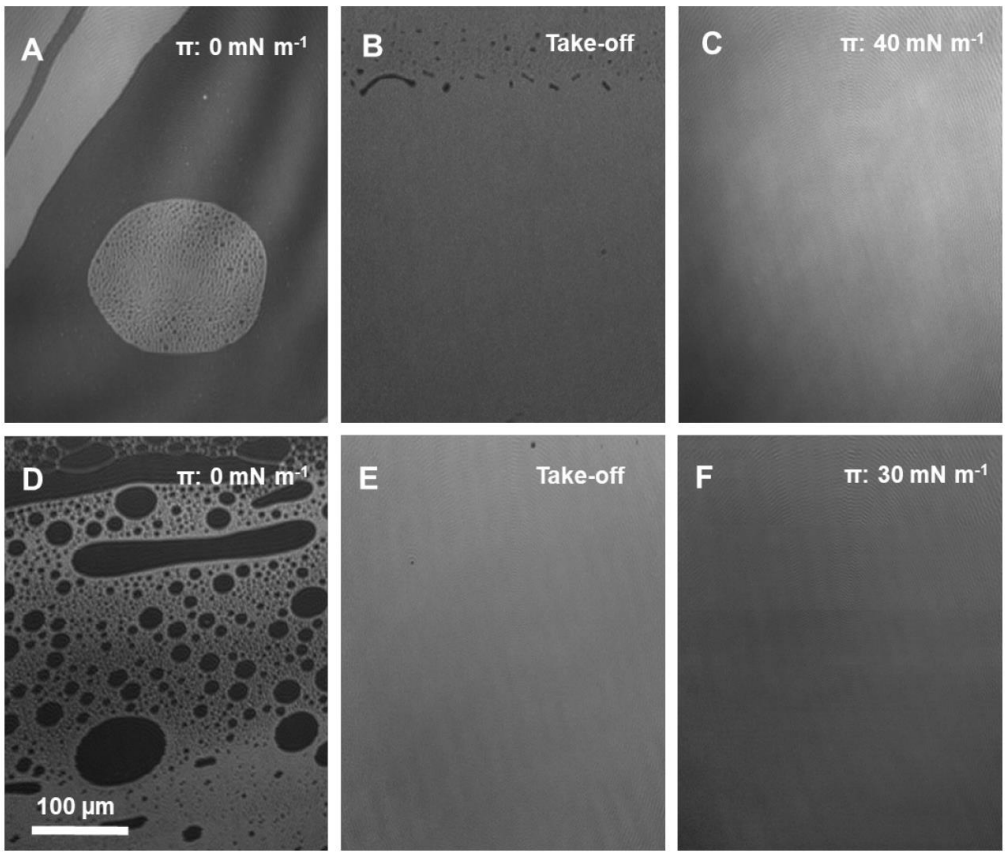

Figure S1. BAM micrographs of the layer of **1** formed on a 10 µM $CuCl_2$ aqueous solution (A-C) and a 10 µM $NiCl_2$ solution (D-F). A gas and liquid phases are identified before the take-off at the air-aqueous solution interface. Upon compression, a homogeneous layer is formed at the interface. In contrary to our recent publication on a similar amphiphile of **1** deprived the methylene bridge between the carboxy group and the arene ring, *i.e. p*-carboxy calix[4]arene derivative,[4] there is no sign of crystallinity in the BAM images of the self-assembled layer of **1**.

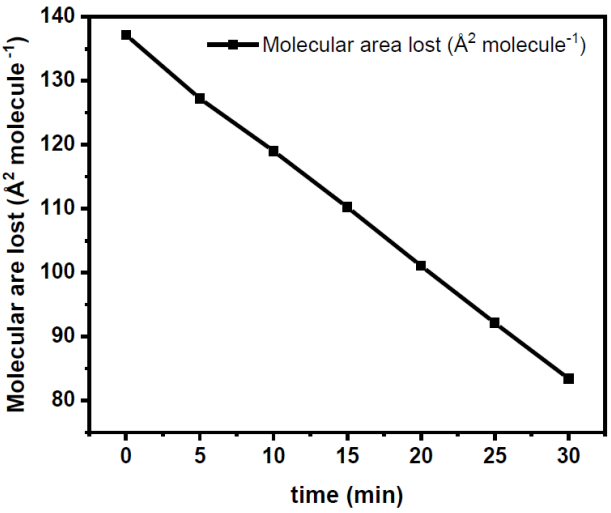

Figure S2. Stability test of the monolayer of **1** formed at the air-10 μM $CuCl_2$ solution interface at π: 40 mN m^{-1}. The linear losing of the molecular area over time, recorded from the Langmuir isotherm, could be assigned to flipping and turning of the amphiphiles of **1** into subphase.

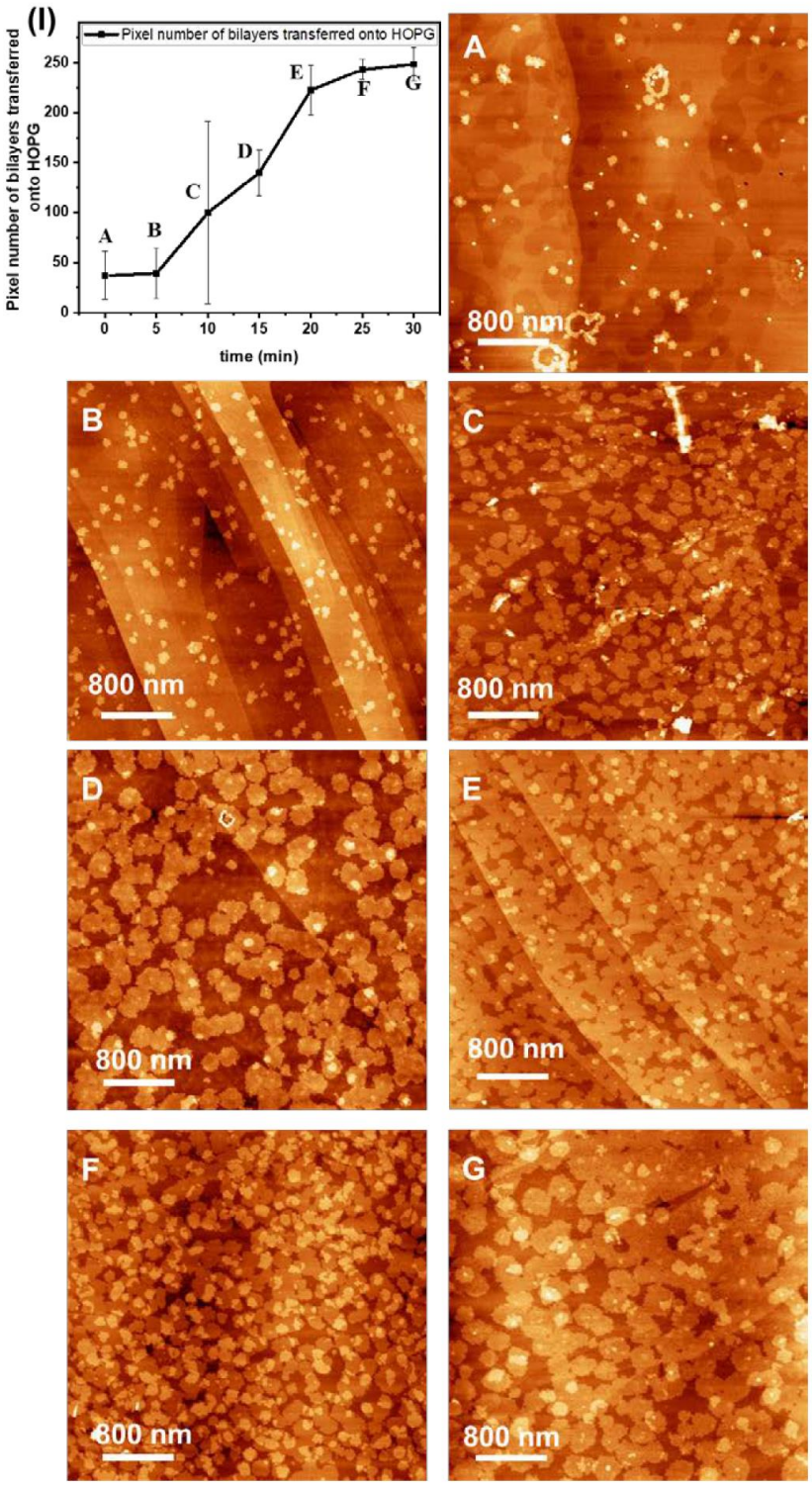

Figure S3. AFM analysis of the bilayers of **1** formed upon interaction with Cu^{2+} ions. The layer of **1** was transferred from the interface onto HOPG after different relaxation time of 0 (A), 5 (B), 10 (C), 15 (D), 20 (E), 25 (F) and 30 min (G).The plot (I) shows the pixel numbers of bilayer domains, counted from the AFM images, versus the relaxation time in which the layer was transferred from the interface. The linear regime of increasing the percentage of formed bilayers over the relaxation time shows that the degree of bilayer formation is kinetically controllable.

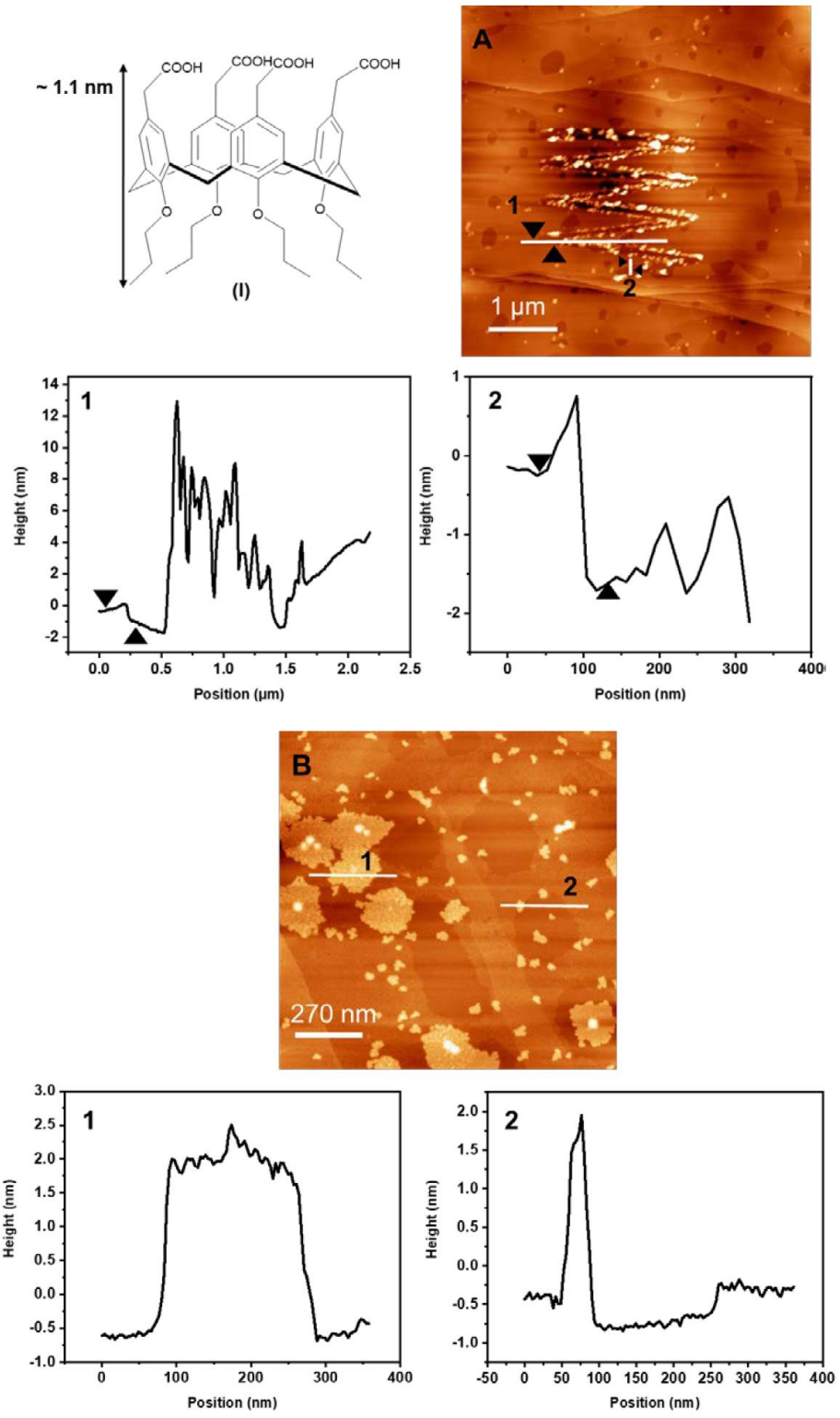
~ 1.1 nm
COOH
COOHCOOH
COOH
(I)
A
1
2
1 μm
1
Height (nm)
Position (μm)
2
Height (nm)
Position (nm)
B
1
2
270 nm
1
Height (nm)
Position (nm)
2
Height (nm)
Position (nm)

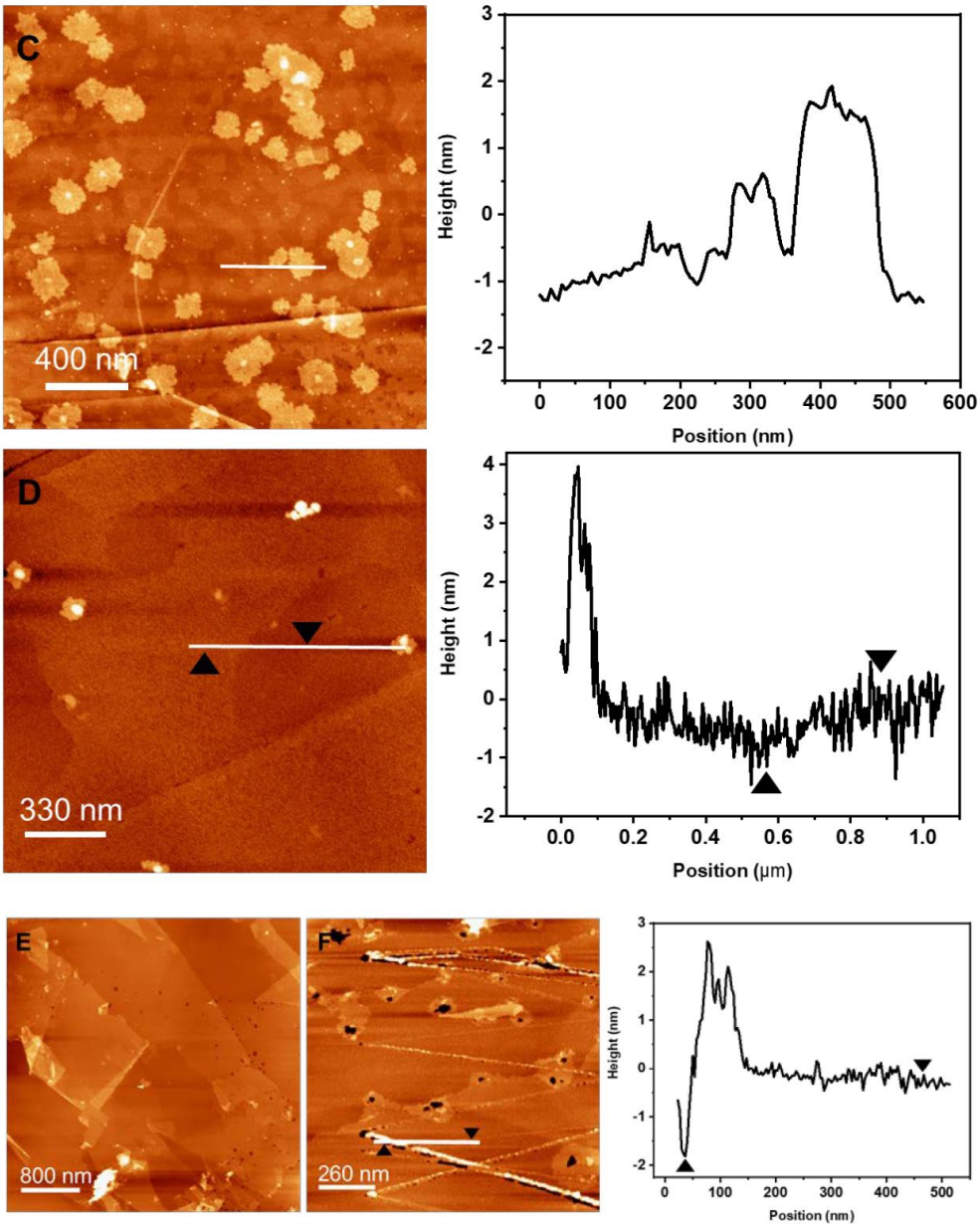

Figure S4. AFM height analysis of the transferred layers of **1** from a 10 μM $CuCl_2$ subphase (A-D) and a 10 μM $NiCl_2$ subphase (E-F) on HOPG by the LS method. The AFM height analysis of the layers of **1** were carried out on intentionally scratched layer in order to confirm the presence of a monolayer of **1** (A & F). The lines in the images indicate where the height profiles were recorded. The AFM results confirmed the presence of a monomolecular layer of **1** with an average height of 1.3 ± 0.2 nm. The measured height from the AFM is in a good agreement with the expected height of **1**, derived from the chemical structure of the similar analogues of **1** (~1 nm) (I).[4] The deviation from 1 nm could come from the ambient-condition AFM measurements[5] and also partially rearrangement of the molecules because of water evaporation. The height analysis on the bilayer domains (B-D) confirms the formation of two layers of **1** (3 ± 0.5 nm). A large area of 4 × 4 μm of highly crystalline monolayer of **1** upon interaction with Ni^{2+} is shown in (E), in absence of any formed bilayers.

Table S1. Contact angle measurements on the MOCNs of **1** transferred from a 10 μM $CuCl_2$ and a 10 μM $NiCl_2$ subphase. HOPG was considered as a reference sample. The increasing of the contact angle values of layers transferred after relaxation time is confirming higher degree of bilayer formation, *i.e.* more hydrophobic layers.

Sample	Contact angle(°)
HOPG (reference sample)	98.8 ± 6
Monolayer of **1** transferred from 10 μM $CuCl_2$ – with no relaxation time	86.6 ± 3.03
Monolayer of **1** transferred from 10 μM $CuCl_2$ – after 10 min relaxation time	93.3 ± 1.16
Monolayer of **1** transferred from 10 μM $CuCl_2$ – after 20 min relaxation time	96.3 ± 0.29
Monolayer of **1** transferred from 10 μM $CuCl_2$ – after 30 min relaxation time	96.5 ± 2.03
Monolayer of **1** transferred from 10 μM $NiCl_2$ – with no relaxation time	81.6 ± 2.34

Table S2. C1s XPS peak assignment for layer of **1** transferred on HOPG, by the LS method, from a 10 μM $CuCl_2$ (A) and a 10 μM $NiCl_2$ (B) solutions.[6] The derivatives were obtained by fitting the spectra.

(A)		Binding energy (eV)
C 1s	π - π*	291.3
	COOH	288.8
	C-O (sp^3)	286.0
	C-C (sp^3)	284.8
	C=C (sp^2)	284.5
(B)		Binding energy (eV)
C 1s	π - π*	291.6
	COOH	289.2
	C-O (sp^3)	286.9
	C-C (sp^3)	285.7
	C=C (sp^2)	284.5

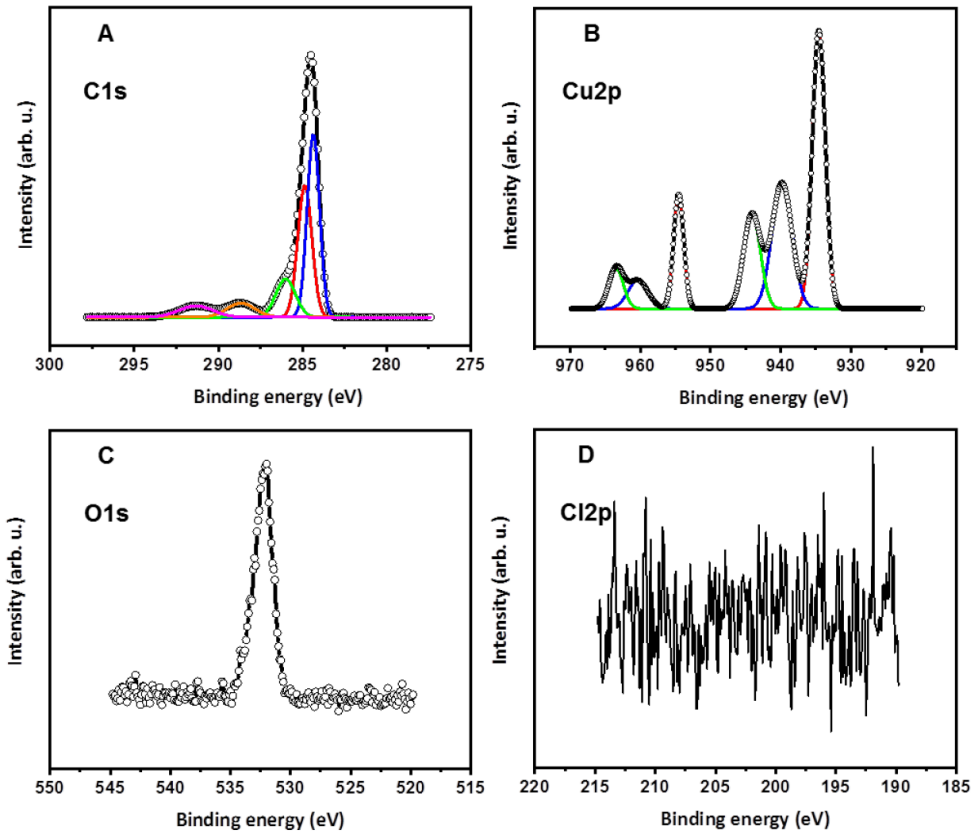

Figure S5. XP spectra of the MOCN of **1** transferred onto HOPG from 10 μM $CuCl_2$ by the LS method for C1s, Cu2p, O1s and Cl2p peaks, respectively (A-D). Copper XP spectrum in the MOCN of **1** shows two satellite peaks in 939.7 and 959.4 eV, characteristic features of Cu in CuO.[7] The binding energy and satellites of the copper XP spectrum indicate the copper oxidation state is +2 for the MOCN of **1**.[8] The absence of a Cl2p signal in the XPS results of the MOCN of **1** evidences the balanced charge in the system without any counter ion, *i.e.* Cl^-, due to dissociation of $CuCl_2$ and coordination of deprotonated carboxyl groups with Cu^{2+} ions. The ratio between carboxyl groups and Cu centers, presented in the MOCN of **1**, was calculated by integration of the area of carboxyl peak in the C1s and Cu in the Cu2p spectra. A precise interpretation of the O1s spectrum is challenging because of multiple peaks overlapping for different O entities of **1** and water molecules.

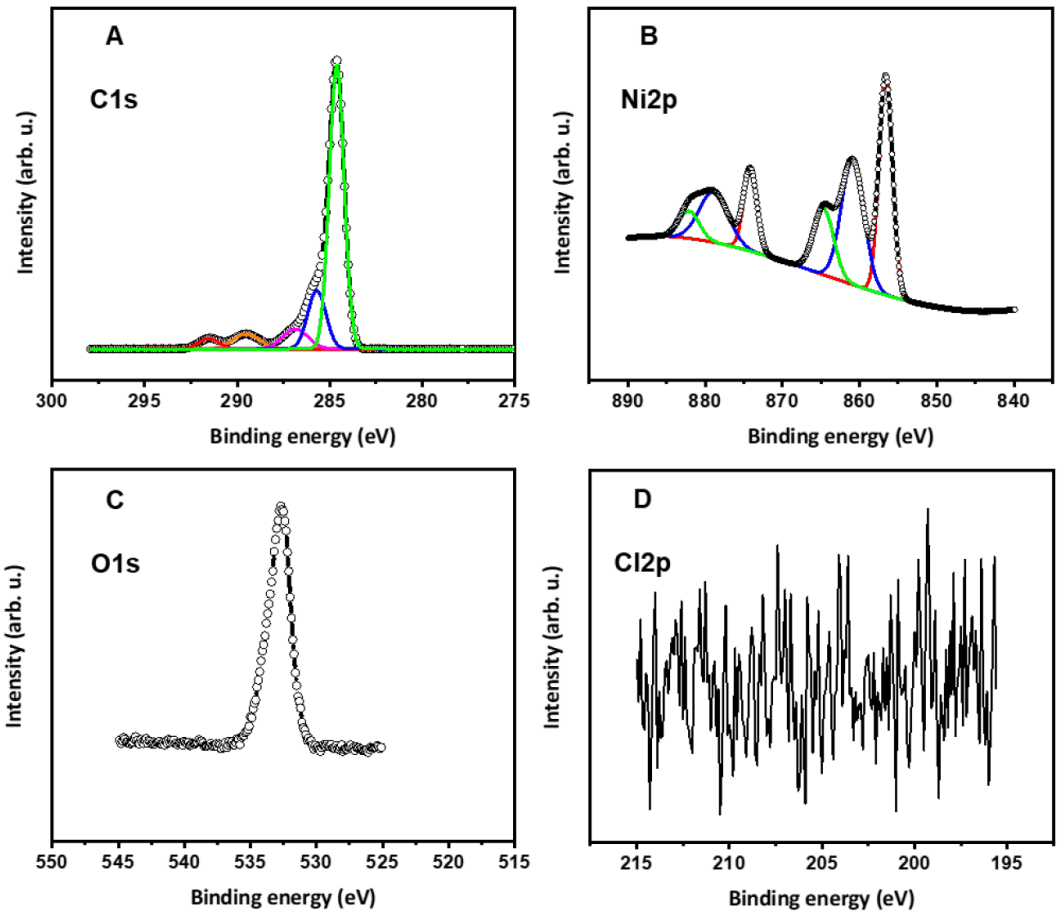

Figure S6. XP spectra of the MOCN of **1** transferred onto HOPG from a 10 μM $NiCl_2$ by the LS method for C1s, Ni2p, O1s and Cl2p peaks, respectively (A-D). Nickel XP spectrum in the MOCN of **1** shows two characteristic core level peaks in 855.6 and 873.34 eV, characteristic features of Ni in NiO.[7] The binding energy and satellites of the nickel spectrum indicate the nickel oxidation state is +2.[9] The absence of a Cl2p signal in the XPS results of the MOCN of **1** shows the balanced charge in the system without any counter ion. The ratio between the carboxyl groups and Ni^{2+} ions was measured to be 4:1 calculated by integration of the area of the carboxyl peak in the C1s and Ni in the Ni2p spectra. A precise interpretation of the O1s spectrum is challenging because of multiple peaks overlapping for different O entities of **1** and water molecules.[6]

References

[1] N. Moridi, C. Wackerlin, V. Rullaud, R. Schelldorfer, T. A. Jung, P. Shahgaldian, *Chem. Commun.* **2013**, *49*, 367-369.

[2] Y. M. Shirshov, S. A. Zynio, E. P. Matsas, G. V. Beketov, A. V. Prokhorovich, E. F. Venger, L. N. Markovskiy, V. I. Kalchenko, A. V. Soloviov, R. Merker, *Supramol. Sci.* **1997**, *4*, 491-494.

[3] M. Moradi, N. L. Opara, L. G. Tulli, C. Wäckerlin, S. J. Dalgarno, S. J. Teat, M. Baljozovic, O. Popova, E. v. Genderen, A. Kleibert, H. Stahlberg, J. P. Abrahams, C. Padeste, P. F.-X. Corvini, T. A. Jung, P. Shahgaldian, *Sci. Adv.* **2018**, In press.

[4] M. Moradi, L. G. Tulli, J. Nowakowski, M. Baljozovic, T. A. Jung, P. Shahgaldian, *Angew. Chem. Int. Ed.* **2017**, *56*, 14395–14399

[5] T. Bauer, Z. Zheng, A. Renn, R. Enning, A. Stemmer, J. Sakamoto, A. D. Schlüter, *Angew. Chem. Int. Ed.* **2011**, *50*, 7879-7884.

[6] L. Zhang, L. Ji, P.-A. Glans, Y. Zhang, J. Zhu, J. Guo, *Phys. Chem. Chem. Phys.* **2012**, *14*, 13670-13675.

[7] John F. Moulder, W. F. Stickle, Peter E. Sobol, K. D. Bomben, *Handbook of X-ray Photoelectron Spectroscopy*, USA, **1992**.

[8] a) R. Makiura, S. Motoyama, Y. Umemura, H. Yamanaka, O. Sakata, H. Kitagawa, *Nat. Mater.* **2010**, *9*, 565-571; b) Y. Wang, J. Im, J. W. Soares, D. M. Steeves, J. E. Whitten, *Langmuir* **2016**, *32*, 3848-3857.

[9] Y. Wang, C. Zhang, H. Li, G. Zhu, S.-S. Bao, S. Wei, L.-M. Zheng, M. Ren, Z. Xu, *J. Mater. Chem. B* **2015**, *3*, 296-305.

CONCLUSION AND OUTLOOK

Conclusion

This thesis aimed to describe a novel approach based on the molecular design of organic building blocks to fabricate molecularly precise 2D organic networks. Using the concepts of supramolecular chemistry and crystal engineering, we synthesized the first 2D free-standing and crystalline organic networks of calix[4]arene amphiphilic synthons. Calix[4]arene organic building blocks equipped with chemical functional groups were used to produce self-assembled 2D organic networks via the formation of coordination bonds or supramolecular interactions. The air-water interface was used to orient and confine the molecular modules in a 2D plane for supramolecular aggregation or the interfacial reaction.

2D metal-organic coordination network (MOCN) of C_3-p-carboxy-calix amphiphiles – This thesis reports the first example of a 2D MOCN of *C_3-p*-carboxy-calix synthons coordinating Cu^{2+} ions with an octahedral coordination motif.

We confirmed that *C_3-p*-carboxy-calix molecules self-assemble into 2D crystalline networks with and without ionic centers. Furthermore, the addition of Cu^{2+} ions to the water in the Langmuir-Blodgett (LB) trough (subphase) drastically altered the morphology of the 2D layer to a dendritic multicrystalline monolayer underlining the effect of the increased intermolecular bonding mediated by the coordination reaction.

The Langmuir-Schaefer (LS) deposition method was used to transfer the self-assembled monolayer from the air-liquid interface onto a solid substrate for a series of surface analysis techniques. *X*-ray photoelectron spectroscopy (XPS) analysis confirmed the formation of coordination bonds between the carboxy functional groups and copper ions. Atomic force microscopy (AFM) of the MOCNs of *C_3-p*-carboxy-calix building units revealed a crystalline monolayer consisting of domains with different orientations and stripe morphologies. Transmission electron microscopy (TEM) analysis proved the 2D MOCNs of *C_3-p*-carboxy-calix are highly stable and can span perforated TEM grids with pore sizes up to $5 \times 5\ \mu m^2$.

Moreover, high-resolution TEM (HRTEM) images showed the free-standing MOCN of *C_3-p*-carboxy-calix amphiphiles act as a template for crystallization of copper oxide domains (Figure 1); further investigations are needed to fully understand this phenomenon.

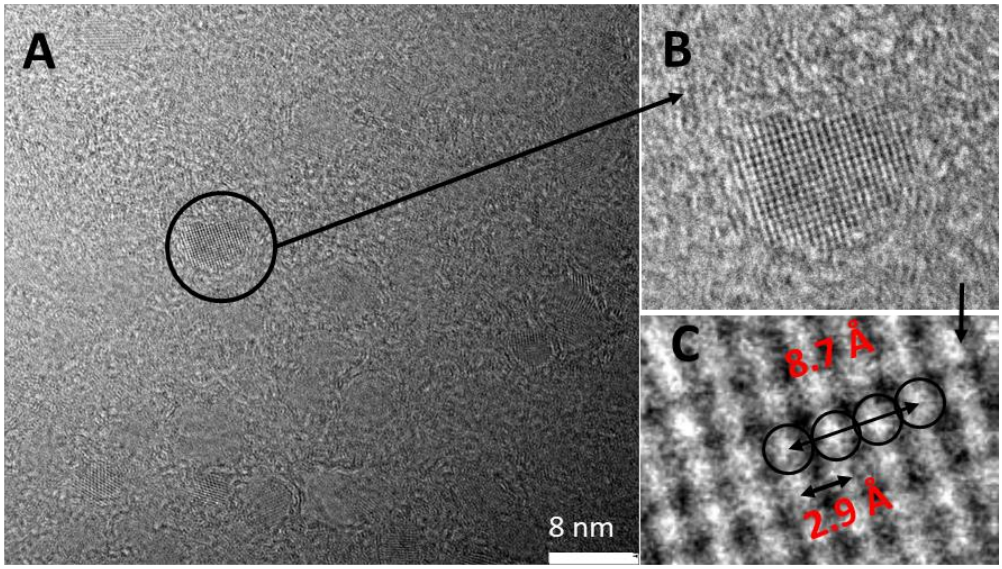

Figure 1: (A) HRTEM analysis on the free-standing monolayer of the MOCN of *C_3-p*-carboxy-calix amphiphiles. (B & C) Zoomed images on the crystalline domains of CuO with unit cell size of 2.9 Å.

2D supramolecular-organic network (SON) of C_3-p-me-CN-calix amphiphiles – The molecular design strategy allowed us to fabricate, for the first time, a robust free-standing 2D crystalline SON of *C_3-p*-me-cyano-calix via self-assembly driven by weak and moderately directional dipole-dipole interactions.

By replacing the carboxy groups of the *C_3-p*-carboxy-calix with methyl cyano functional groups, we aimed to fabricate self-assembled monolayers via dipole-dipole interactions between the cyano binding moieties. The layers were produced by the LS method, transferred from the interface onto highly oriented pyrolytic graphite (HOPG) substrate, and analyzed using a wide range of surface analysis techniques including AFM, XPS, near-edge *X*-ray absorption fine spectroscopy and TEM.

Molecular-resolution AFM images showed single *C_3-p*-me-cyano-calix (and missing building units) were arranged in a square packing fashion within the crystalline 2D SON. TEM analysis proved the stability of the layer, which can span perforated TEM grids with holes as large as 3 × 3 µm. Electron diffraction analysis of the free-standing SON confirmed the layer consisted of an extended array of molecules composed of square, symmetric unit cells, in perfect agreement with the AFM results.

Therefore, the in-depth analysis of this system confirmed 2D SONs of calix[4]arene derivatives can be fabricated via self-assembly due to non-covalent interactions between the building blocks.

In-situ bilayer formation of MOCN based on C_3-p-me-carboxy-calix amphiphiles – A methylene bridge between the carboxy functional group and the arene ring of the *C_3-p*-carboxy-calix molecules was added to provide more conformational freedom for the carboxy groups and enable adoption of different coordination geometries upon coordinating various

ions in the subphase. Langmuir isotherm studies of the *C_3-p*-carboxy-calix MOCN at the interface and XPS and AFM analysis of the MOCN transferred from the interface onto HOPG substrate confirmed that *C_3-p*-me-carboxy-calix amphiphiles coordinate Cu^{2+} ions and form bilayers in situ at the interface due by adopting a $\{Cu_2(O_2CR)_4\}$ paddle-wheel coordination geometry.

Since these amphiphiles have more freedom and flexibility to adopt different coordination geometries, the molecules can also coordinate Ni^{2+} ions and — in contrast to the bilayer on coordination of Cu^{2+} ions — generate a crystalline monolayer via formation of $\{NiO_6\}$ octahedral coordination geometry. Both the monolayers and bilayers of these *C_3-p*-me-carboxy-calix coordination networks were stable as free-standing layers.

2D free-standing calix[4]arene-based metal-organic networks – We showed that the stable free-standing layers of 2D MOCN formed from the *C_3-p*-carboxy-calix and *C_3-p*-me-carboxy-calix building blocks can be utilized as sample supports for the imaging of single biomolecules/assemblies and nanoparticles.

We deposited viruses (*e.g.* granulovirus and tobacco mosaic virus [TMV]), enzymes (catalase nanocrystals and urease solution), protein crystals and single iron nanoparticles on the free-standing MOCNs. Figure 2 illustrates some successful deposition experiments on the free-standing MOCN of calix[4]arene amphiphiles.

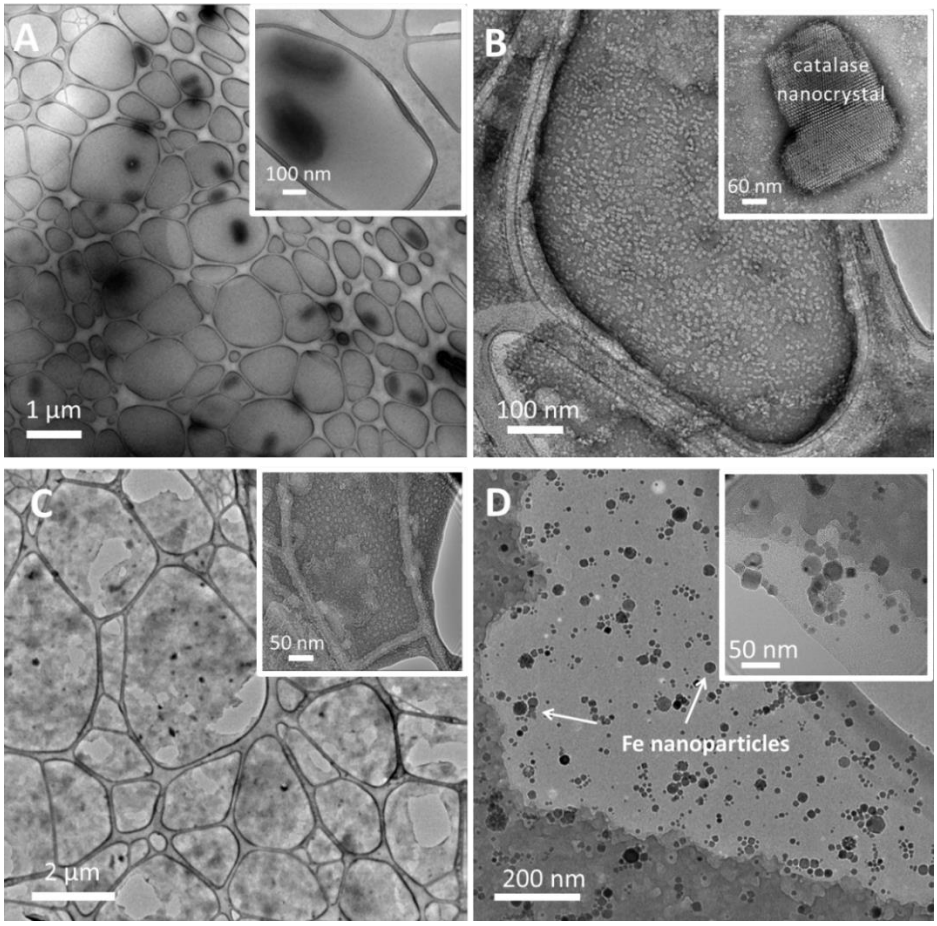

Figure 2: TEM images of the deposited biomolecules, enzymes and viruses on the MOCN of calix[4]arene amphiphiles transferred from the interface onto TEM grids. (A) Granulovirus nanocrystals, kindly provided by Kenneth Goldie and Prof. Peter Metcalf from Auckland. (B) Uranyl acetate catalase nanocrystal. (C) Protein crystals deposition on the MOCN of calix[4]arene amphiphiles coordinated Ni^{2+} ions. The protein solution was kindly provided by Jarek Sędzicki and purified by Frank Lehmann in C-CINA bio center in Basel, Switzerland. (D) TEM analysis on the deposited Fe nanoparticles. The deposition experiment was done by Tatiana Savchenko in PSI, Switzerland.

To successfully image biomolecules, which only scatter the electron beam weakly, we designed “bilayer support substrates” by transferring free-standing layers of calix[4]arene networks onto a free-standing graphene monolayer, and then deposited the biomolecules on the calix[4]arene-based bilayer membranes. We expect that the specific diffraction pattern of graphene can be easily subtracted, as a background, from the diffraction pattern produced by the molecules deposited on the support. Moreover, denaturation of the deposited biomolecules is suppressed by the hydrophilic nature of the calix[4]arene-based membrane. Figure 3 shows our first trials of deposition experiments on bilayer calix[4]arene/graphene sample supports using TMV molecules and urease particles.

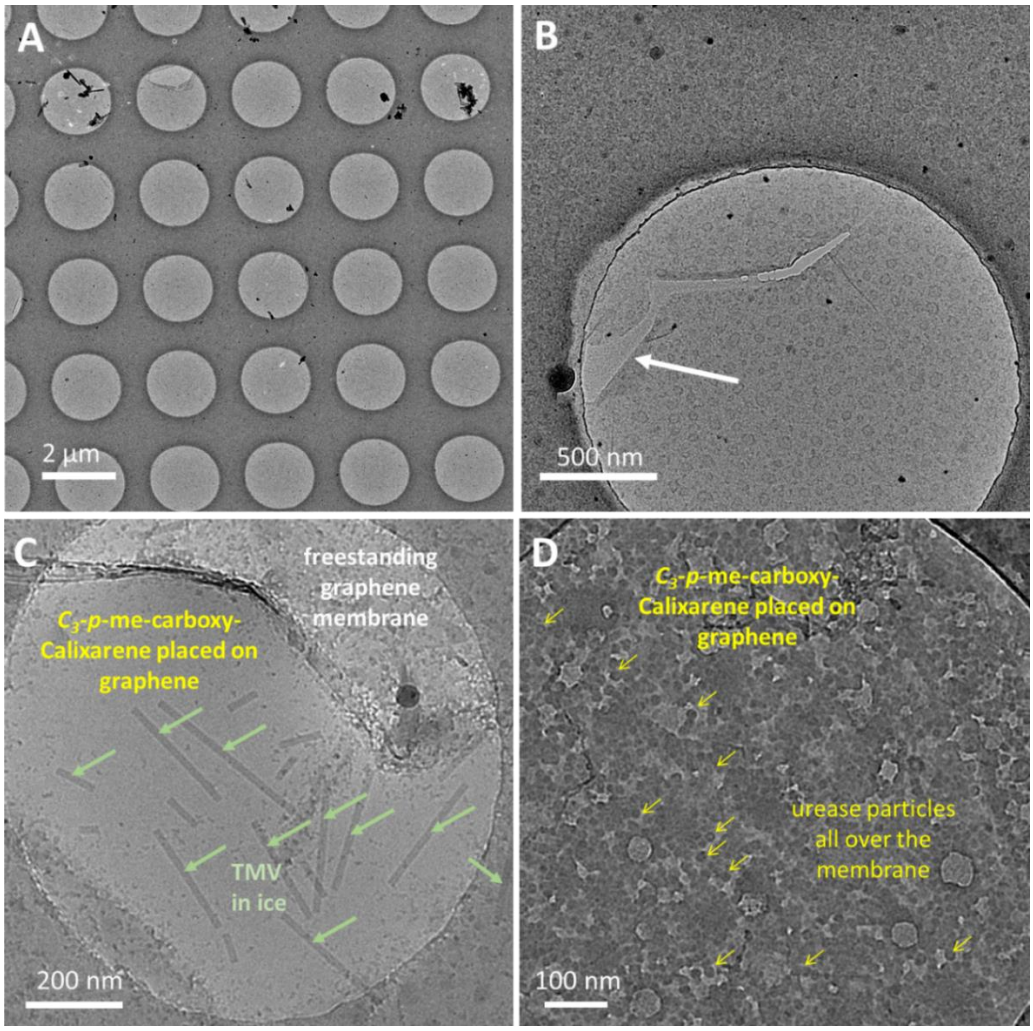

Figure 3: (A & B) TEM images of the bilayered calix[4]arene and graphene membranes. In (B) the layers of graphene and free-standing MOCN of calix[4]arene amphiphiles are visible in the ruptured part of the membrane, shown by the white arrow. TEM images of the deposited (C) TMV molecules and (D) urease particles on the calix[4]arene-based bilayered membranes.

Outlook

On the basis of the work described in this thesis, organic networks of calix[4]arene derivatives can be considered as a new generation of sample carriers for cryo-TEM and *X*-ray structural studies of biomolecules and magnetic nanoparticles.

Employing the molecular design strategy based on interfacial self-assembly introduced in this PhD thesis enables fabrication of other non-trivial structures with unique properties. For example:

- New and complex 2D organic networks could be synthesized by using preformed metal complexes, *i.e.* secondary building units instead of single ions.
- 2D covalent-organic frameworks could be fabricated from calix[4]arene amphiphiles functionalized with *e.g.* pyrazolyl or amino chemical groups.
- The calixarenes could be replaced by other macrocycles such as cyclodextrin, crown ethers and pillararenes. The 2D architectures of chiral amphiphilic crown ethers or pillararenes could potentially be employed as templates to recognize enantiomers of biomolecules.
- The properties and functions of the organic networks can be precisely tuned for example by changing the lipophilicity of the amphiphilic building units.

REFERENCES

1. Tan, C. *et al.* Recent advances in ultrathin two-dimensional nanomaterials. *Chem. Rev.* **117**, 6225-6331 (2017).
2. Dong, R., Zhang, T., Feng, X. Interface-assisted synthesis of 2D materials: trend and challenges. *Chem. Rev.* **118**, 6189-6235 (2018).
3. Zhao, M. *et al.* Two-dimensional metal–organic framework nanosheets: synthesis and applications. *Chem. Soc. Rev.* **47**, 6267-6295 (2018).
4. Böker, A., He, J., Emrick, T., Russell, T. P. Self-assembly of noparticles at interfaces. *Soft Matter* **3**, 1231-1248 (2007).
5. Toor, A., Feng, T., Russell, T. P. Self-assembly of nanomaterials at fluid interfaces. *Eur. Phys. J. E* **39**, 57 (2016).
6. Van der waals, J. D. *On the continuity of the gaseous and liquid states.* Doctoral Dissertation Thesis, Universiteit Leiden, (1873).
7. Fischer, E. Einfluss der configuration auf die wirkung der enzyme. *Ber. Dtsch. Chem. Ges.* **27**, 2985-2993 (1894).
8. Steed, J. W., Atwood, J. L., Gale, P. A. *Definition and emergence of supramolecular chemistry. In supramolecular chemistry: from molecules to nanomaterials*. (John Wiley & Sons, 2012).
9. Latimer, W. M., Rodebush, W. H. Polarity and ionization from the standpoint of the lewis theory of valence. *JACS* **42**, 1419-1433 (1920).
10. Pauling, L. *The nature of the chemical bond and the structure of molecules and crystals: an introduction to modern structural chemistry*. (Cornell University Press, USA, 1986).
11. Kaufmann, G. B., Werner, A. *Founder of coordination chemistry*. (Springer Verlag: Berlin and New York, 1966).
12. Pedersen, C. J. Cyclic Polyethers and their complexes with metal salts. *JACS* **89**, 7017-7036 (1967).
13. Lehn, J.-M. Supramolecular chemistry—scope and perspectives molecules, supermolecules, and molecular devices (Nobel Lecture). *Angew. Chem. Int. Ed.* **27**, 89-112 (1988).
14. Gutsche, C. D., Muthukrishnan, R. Calixarenes. 1. analysis of the product mixtures produced by the base catalyzed condensation of formaldehyde with *para*-substituted phenols. *J. Org. Chem.* **43**, 4905-4906 (1978).
15. Cohen, Y., Slovak. S., Avram., L. *Calixarenes and beyond,* (ed J. L. Sessler P. Neri, M.-X. Wang), 811–842 (Springer, 2016).
16. Coletta, M., Brechin, E. K., Dalgarno, S. J. *Calixarenes and beyond,* (ed J. L. Sessler P. Neri, M.-X. Wang), 671-689 (Springer, 2016).
17. Salvio, R., Cacciapaglia, R., Casnati, A. *Calixarenes and beyond,* (ed J. L. Sessler P. Neri, M.-X. Wang), 691-718, (Springer, 2016).
18. Feynman, R. There's plenty of room at the ottom. *Eng. Sci.*, 22-36 (1960).
19. Schmidt, G. M. J. Photodimerization in the solid state. *Pure Appl. Chem.* **27**, 647-678 (1971).
20. Schmidt, G. M. J. 385. Topochemistry. Part III. the crystal chemistry of some trans-cinnamic acids. *JACS (Resumed)*, 2014-2021 (1964).
21. Elacqua, E., Laird, R. C., MacGillivray, L. R., *Supramolecular chemistry: from molecules and nanomaterials,* (ed P. A. Gale J. W. Steed) (Wiley, 2012).
22. MacGillivray, L. R. Organic synthesis in the solid state via hydrogen-bond-driven self-assembly. *Org. Chem.* **73**, 3311-3317 (2008).
23. Desiraju, G. R., Sarma, J. A. R. P. Crystal engineering via donor–acceptor interactions. *X*-Ray crystal structure and solid state reactivity of the 1 : 1 complex, 3,4-dimethoxycinnamic acid–2,4-dinitrocinnamic acid. *Chem. Commun.*, **1**, 45-46 (1983).
24. Tiekink, E. R. T., Vittal, J. J., *Frontiers in crystal engineering*. (John Wiley & Sons, Ltd, Chichester, UK, 2006).
25. Moulton, B., Zaworotko, M. J., From molecules to crystal engineering: supramolecular isomerism and polymorphism in network solids. *Chem. Rev.* **101**, 1629-1658 (2001).

26. Yaghi, O. M. *et al.* Reticular synthesis and the design of new materials. *Nature* **423**, 705-714 (2003).
27. Desiraju, G. R. *Crystal Engineering: The design of organic solids (Materials Science Monographs)*. (Elsevier, Amsterdam, 1989).
28. Desiraju, G. R. Crystal engineering: from molecule to crystal. *JACS* **135**, 9952-9967 (2013).
29. Desiraju, G. R. Designer crystals: intermolecular interactions, network structures and supramolecular synthons. *Chem. Commun.*, **1**, 1475-1482 (1997).
30. Maddox, J. Crystals from first principles. *Nature* **335**, 201 (1988).
31. Kalmutzki, M. J., Hanikel, N., Yaghi, O. M. Secondary building units as the turning point in the development of the reticular chemistry of MOFs. *Sci. Adv.* **4**, 1-16 (2018).
32. Abrahams, B. F., Hoskins, B. F., Michail, D. M., Robson, R. Assembly of porphyrin building blocks into network structures with large channels. *Nature* **369**, 727-729 (1994).
33. Eddaoudi, M. *et al.* Modular chemistry: secondary building units as a basis for the design of highly porous and robust metal−organic carboxylate frameworks. *Acc. Chem. Res.* **34**, 319-330 (2001).
34. Yaghi, O. M., Li, H., Davis, C., Richardson, D., Groy, T. L. Synthetic strategies, structure patterns, and emerging properties in the chemistry of modular porous solids. *Acc. Chem. Res.* **31**, 474-484 (1998).
35. Batten, S. R., Robson, R. Interpenetrating nets: ordered, periodic entanglement. *Angew. Chem. Int. Ed.* **37**, 1460-1494 (1998).
36. Yaghi, O. M., O'Keeffe, M., Kanatzidis, M. Design of solids from molecular building blocks: golden opportunities for solid state chemistry. *Solid State Chem.* **152**, 1-2 (2000).
37. Yaghi, O. M., Li, H. Hydrothermal synthesis of a metal-organic framework containing large rectangular channels. *JACS* **117**, 10401-10402 (1995).
38. Shetty, D. *et al.* Calix[4]arene-based porous organic nanosheets. *ACS Appl. Mater. Interfaces* **10**, 17359-17365 (2018).
39. Kitagawa, S., Kitaura, R., Noro, S.-i. Functional porous coordination polymers. *Angew. Chem. Int. Ed.* **43**, 2334-2375 (2004).
40. Makiura, R. *et al.* Towards rational modulation of in-plane molecular arrangements in metal–organic framework nanosheets. *ChemPlusChem* **79**, 1352-1360 (2014).
41. Yamada, T., Otsubo, K., Makiura, R., Kitagawa, H. Designer Coordination polymers: dimensional crossover architectures and proton conduction. *Chem. Soc. Rev.* **42**, 6655-6669 (2013).
42. Rao, C. N. R., Waghmare, U. V. *2D inorganic materials beyond graphene*. (World Scientific, 2017).
43. Liu, H. *et al.* Synthetic two-dimensional organic structures. *Chin. J. Polym. Sci.* **36**, 425-444 (2018).
44. Cai, S.-L. *et al.* The organic flatland—recent advances in synthetic 2D organic layers. *Adv. Mater.* **27**, 5762-5770 (2015).
45. Xu, M., Liang, T., Shi, M., Chen, H. Graphene-like two-dimensional materials. *Chem. Rev.* **113**, 3766-3798 (2013).
46. Butler, S. Z. *et al.* Progress, challenges, and opportunities in two-dimensional materials beyond graphene. *ACS Nano* **7**, 2898-2926 (2013).
47. Jiang, C., Markutsya, S., Pikus, Y., Tsukruk, V. V. Freely suspended nanocomposite membranes as highly sensitive sensors. *Nat. Mater.* **3**, 721-728 (2004).
48. Atwood, J. L., Barbour, L. J., Jerga, A. Storage of methane and freon by interstitial van der Waals confinement. *Science* **296**, 2367-2369 (2002).
49. Corbellini, F. *et al.* Assembly of a supramolecular capsule on a molecular printboard. *JACS* **126**, 17050-17058 (2004).
50. Shetty, D. *et al.* An ultra-absorbent alkyne-rich porous covalent polycalix[4]arene for water purification. *J. Mater. Chem. A* **5**, 62-66 (2017).
51. Tulli, L. G. Shahgaldian P., *Calixarenes and beyond,* (ed J. L. Sessler P. Neri, M.-X. Wang) 987–1010 (Springer, 2016).
52. Braslau, A. *et al.* Surface roughness of water measured by *X*-Ray reflectivity. *Phys. Rev. Lett.* **54**, 114-117 (1985).
53. Wirth, M. J., Burbage, J. D. Reorientation of acridine orange at liquid alkane/water interfaces. *J. Phys. Chem. A* **96**, 9022-9025 (1992).

54. Eddaoudi, M. *et al.* Systematic design of pore size and functionality in isoreticular MOFs and their application in methane storage. *Science* **295**, 469-472 (2002).
55. Li, J.-R., Kuppler, R. J., Zhou, H.-C. Selective gas adsorption and separation in metal–organic frameworks. *Chem. Soc. Rev.* **38**, 1477-1504 (2009).
56. Skorjanc, T. *et al.* Redox-responsive covalent organic nanosheets from viologens and calix[4]arene for iodine and toxic dye capture. *Chem. Eur. J.* **24**, 8648-8655 (2018).
57. Li, H., Wu, J., Yin, Z., Zhang, H. Preparation and applications of mechanically exfoliated single-layer and multilayer MoS_2 and WSe_2 nanosheets. *Acc. Chem. Res.* **47**, 1067-1075 (2014).
58. Wang, X. *et al.* Reversed Thermo-switchable molecular sieving membranes composed of two-dimensional metal-organic nanosheets for gas separation. *Nat. Commun.* **8**, 14460-14470 (2017).
59. Zheng, J. *et al.* High Yield Exfoliation of two-dimensional chalcogenides using sodium naphthalenide. *Nat. Commun.* **5**, 2995-3002 (2014).
60. Paton, K. R. *et al.* Scalable production of large quantities of defect-free few-layer graphene by shear exfoliation in liquids. *Nat. Mater.* **13**, 624-630 (2014).
61. Ma, R. *et al.* Topochemical synthesis of monometallic (Co^{2+}–Co^{3+}) layered double hydroxide and its exfoliation into positively charged $Co(OH)_2$ nanosheets. *Angew. Chem. Int. Ed.* **47**, 86-89 (2008).
62. Zeng, Z. *et al.* An effective method for the fabrication of few-layer-thick inorganic nanosheets. *Angew. Chem. Int. Ed.* **51**, 9052-9056 (2012).
63. Huang, A., Bux, H., Steinbach, F., Caro, J. Molecular-sieve membrane with hydrogen permselectivity: ZIF-22 in LTA topology prepared with 3-aminopropyltriethoxysilane as covalent linker. *Angew. Chem. Int. Ed.* **49**, 4958-4961 (2010).
64. Kubo, M., Chaikittisilp, W., Okubo, T. Oriented films of porous coordination polymer prepared by repeated in-situ crystallization. *Chem. Mater.* **20**, 2887-2889 (2008).
65. Scherb, C., Schödel, A., Bein, T. Directing the structure of metal–organic frameworks by oriented surface growth on an organic monolayer. *Angew. Chem. Int. Ed.* **47**, 5777-5779 (2008).
66. Motoyama, S., Makiura, R., Sakata, O., Kitagawa, H. Highly crystalline nanofilm by layering of porphyrin metal−organic framework sheets. *JACS* **133**, 5640-5643 (2011).
67. Shekhah, O. Layer-by-layer method for the synthesis and growth of surface mounted metal-organic frameworks (SURMOFs). *Materials* **3**, 1302-1315 (2010).
68. Kim, K. K. *et al.* Synthesis of monolayer hexagonal boron nitride on Cu foil using chemical vapor deposition. *Nano Letters* **12**, 161-166 (2012).
69. Qin, H., Li, F., Wang, D., Lin, H., Jin, J. Organized molecular interface-induced noncrystallizable polymer ultrathin nanosheets with ordered chain alignment. *ACS Nano* **10**, 948-956 (2016).
70. Varaksa, N., Pospíšil, L., Magnera, T. F., Michl, J. Self-assembly of a metal-ion-bound monolayer of trigonal connectors on mercury: an electrochemical Langmuir trough. *PNAS* **99**, 5012-5017 (2002).
71. Culp, J. T., Park, J.-H., Stratakis, D., Meisel, M. W., Talham, D. R. Supramolecular assembly at interfaces: formation of an extended two-dimensional coordinate covalent square grid network at the air−water interface. *JACS* **124**, 10083-10090 (2002).
72. Bauer, T. *et al.* Synthesis of free-standing, monolayered organometallic sheets at the air/water interface. *Angew. Chem. Int. Ed.* **50**, 7879-7884 (2011).
73. Makiura, R. *et al.* Surface nano-architecture of a metal–organic framework. *Nat. Mater.* **9**, 565-571 (2010).
74. Hmadeh, M. *et al.* New porous crystals of extended metal-catecholates. *Chem. Mater.* **24**, 3511-3513 (2012).
75. Zhao, M. *et al.* Ultrathin 2D metal–organic framework nanosheets. *Adv. Mater.* **27**, 7372-7378 (2015).
76. Kambe, T. *et al.* π-Conjugated nickel bis(dithiolene) complex nanosheet. *JACS* **135**, 2462-2465 (2013).
77. Takada, K. *et al.* Electrochromic bis(terpyridine)metal complex nanosheets. *JACS* **137**, 4681-4689 (2015).
78. Sakamoto, R. *et al.* A photofunctional bottom-up bis(dipyrrinato)zinc(II) complex nanosheet. *Nat. Commun.* **6**, 6713 (2015).

79. Clough, A. J. *et al.* Metallic Conductivity In a two-dimensional cobalt dithiolene metal–organic framework. *JACS.* **139**, 10863-10867 (2017).
80. Clough, A. J., Yoo, J. W., Mecklenburg, M. H., Marinescu, S. C. Two-dimensional metal–organic surfaces for efficient hydrogen evolution from water. *JACS* **137**, 118-121 (2015).
81. Mali, K. S., Pearce, N., De Feyter, S., Champness, N. R. Frontiers of supramolecular chemistry at solid surfaces. *Chem. Soc. Rev.* **46**, 2520-2542 (2017).
82. Lin, Y. *et al.* Self-assembled 2D free-standing janus nanosheets with single-layer thickness. *JACS* **139**, 13592-13595 (2017).
83. Zhang, K.-D. *et al.* Toward a single-layer two-dimensional honeycomb supramolecular organic framework in water. *JACS* **135**, 17913-17918 (2013).
84. An, Q. *et al.* A facile method for preparing one-molecule-thick free-standing organic nanosheets with a regular square shape. *Chem. Commun.* **46**, 725-727 (2010).
85. Pfeffermann, M. *et al.* Free-standing monolayer two-dimensional supramolecular organic framework with good internal order. *JACS* **137**, 14525-14532 (2015).
86. Dong, R. H. *et al.* Large-area, free-standing, two-dimensional supramolecular polymer single-layer sheets for highly efficient electrocatalytic hydrogen evolution. *Angew. Chem. Int. Ed.* **54**, 12058-12063 (2015).
87. Bai, W., Jiang, Z. W., Ribbe, A. E., Thayumanavan, S. Smart organic two-dimensional materials based on a rational combination of non-covalent interactions. *Angew. Chem. Int. Ed.* **55**, 10707-10711 (2016).
88. Payamyar, P., King, B. T., Öttinger, H. C. & Schlüter, A. D. Two-dimensional polymers: concepts and perspectives. *Chem. Commun.* **52**, 18-34 (2016).
89. Gee, G., Rideal E. K., F. R.S., Reaction in monolayers of drying oils I - the oxidation of the maleic anhydride compound of β-elaeostearin. *Proc. Royal Soc.* **153**, 116-128 (1935).
90. Kissel, P. *et al.* A two-dimensional polymer prepared by organic synthesis. *Nat. Chem.* **4**, 287-291 (2012).
91. Murray, D. J. *et al.* Large area synthesis of a nanoporous two-dimensional polymer at the air/water interface. *JACS* **137**, 3450-3453 (2015).
92. Lange, R. Z., Hofer, G., Weber, T., Schlüter, A. D. A two-dimensional polymer synthesized through topochemical [2 + 2]-cycloaddition on the multigram scale. *JACS* **139**, 2053-2059 (2017).
93. Müller, V. *et al.* Structural characterization of a covalent monolayer sheet obtained by two-dimensional polymerization at an air/water interface. *Angew. Chem. Int. Ed.* **56**, 15262-15266 (2017).
94. Müller, V. *et al.* A two-dimensional polymer synthesized at the air/water interface. *Angew. Chem. Int. Ed.* **57**, 10584-10588 (2018).
95. Côté, A. P. *et al.* Porous, crystalline, covalent organic frameworks. *Science* **310**, 1166-1170 (2005).
96. Spitler, E. L. *et al.* A 2D covalent organic framework with 4.7 nm pores and insight into its interlayer stacking. *JACS* **133**, 19416-19421 (2011).
97. Tulli, L. G. *et al.* Interfacial binding of divalent cations to calixarene-based Langmuir monolayers. *Langmuir* **31**, 2351-2359 (2015).
98. Tulli, L. G. *et al.* Polymorphism control of an active pharmaceutical ingredient beneath calixarene-based Langmuir monolayers. *Chem. Commun.* **50**, 3938-3940 (2014).
99. Moradi, M. *et al.* Two-dimensional calix[4]arene-based metal-organic coordination networks of tunable crystallinity. *Angew. Chem. Int. Ed.* **56**, 14395–14399 (2017).
100. M. Moradi *et al.* Supramolecular architectures of molecularly thin yet robust free-standing layers. *Sci. Adv.* In press. (2018).
101. Moradi, M. *et al.* Controlling in-situ formation of bilayer *vs* monolayer of metal-organic coordination networks. Submitted. (2018).